INAUGURAL–DISSERTATION
zur
Erlangung der Doktorwürde
der
Naturwissenschaftlich–Mathematischen
Gesamtfakultät
der
Ruprecht–Karls–Universität
Heidelberg

vorgelegt von
Lic.-Ing. Hernán Andrés Olguín Astudillo
aus Valparaíso, Chile

Tag der mündlichen Prüfung: 17.07.2015

Theoretical and Numerical Analysis of Laminar Spray Flames for Use in Turbulent Spray Combustion Modeling

Gutachter: Prof. Dr. Eva Gutheil
apl. Prof. Dr. Hans-Robert Volpp

Gedruckt mit Unterstützung des Deutschen Akademischen Austauschdienst

Contents

Abstract

Spray combustion under turbulent conditions occurs in many technical devices. Therefore, the proper prediction of the characteristics of turbulent spray flames is of vital importance for the design of new combustion technologies in view of efficiency and pollutant reduction, where the latter requires consideration of detailed chemical reaction mechanisms. Unfortunately, a direct inclusion of detailed chemical reactions dramatically increases the computational cost of the numerical simulations of technical combustion processes, and it is prohibitive in practical situations. Models based on the assumption that turbulent flames can be seen as an ensemble of laminar stretched flame structures, the so-called flamelet models, represent a very promising approach for the cost effective inclusion of detailed chemical reaction mechanisms in the simulation of turbulent spray flames.

Several flamelet models are currently available in the literature for the simulation of pure non-premixed and pure premixed gas flames. Additionally, some two-regime flamelet formulations have been proposed in the last years for situations where non-premixed and premixed gas combustion coexist and interact. These models, however, are not adequate for the simulation of turbulent spray combustion, since they do not take into account spray evaporation, which strongly affects the flame structure. Although a spray flamelet model has been proposed for the simulation of flames where non-premixed and evaporation-dominated combustion regimes coexist, most studies of turbulent spray flames use gas flamelet models, neglecting the effects of evaporation on the flame structure.

In the present thesis, a common framework is developed in which the several single and two-regime flamelet models existing in the literature can be described and combined in order to advance the development of a comprehensive multi-regime spray flamelet model for turbulent spray flames. For this purpose, a set of multi-regime spray flamelet equations in terms of the mixture fraction and a reaction progress variable is derived, which describes all combustion regimes appearing in spray flames. The flamelet equations available in the literature for single and two-regime flames are retrieved from these multi-regime spray flamelet equations as special cases. Additionally, exact transport equations of the mixture fraction and its scalar dissipation rate are derived, which are then used to evaluate the validity of several assumptions commonly made in the literature during their derivation, such as the use of unity Lewis number and the negligence of spatial variations of the mean molecular weight of the mixture. These assumptions had not yet been tested for the calculation of the scalar dissipation rate of the mixture fraction in spray flames, and their validation is of vital importance for the formulation of any spray flamelet model.

Numerical simulations of axi-symmetric laminar mono-disperse ethanol/air counterflow spray flames are carried out to analyze the influence of spray evaporation on the flame structure. Parametric studies of the influence of the initial droplet radius and strain rate are presented, which clearly illustrate the major importance of evaporation in the determination of the flame structure. Additionally, the relative importance of non-premixed and premixed combustion regimes in the previously analyzed counterflow spray flames is studied by means of the derived multi-regime spray flamelet equations. The results show that premixed effects can be neglected in this kind of flame with all fuel injected in liquid phase.

Moreover, the derived transport equations of mixture fraction and its scalar dissipation rate are solved for the counterflow spray flames considered in this work considering and without considering the assumptions of unity Lewis number and spatially uniform mean molecular weight of the mixture. The results are compared, and it is found that the assumption of unity Lewis number may lead to non-physical values of the scalar dissipation rate of the mixture fraction, whereas the use of a mass-averaged diffusion coefficient of the mixture is an acceptable approximation. Effects associated with the spatial variation of the mean molecular weight of the mixture are found to be small at low strain rate and negligible at high strain rates. These results confirm the validity of the use of Fick's diffusion law in highly strained flames.

Finally, a set of non-premixed spray flamelet equation is obtained by neglecting premixed effects in the previously derived multi-regime spray flamelet equations. This set of equations, which is valid in situations where non-premixed and evaporation-dominated combustion regime coexist, is similar to the classical non-premixed gas flamelet equations, but it contains two additional terms for the description of evaporation effects. These equations are then used to evaluate the relative importance of the effects attributable to evaporation. The results show that they are always relevant and they should be always considered.

Keywords: spray flamelet modeling, counterflow ethanol/air flames, scalar dissipation rate

Zusammenfassung

In den meisten technischen Verbrennungsprozessen wird der Brennstoff dem Brennraum in flüssiger Form zugeführt. Daher ist die richtige Vorhersage der Eigenschaften von turbulenten Sprayflammen entscheidend für die Entwicklung neuer Verbrennungstechnologien in Hinblick auf ihre Leistungsfähigkeit und Schadstoffreduzierung, wobei letzteres die Berücksichtigung detaillierter chemischer Reaktionsmechanismen erfordert. Leider erhöht eine direkte Einbeziehung der detaillierten chemischen Reaktionen drastisch die Rechenkosten der numerischen Simulation von technischen Verbrennungsprozesse und ist deshalb in praktischen Situationen nicht möglich. Flamelet-Modelle stellen einen vielversprechenden Ansatz für die kosteneffiziente Einbeziehung detaillierter chemischer Reaktionsmechanismen bei der Simulation turbulenter Sprayflammen dar.

Derzeit existieren Flamelet-Modelle, die für die Simulation von nicht-vorgemischten und vorgemischten Gasflammen geeignet sind. Darüber hinaus sind in den letzten Jahren einige Zwei-Regime Flamelet Formulierungen für Situationen hergeleitet worden, in denen nicht-vorgemischte und vorgemischte Gasflammen koexistieren und interagieren.

Diese Modelle sind jedoch leider nicht für die Simulation der turbulenten Sprayverbrennung geeignet, da sie keine Verdampfungseffekte berücksichtigen, die die Flammenstruktur stark beeinflussen. Obwohl ein Spray-Flamelet-Modell für die Simulation von Flammen vorgeschlagen wurde, in denen nicht-vorgemischte Verbrennung und Verdampfung interagieren, werden in den meisten Studien über turbulente Sprayflammen Gas-Flamelet-Modelle verwendet. Auf diese Weise wird die Auswirkung der Verdampfung auf die Flammenstruktur vernachlässigt.

In der vorliegenden Arbeit wird ein Gesamtmodell entwickelt, in dem alle verschiedene Regime, in der Fachliteratur vorhandenen Flamelet-Modelle beschrieben werden können. Ziel ist es einen Beitrag zur Entwicklung eines umfassenden Multi-Regime Spray-Flamelet-Modells für turbulente Sprayflammen zu leisten. Zu diesem Zweck werden Multi-Regime-Spray-Flamelet Gleichungen abgeleitet, die alle Verbrennungsregime in Sprayflammen beschreiben. Die in der Fachliteratur vorhandenen Flamelet-Gleichungen für Ein- und Zwei-Regime Flammen sind indiesen Multi-Regime Spray-Flamelet-Gleichungen als Spezialfälle erhalten.

Weiterhin werden Transportgleichungen für den Mischungsbruch und seine skalare Dissipationsgeschwindigkeit hergeleitet. Diese Transportgleichungen werden dann verwendet, um die Gültigkeit mehrerer gebrÃ¤uchlicher Annahmen zu bewerten. Dazu zählen einer Annahme, dass die Lewis Zahl gleich eins ist und die Vernachlässigung der räumlichen Variationen des mittleren Molekulargewichts der Mischung. Diese An-

nahmen sind noch nicht für die Vorhersage der skalaren Dissipationsgeschwindigkeit in Sprayflammen geprüft worden, und ihre Validierung ist von entscheidender Bedeutung für die Formulierung eines Multi-Regime Spray-Flamelet-Modells.

Es werden numerische Simulationen von achsensymmetrischen, laminaren, monodispersen Ethanol/Luft Gegenstrom Spray-Flammen durchgeführt, um den Einfluss der Verdampfung auf die Flammenstruktur zu analysieren. Parametrische Untersuchungen des Einflusses der Größe des Anfangs-Tropfenradius und der Streckungsgeschwindigkeit werden vorgenommen, die die große Bedeutung der Verdampfung auf die Flammenstruktur verdeutlichen. Zusätzlich wird die relative Bedeutung der nicht-vorgemischten und vorgemischten Verbrennungsregime in den zuvor analysierten Gegenstrom-Spray-Flammen mit Hilfe der abgeleiteten Multi-Regime Spray-Flamelet-Gleichungen untersucht. Die Ergebnisse zeigen, dass, vorgemischte Effekte in diesen Flammen vernachlässigt werden können, wenn der Kraftstoff in flüssiger Phase eingespritzt wird.

Darüber hinaus werden die hergeleiteten Transportgleichungen für den Mischungsbruch und seine skalare Dissipationsgeschwindigkeit für die in dieser Arbeit betrachteten Gegenstrom-Spray-Flammen gelöst. Dies geschieht unter Berücksichtigung und Vernachlässigung der Annahmen der Lewis Zahl gleich eins und eines konstanten mittleren Molekulargewicht der Mischung. Ein Vergleich der Ergebnisse zeigt, dass die Annahme der Lewis Zahl gleich eins zu nicht physikalischen Ergebnissen der skalaren Dissipationsgeschwindigkeit führen kann. Die Verwendung eines masse-gemitteltenen Diffusionkoeffizienten der Mischung stellt hingegen eine gute Näherung dar. Die räumliche Veränderung des mittleren Molekulargewichts der Mischung ist gering für kleine Streckungsgeschwindigkeiten und vernachlässigbar für hohe Streckungsgeschwindigkeiten. Diese Ergebnisse bestätigen die Gültigkeit der Verwendung von Fick's Diffusionsgesetz in stark gestreckten Flammen.

Schließlich werden nicht-vorgemischte Spray-Flamelet-Gleichungen durch die Vernachlässigung vorgemischter Effekte in den zuvor abgeleiteten Multi-Regime Spray-Flamelet-Gleichungen hergeleitet. Diese Gleichungen sind für Situationen geeignet, in denen nicht-vorgemischte Verbrennung und Verdampfung koexistieren. Sie enthalten die klassischen nicht-vorgemischten Gas-Flamelet-Gleichungen als Spezialfall, wenn die beide Terme zur Beschreibung der Verdampfung gleich Null sind.

Die Spray-Flamelet-Gleichungen werden dann verwendet, um die Bedeutung der Verdampfung zu bewerten. Die Ergebnisse zeigen, dass diese immer relevant ist und berücksichtigt werden muss.

Schlagworte: Spray-Flamelet-Modellierung, Gegenstrom Ethanol/Luft Flammen, skalare Dissipationsgeschwindigkeit

1. Introduction

1.1 Background

Combustion can be found in many practical devices used for transportation, electricity generation, domestic heating and industrial processes. Examples are, among others, internal combustion engines, gas turbines, rockets, and industrial furnaces. Combustion is currently the most important available means for transforming primary energy into secondary usable energy. During the last decades, the main sources of primary energy for combustion processes have been fossil fuels such as coal, oil and natural gas. According to the International Energy Agency (IEA), the demand of these fuels constantly increased during the last decades (see Fig. 1.1) and covered over 90% of the total world demand of primary energy in 2012 [1] (see Fig. 1.2). Currently proven reserves of these fuels are such that they could provide the world's energy needs for several decades [2, 3] and new storages are continuously discovered. Thus, the dominant position of combustion is expected to be maintained in the foreseeable future [3].

In most technical applications, combustion occurs under turbulent conditions. Additionally, several technical devices operate with liquid fuels, which are injected into the combustion chamber as a spray. In 2012, liquid fuels represented over 30% of the total

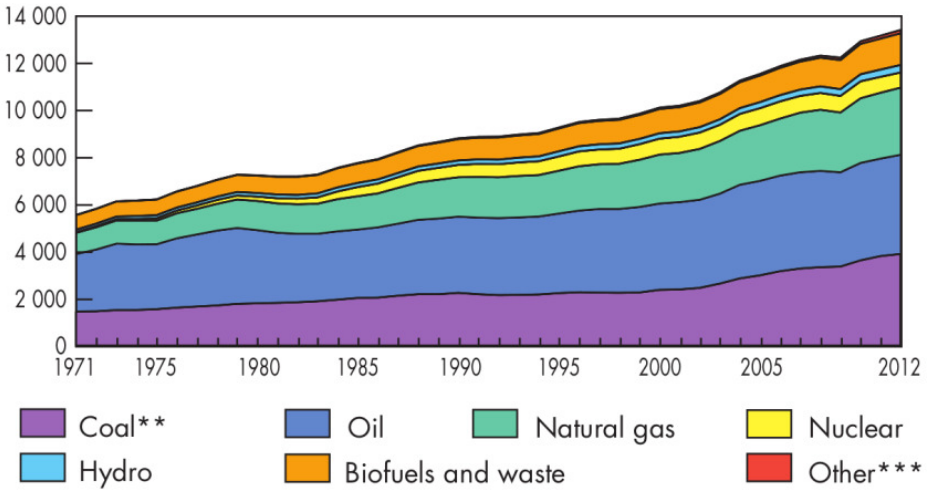

Figure 1.1: World demand of primary energy in the period 1971-2012 [1]

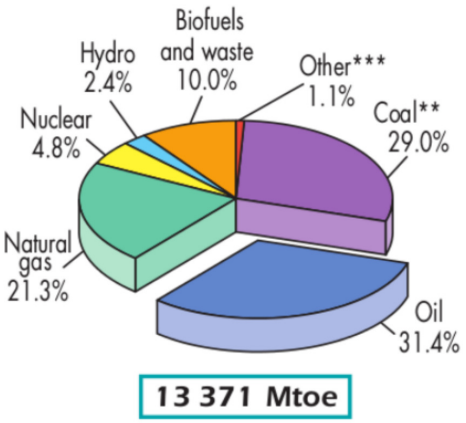

Figure 1.2: World primary energy supply by source in 2012 [1]

world demand of primary energy (see Fig. 1.2). This big proportion can be attributed to their several advantages over other alternatives such as availability and considerably higher safety and easiness of transport and storage. Thus, the study of turbulent spray combustion is of great interest for improving currently used combustion devices and for the development of new, less contaminant and more efficient combustion technologies.

Unfortunately, as useful as it is, combustion is always associated with the emission of pollutants. Currently, human caused emissions of carbon dioxide are believed to be directly linked to the global warming and other environmental issues of big concern such as the rise in sea level and the recession of glaciers [4]. Therefore, every year combustion technologies are required to meet stricter emission legislations, especially regarding CO_2 and NO_x [2]. Thus, the final goal of combustion research is the design of combustion systems with high efficiency and reliability and a minimum emission of air pollutants. Numerical simulations are a very valuable tool with the potential of playing a determinant role in the achievement of these goals [5, 6, 7, 8, 9, 10, 11].

The use of alternative fuels generated from vegetal feedstocks, commonly referred to as biofuels, can enormously contribute to reduce the negative environmental impact of combustion [12, 13, 14]. Currently, biofuels are considered an important means of progress for limiting greenhouse gas emissions and improving air quality [12, 13, 14]. They are considered to be carbon neutral, since any carbon dioxide released from their burning was previously captured from the atmosphere during the growing of the bio-feedstock that was used for their production (see exemplarily Fig. 1.3). Moreover, biofuels provide energetic independence, since natural bioresources are geographically more evenly distributed than fossil fuels. For these reasons, and because they have the potential of being sustainably produced, biofuels are currently considered a very

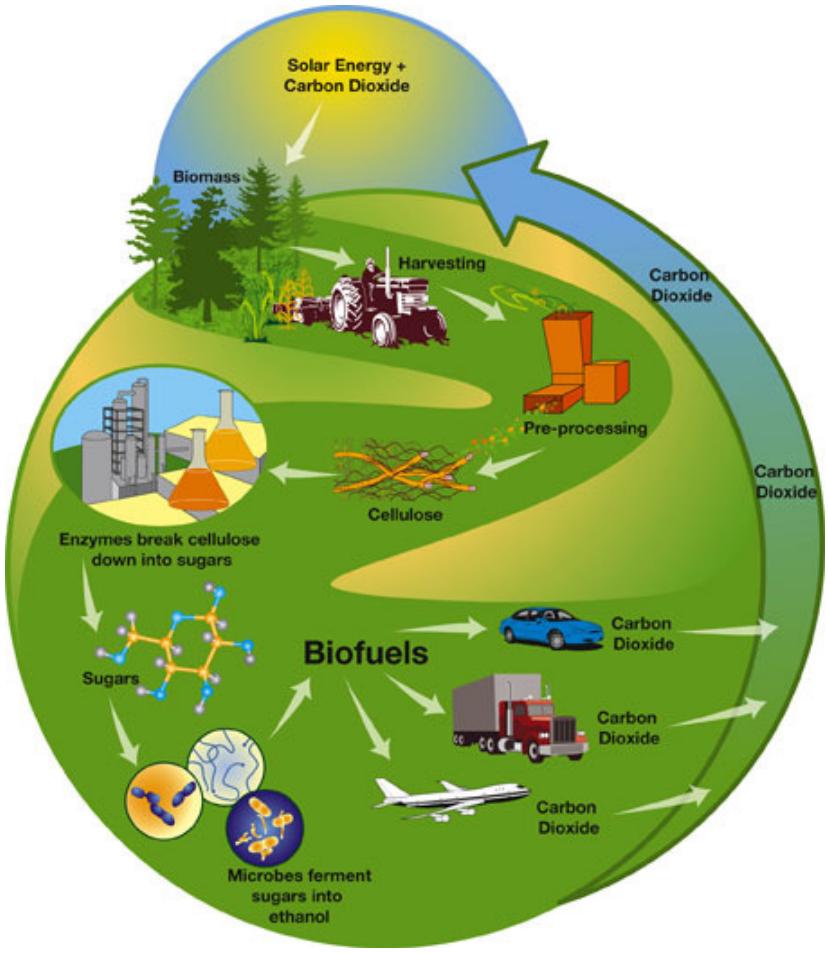

Figure 1.3: Schematic representation of the production cycle of biofuels [15]

promising alternative for replacing fossil fuels [12, 13, 14].

The first developments of biofuels were based on the conversion of sugar plants into ethanol via fermentation, and the upgrading of vegetable oils via transesterification [16]. The seemingly easy implementation of ethanol in existing infrastructure and its relatively low cost of production have attracted big interest on this biofuel during the last decades [13, 16]. Currently, ethanol is the most widely used biofuel in the world, accounting for the 90% of the total production of biofuels [17]. Compared with gasoline, ethanol contains only a small amount of sulphur [14, 18, 19]. Thus, mixing ethanol with gasoline helps to reduce the fuel's sulphure content and thereby lowers the emissions of sulphur oxides, a major component of acid rain, and a carcinogen [14]. However, its corrosivity and low energy density prevent its use as pure fuel without major modifications in engines [20, 21]. Thus, an adequate and permanent integration of ethanol into the world's energy matrix requires further research and the development of appropriate predictive tools for allowing the study of the effects of engine modifications

on engine's global performance and pollutant formation.

During the past years, butanol has been attracting special interest from the scientific community [22]. This fuel has a very similar energy density to gasoline and a much lower corrosivity than ethanol, which would allow its direct application in engines [23, 24, 25, 26, 27]. Historically, butanol has been mainly produced from biomass by the Acetone, Butanol, Ethanol fermentation process (ABE), which was not economically attractive. However, recently developed major improvements in its production process [28] restarted the interest in butanol as a viable alternative fuel and motivated several studies regarding its chemical and physical properties. In the last few years, several reaction mechanisms have been developed for the different isomers of butanol [23, 29, 30, 31, 32, 33]. However, despite of this increased interest, the development of butanol is still in a very early stage and more research in this field is warranted for the years to come.

Additionally to ethanol and butanol, several other alternative fuels have been studied in the last years. Examples are methanol, longer chain alcohols, furan-based molecules, and bio-derived synthetic hydrocarbons [16]. Currently, it remains an open question which of all the available biofuels is the best candidate to replace fossil fuels in the long term. Economical, environmental and technical aspects are all very important factors to consider to answer this question [12, 13, 14]. The fuel of the future has to be economically viable to produce at big scales and it has to be as similar as possible to current fossil fuels, so that only small modifications to the existing infrastructure have to be done for its use. Finally, probably the most important factor to be considered is the performance and the pollutant's emissions of combustion devices when these alternative fuels are employed. Thus, the importance of numerical simulations of combustion becomes evident, since they can considerably contribute to answering these questions.

1.2 Numerical Simulation of Turbulent Spray Flames

The advantages of numerical simulations are numerous: they represent a feasible and economic way of studying the performance of new designs of combustion devices, they can avoid the need of carrying out very expensive experiments, they are very useful in determining the influences of different individual parameters in combustion processes and they can provide multi-scale information, which may not be available by other means [5, 6, 7, 8, 9, 10, 11].

Unfortunately, combustion processes are very complex and several difficulties are associated with numerical simulations of turbulent flames, as it has been proved by

several decades of active research in this challenging field [7, 8, 9, 10, 11]. The major complications arise from the fact that several complex phenomena take place at different time and length scales and interact with each other in combustion chambers. In particular, the study of combustion includes many difficult subjects such as fluid mechanics, thermodynamics, mass and heat transfer and chemical kinetics, which are very complex in their own. Moreover, the use of liquid fuels introduces many additional difficulties to the numerical simulations. These complications are mainly related with the processes of liquid atomization, droplet movement, heating and evaporation, interphase interactions and the additional time and length scales associated with the liquid phase [34, 35]. The interaction between all these processes results in a very big and stiff set of partial differential equations, which is very difficult to solve.

Currently, turbulent spray combustion modeling is a very active research topic with plenty of open issues [34, 35, 36]. The development of models for spray injection and atomization are among the most important open issues in this field. These phenomena are still not well understood even though they are of vital importance for the proper simulation of turbulent spray flames [34, 35]. A common practice employed to avoid the complications associated with the modeling of the injection and atomization processes is the consideration of an already atomized spray, where the initial droplet distributions are obtained from experimental data. This considerably simplifies the simulation process and reduces the computational effort required for the simulations [34, 35].

As pointed out before, most technical applications involve turbulence, which is often referred to as the biggest unsolved problem in classical mechanics [37, 38]. The development of turbulence models is a very complex task. For reacting flows, specific complications appear when turbulence models are applied to the transport equations of chemical species, since unclosed terms appear due to the non-linearities associated with the chemical reaction source terms. Thus, turbulent combustion closure models are required [5, 39], which is another open modeling issue of big relevance.

Moreover, the fact that detailed reaction mechanisms are required for the proper prediction of pollutant formation introduces additional difficulties. Unfortunately, detailed chemical reaction mechanisms involve a big number of species and reactions, even for simple fuels. For this reason, their direct inclusion dramatically increases the computational cost of the numerical simulations of technical combustion processes, and it is prohibitive in practical situations. Currently, the development of adequate approaches for a cost effective inclusion of detailed chemistry in numerical simulations represent a very big challenge in turbulent (spray) combustion modeling [5, 39, 34, 35]. In the next chapter, a review of the several turbulent combustion models available in the literature is given, with special emphasis on flamelet models, which are the main topic of the present thesis. Flamelet models are an especially promising alternative for including

detailed chemical reaction mechanisms in the simulation of turbulent flames due to their low computational cost and easiness of implementation. A brief introduction to these models is given in the next section (1.3)

1.3 Flamelet Modeling

Flamelet models are a very promising approach for the inclusion of detailed chemical reaction mechanisms in the simulation of turbulent spray flames. The main idea behind flamelet models is that a turbulent flame can be considered as an ensemble of stretched laminar flames (commonly referred to as flamelets) [40]. Thus, during the simulation of a turbulent flame, species mass fractions can be obtained by averaging appropriate laminar flamelet structures instead of solving the transport equations of chemical species, which dramatically reduces the computational cost of numerical simulations [40].

The approach is further simplified by the use of a-priori generated laminar flamelet structures, which are tabulated in a flamelet library as a function of appropriate characteristic parameters. The posterior inclusion of these pre-tabulated structures in the computation of a turbulent flame requires the consideration of a Probability Density Function (PDF) of the characteristic parameters for taking into account turbulent fluctuations [40]. The structures required for the tabulations can be generated by different approaches. The simplest of them is the direct consideration of counterflow flames [41, 42, 43]. The second possible approach is the consideration of the so called flamelet equations, which correspond to transformations of the full transport equations of chemical species that mathematically describe the flame structure in a one-dimensional framework. During the construction of the library, the specific combustion regime of the turbulent flame to be simulated is a major factor to take into account, since different combustion regimes require the consideration of different flamelet structures [42, 44, 45, 46]. Therefore, different flamelet-based models can be found in the literature. The exact form of the flamelet equations and the specific coordinate system in which they are formulated are also chosen depending on the particular combustion regime considered.

Thus, classical formulations of flamelet-based models adopted very strict assumptions regarding the different combustion regimes that may occur in turbulent flames and either pure non-premixed [40, 47] or pure premixed [48, 49] combustion regimes were considered. The success of these classical gas flamelet models in the simulation of turbulent gas flames has motivated their application to the simulation of turbulent spray flames [41, 50, 51, 52, 53]. Liquid fueled combustion, however, is known to produce premixed, non-premixed and evaporation dominated modes of burning, which can simultaneously coexist and interact. In particular, for spray flames, evaporation may

greatly influence the spray flamelet structure [54, 55, 56, 57, 58, 42, 59, 60]. Recent studies [61, 62, 63, 64] in the framework of Conditional Momentum Closure (CMC) models for turbulent spray combustion also highlighted the need for including the spray evaporation source term into spray flame modeling. Therefore, classical flamelet formulations are not appropriate for the simulation of turbulent spray flames. Recently, several attempts have been made to extend classical mono-regime gas flamelet formulations to more complex situations, where at least two combustion regimes coexist [42, 59, 45, 65, 43].

Hollmann and Gutheil [42] and Gutheil [59] have extended the classical non-premixed gas flamelet model to spray flames, where non-premixed and evaporation-dominated combustion regimes take place simultaneously. This formulation consistently employs a spray flamelet library based on laminar counterflow spray flame structures, and it has been successfully used to simulate methanol/air and ethanol/air turbulent spray flames [42, 66, 67]. Nguyen et al. [65] derived a set of two-regime flamelet equations for the description of gas flames, where non-premixed and premixed combustion regimes coexist. Similarly, Knudsen and Pitsch [45, 46] have developed a set of two-regime flamelet equations, which can simultaneously capture non-premixed and premixed combustion regimes and which are used to locally determine the relative importance of each of them in a turbulent flame. Based on the results of this evaluation, mono-regime premixed and non-premixed gas flamelet libraries are selectively weighted and applied for the inclusion of detailed chemical reaction mechanisms [45, 46].

Despite of the progress made in the development of more complex two-regime flamelet models, the formulation of a comprehensive model able to capture all combustion regimes found in turbulent spray flames remains a very challenging task, and it is still an open research field. Thus, the development of a common framework for combining currently available flamelet models is highly desirable for the further development of spray flamelet models.

1.4 Research Objectives

The present work has four major objectives. The first of them is to generate a common framework for the existing two-regime flamelet models in order to advance in the formulation of a comprehensive spray flamelet model. For this purpose, a set of multi-regime spray flamelet equations is derived, which takes into account evaporation effects explicitly and is suitable to describe all combustion regimes appearing in spray flames. These equations comprise the two-regime [45, 46] and single-regime flamelet equations [40] available in the literature.

The second objective of this work is the verification of the spray flamelet model of

Hollmann and Gutheil's [42]. Specifically, it is evaluated if it is adequate to assume that only non-premixed and evaporation effects coexist in counterflow spray flames when all fuel is injected in liquid phase. For this purpose, terms associated with premixed effects are neglected in the derived multi-regime spray flamelet equations. By doing this, a two-regime formulation taking into account non-premixed and evaporation effects is obtained, which provides the theoretical fundamentals for the spray flamelet model of Hollmann and Gutheil [42] and will be referred as the non-premixed spray flamelet equations. The different terms in these equations are then evaluated for laminar ethanol/air spray flames in the counterflow configuration and the total budget of the terms balancing the chemical source in the flamelet equations is compared with the terms balancing it in the transport equation of chemical species in physical space for testing their equivalence, which implies that the influence of premixed effects can be neglected in the studied flames.

The third objective of this work is the evaluation of several assumptions made in the literature during the derivation of transport equations for the mixture fraction and its scalar dissipation rate. These two variables are of vital importance for the implementation of flamelet models, since they are widely used as characteristic parameters for the tabulation of the laminar flamelet structures. In particular, the validity of the use of Fick's diffusion law and the associated negligence of spatial variations in the mean molecular weight of the mixture, as well as the use of the assumption of unity Lewis number and the consideration of a mass averaged species diffusion coefficient are evaluated. For this sake, exact formulations of transport equations for mixture fraction and its scalar dissipation rate are derived and solved using the different assumptions commonly made in the literature. The results are compared with values of the mixture fraction and its scalar dissipation rate directly obtained by their definition in order to evaluate the validity of the assumptions introduced.

Finally, the non-premixed spray flamelet equations are also employed for the evaluation of the relative importance of evaporation on the spray flamelet structure. This evaluation represents the fourth objective of this work.

The outline of this dissertation is as follows. In chapter 2, a review of the state of the art in turbulent combustion modeling with emphasis on flamelet modeling is given. The governing equations, the derivation of the transport equations of mixture fraction and its scalar dissipation rate and of the multi-regime spray flamelet equations, as well as the numerical scheme employed in this work are presented in chapter 3. Chapter 4 presents results and discussions. Finally, conclusions and perspectives of future work are given in chapter 5.

2. State of the Art

In this chapter, a review of the state of the art in turbulent combustion modeling with emphasis on flamelet modeling is given. In turbulent spray flames, several complex phenomena take place simultaneously and interact with each other. These interactions are very strong and cannot be neglected. Especially important are the turbulence/-chemistry interactions, which are the main differentiating feature of turbulent reacting flows when compared with turbulent non-reacting flows. Different approaches can be used for the description of the turbulent flow field. In terms of the level of details employed, simulations of turbulent reacting flows can be categorized in three different groups. The most detailed approach consists in the resolution of all spatial and temporal scales of turbulence by considering the full instantaneous equations for mass, momentum, species mass fraction and energy conservation without employing turbulence models. This approach is called Direct Numerical Simulation (DNS) and it is commonly associated with a very high computational cost, which makes it prohibitive in practical situations [37, 39]. A less detailed approach is Large Eddy Simulations (LES) [37, 39], where only large turbulent scales are directly solved and small scales are modeled. By doing this, the computational cost of the simulations is reduced. However, LES are still computationally expensive and applications to real engineering problems are still in a very early stage [39]. Finally, the most inexpensive approach for the description of turbulent (reacting) flows are Reynolds Averaged Navier Stokes (RANS) methods [37, 39]. In this method, the governing equations for mass, momentum, species mass fractions and energy conservation are time averaged. In constant density flows, the averaging process consists in splitting any quantity ϕ into [5, 39]

$$\phi = \overline{\phi} + \phi', \tag{2.1}$$

where $\overline{\phi}$ is the mean value of ϕ and ϕ' is a fluctuating component. In the case of combustion, however, the fluid is compressible and a mass weighted average (called Favre average) is normally preferred [68, 39]. The Favre-average value of the variable ϕ is calculated as [5, 39]

$$\tilde{\phi} = \frac{\overline{\rho\phi}}{\overline{\rho}}. \tag{2.2}$$

Thus, the instantaneous quantities can be split into a Favre-averaged mean value and a fluctuation as [39, 68]

$$\phi = \tilde{\phi} + \phi'', \tag{2.3}$$

where, by definition

$$\widetilde{\phi''} = \frac{\overline{\rho\phi''}}{\overline{\rho}} = 0. \tag{2.4}$$

Although the consideration of averaged quantities instead of instantaneous ones considerably reduces the computational cost of the simulations of turbulent reacting flows, this practice leads to the rise of probably the biggest problem found in turbulence/-chemistry interactions modeling, namely the averaging of the chemical reaction rates appearing in the species transport equations. Since reaction rates are highly non-linear, the average reaction rate cannot be easily expressed as a function of Favre averaged scalars. The most direct approach for solving this problem is to expand the reaction rates as a function of species mass fractions and temperature. For example, considering global chemistry, the mean reaction rate of the fuel can be written as [5, 39]

$$\begin{aligned} \overline{\dot{\omega}}_F = & - A\,\overline{\rho}\,\tilde{T}^b\,\tilde{Y}_F\,\tilde{Y}_O\,\exp\left(-\frac{T_A}{\tilde{T}}\right) \\ & \times \left[1 + \frac{\widetilde{Y_F''Y_O''}}{\tilde{Y}_F\tilde{Y}_O} + (P_1 + Q_1)\left(\frac{\widetilde{Y_F''T''}}{\tilde{Y}_F\tilde{T}} + \frac{\widetilde{Y_O''T''}}{\tilde{Y}_O\tilde{T}}\right) + ...\right], \end{aligned} \tag{2.5}$$

where P_n and Q_n are determined as

$$P_n = \sum_{k=1}^{n} (-1)^{n-k}\,\frac{(n-1)!}{(n-k)![(k-1)!]^2 k}\left(\frac{T_A}{\tilde{T}}^k\right) \tag{2.6}$$

and

$$Q_n = \frac{b(b+1)...(b+n-1)}{n!}, \tag{2.7}$$

respectively. This approach leads to several difficulties. First, several unclosed terms appear in Eq. (2.5), which require modeling through algebraic expressions or additional transport equations. Moreover, the non-linearities associated with the problem prevents the negligence of high order terms, since this practice can lead to considerably big errors. Finally, Eq. (2.5) is only valid for a reaction mechanism consisting of a single irreversible chemical reaction. Expressions for the mean reaction rates using more realistic chemical reaction mechanisms are even more complex. Thus, this direct approach is very impractical and its application is very difficult and limited [68, 39].

Several other approaches have been developed for the consideration of chemical reaction mechanisms in the simulation of turbulent flames. In the remainder of this chapter, a revision of the state of the art in turbulent combustion modeling with special emphasis on flamelet modeling is given. In particular, the main turbulent combustion models different than the flamelet model will be summarized in section 2.1 and the several flamelet models available in the literature are reviewed in section 2.2.

2.1 Turbulent Combustion Modeling

Several approaches different to flamelet models exist in the literature for the consideration of chemical reactions in the simulation of turbulent (spray) flames. The main available methods are summarized in the present section. A more detailed description, as well as additional methods, can be found in the review paper of Veynante and Vervisch [5].

2.1.1 Infinitely Fast Chemistry Model

One of the first models proposed for the simulation of non-premixed combustion is the consideration of two streams of fuel and oxidizer, which mix and react in an infinitely fast single step chemical reaction [5, 39]

$$\mathrm{F} + s\mathrm{O} \rightarrow (1+s)\mathrm{P}, \tag{2.8}$$

where F, O and P denote fuel, oxidant and products, respectively, and s is the stoichiometric coefficient. For this situation, the transport equations of fuel mass fraction, oxygen mass fraction and temperature can be written as [5, 39]

$$\frac{\partial Y_\mathrm{F}}{\partial t} + \frac{\partial(\rho u_i Y_\mathrm{F})}{\partial x_i} = \frac{\partial}{\partial x_i}\left(D_\mathrm{F}\frac{\partial Y_\mathrm{F}}{\partial x_i}\right) + \dot{\omega}_\mathrm{F}, \tag{2.9}$$

$$\frac{\partial Y_\mathrm{O}}{\partial t} + \frac{\partial(\rho u_i Y_\mathrm{O})}{\partial x_i} = \frac{\partial}{\partial x_i}\left(D_\mathrm{O}\frac{\partial Y_\mathrm{O}}{\partial x_i}\right) + \dot{\omega}_\mathrm{O}, \tag{2.10}$$

and

$$\frac{\partial T}{\partial t} + \frac{\partial(\rho u_i T)}{\partial x_i} = \frac{\partial}{\partial x_i}\left(\frac{\lambda}{C_p}\frac{\partial T}{\partial x_i}\right) + \left(\frac{Q}{C_p}\right)\dot{\omega}_\mathrm{F} \tag{2.11}$$

respectively. In Eqs. (2.9-2.11), u_i is the gas velocity, ρ is the gas density and D_F and D_O are the diffusion coefficients of fuel and oxidizer into the mixture. $\dot{\omega}_k$ denotes the chemical mass source term of species k, Q is the amount of heat released by combustion, λ is the heat conductivity of the mixture and C_p refers to the specific heat capacity of the mixture. Assuming the same diffusion coefficient for fuel, oxidant and temperature, $D_\mathrm{F} = D_\mathrm{O} = \frac{\lambda}{C_p} = \mathrm{D}$, different combinations of Eqs. (2.9-2.11) can be performed, which yields transport equations for the following variables [5, 39]

$$Z_1 = sY_F - Y_O; \qquad Z_2 = \frac{C_p T}{Q} + Y_F; \qquad Z_3 = \frac{sC_p T}{Q} + Y_O. \tag{2.12}$$

All these transport equations have the same common form [5, 39]

$$\frac{\partial(\rho Z_j)}{\partial t} + \frac{\partial(\rho u_i Z_j)}{\partial x_i} = \frac{\partial}{\partial x_i}\left(D\frac{\partial Z_j}{\partial x_i}\right), \tag{2.13}$$

but are subject to different boundary conditions, which can be summarized as [5, 39]

$$Fuel\ side: \quad Z_1 = sY_{F,-\infty}; \quad Z_2 = \frac{C_pT_{-\infty}}{Q} + Y_{F,-\infty}; \quad Z_3 = \frac{sC_pT_{-\infty}}{Q}; \tag{2.14}$$

$$Air\ side: \quad Z_1 = -Y_{O,\infty}; \quad Z_2 = \frac{C_pT_{\infty}}{Q}; \quad Z_3 = \frac{sC_pT_{\infty}}{Q} + Y_{O,\infty}. \tag{2.15}$$

Normalizing Z_j by their respective values at the fuel and oxidizer streams as [5, 39]

$$\xi_j = \frac{Z_j - Z_{j,O}}{Z_{j,F} - Z_{j,O}}, \tag{2.16}$$

the transport equations of Z_j can be rewritten as [5, 39]

$$\frac{\partial(\rho\xi_j)}{\partial t} + \frac{\partial(\rho u_i \xi_j)}{\partial x_i} = \frac{\partial}{\partial x_i}\left(D\frac{\partial \xi_j}{\partial x_i}\right). \tag{2.17}$$

This normalization process is very useful, since the resulting transport equations of ξ_j have the same boundary conditions, $\xi = 1$ and $\xi = 0$, at the fuel and oxidizer stream, respectively, which means that the same solution is obtained from each of them and, therefore, only a single transport equation for ξ has to be considered. ξ is commonly referred as the mixture fraction, since it indicates the local state of the mixture between fuel and oxidizer. A further advantage of considering normalized quantities is that the species mass fractions and temperature can be related to the single mixture fraction ξ and the injection conditions at the fuel and oxidizer streams by means of Eqs (2.12). This is done by observing that, since the chemistry is assumed to be infinitely fast, reactants cannot coexist and they immediately react when they enter in contact in an infinitely thin reaction zone. Thus, the flame is composed of regions with either excess of fuel (where $Y_{\mathrm{O}} = 0$) or excess of oxidant (where $Y_{\mathrm{F}} = 0$), which are separated by the flame front. Thus, the normalized formulations of Eqs. (2.12), yields the following expression for the calculation of Y_{F}, Y_{O} and T at the side with excess of fuel [5, 39]

$$Y_{\mathrm{F}}(\xi) = Y_{F,-\infty}\left[\frac{\xi - \xi_{st}}{1 - \xi_{st}}\right], \tag{2.18}$$

$$Y_{\mathrm{O}}(\xi) = 0, \tag{2.19}$$

$$T(\xi) = \xi T_{-\infty} + (1-\xi)T_{\infty} + \frac{QY_{F,-\infty}}{C_p}\xi_{st}\frac{(1-\xi)}{(1-\xi_{st})}, \tag{2.20}$$

and the following corresponding relations for the region of the flame with excess of air [5, 39]

$$Y_{\mathrm{F}}(\xi) = 0, \tag{2.21}$$

$$Y_{\mathrm{O}}(\xi) = Y_{O,-\infty}\left[1 - \frac{\xi}{\xi_{st}}\right], \tag{2.22}$$

$$T(\xi) = \xi T_{-\infty} + (1-\xi)T_{\infty} + \frac{QY_{F,-\infty}}{C_p}\xi. \tag{2.23}$$

These relations can be later included in the simulation of non-premixed turbulent flames by [5, 39]

$$\tilde{Y}_{\mathrm{F}} = \int_0^1 Y_{\mathrm{F}}(\xi)\tilde{P}(\xi)\mathrm{d}\xi, \tag{2.24}$$

$$\tilde{Y}_{\mathrm{O}} = \int_0^1 Y_{\mathrm{O}}(\xi)\tilde{P}(\xi)\mathrm{d}\xi, \tag{2.25}$$

and

$$\tilde{T} = \int_0^1 T(\xi)\tilde{P}(\xi)\mathrm{d}\xi, \tag{2.26}$$

where $\tilde{P}(\xi)$ is the Favre probability density function of ξ.

2.1.2 Eddy Break-Up and Eddy Dissipation Concept Models

The Eddy Break-Up (EBU) model has been proposed as a computationally inexpensive alternative for calculating the Favre-averaged chemical reaction mass source in premixed gas flames [69]. This approach is based on a phenomenological analysis of turbulent combustion, assuming high Reynolds and Damköhler numbers, Re and Da, respectively. In the EBU model, the turbulence is assumed to be homogeneous and isotropic, and the chemical reaction rate of the fuel is expressed as a function of local flow properties such as the turbulent kinetic energy and its rate of dissipation [69, 5]

$$\tilde{\dot{\omega}}_{\mathrm{F}} = -C_{\mathrm{EBU}}\overline{\rho}\frac{\epsilon}{k}\sqrt{\widetilde{Y''^2_{\mathrm{F}}}}, \tag{2.27}$$

where Y''_{F} is the fuel mass fraction fluctuation and C_{EBU} denotes a model constant. k is the kinetic energy and ϵ its dissipation rate. The reaction rate can be also formulated in terms of a reaction progress variable, C, as [5]

$$\tilde{\dot{\omega}}_{C} = -C_{\mathrm{EBU}}\overline{\rho}\frac{\epsilon}{k}\sqrt{\widetilde{C''^2}}, \tag{2.28}$$

where the fuel mass fraction fluctuations are replaced by the progress variable fluctuations, C''. The Favre average values of $\widetilde{Y''^2_{\mathrm{F}}}$ and $\widetilde{C''^2}$ have to be modeled, which is normally done by means of transport equations. Unfortunately, the use of Eq. (2.28) leads to some inconsistencies, since the value of $\frac{\partial\tilde{\dot{\omega}}_C}{\partial\tilde{C}} = \infty$ when $\tilde{C} = 0$ and $\tilde{C} = 1$, which is not realistic. For this reason, a different expression is commonly preferred [69, 5]

$$\tilde{\dot{\omega}}_{C} = -C_{\mathrm{EBU}}\overline{\rho}\frac{\epsilon}{k}\tilde{C}(1-\tilde{C}), \tag{2.29}$$

or, in terms of the fuel mass fraction [69, 5]

$$\tilde{\dot{\omega}}_{\mathrm{F}} = -C_{\mathrm{EBU}}\overline{\rho}\frac{\epsilon}{k}\frac{\tilde{Y}_{\mathrm{F}}}{Y_{\mathrm{F},-\infty}}(1-\frac{\tilde{Y}_{\mathrm{F}}}{Y_{\mathrm{F},-\infty}}). \tag{2.30}$$

The EBU model leads to reasonably predictions and it is very easy to implement in CFD codes. However, the quality of the predictions strongly depends on the turbulence model considered, due to the use of the turbulence time scale.

The Eddy Dissipation Concept (EDC), is a direct extension of the EBU model to non-premixed flames [70]. In this model, the kinematic viscosity is employed additionally to the turbulent energy and its dissipation. The fuel burning rate is calculated according to [70, 5]

$$\tilde{\dot{\omega}}_F = \alpha\overline{\rho}\frac{\epsilon}{k}\min\left(\tilde{Y}_F, \frac{\tilde{Y}_O}{s}, \beta\frac{\tilde{Y}_P}{(1+s)}\right), \tag{2.31}$$

where α and β are adjustable parameters. Unfortunately, the EDC model is also strongly affected by the choice of the turbulence model. Additionally, the EBU and EDV models are only valid for one-step chemistry, whereas the proper prediction of pollutant formation during the operation of combustion devices requires the consideration of detailed chemical reaction mechanisms.

2.1.3 Conditional Momentum Closure Models

Conditional Moment Closure (CMC) models have also been proposed for the inclusion of detailed chemistry in the simulation of turbulent flames [71]. The main idea behind this approach is that the fluctuations of temperature and compositions can be linked to the fluctuations of one or two characteristic variables. Then, the transport equations for species mass fractions and enthalpy can be reformulated in terms of conditional averages, which are the averages of all these scalars having the same value of the key variables. For this, a conditional PDF is employed. The typical formulation of the CMC equations is [71]

$$\begin{aligned}\frac{\partial Q_\alpha}{\partial t} &+ \langle u_i \mid \eta\rangle\frac{\partial Q_\alpha}{\partial x_i} = \langle N \mid \eta\rangle\frac{\partial^2 Q_\alpha}{\partial \eta^2} + \langle W_\alpha \mid \eta\rangle \\ &- \frac{1}{\rho_\eta \tilde{P}(\eta)}\frac{\partial \rho_\eta \tilde{P}(\eta)\langle u_i'' Y_\alpha'' \mid \eta\rangle}{\partial x_i},\end{aligned}$$

where Q_α is the average mass fraction of chemical species α conditional to the mixture fraction, ρ_η is the gas density conditional to mixture fraction, η is the sample space variable for the mixture fraction, $\tilde{P}(\eta)$ is the density-weighted mixture fraction probability density function, u_i is the gas velocity, Y_α'' are the fluctuations of species mass fractions, N is the scalar dissipation rate of the mixture fraction, W_α is the source term of chemical species due to chemical reactions and "$\langle|\rangle$" denotes conditional average. Equation (2.32) is unclosed and its use requires closure models for $\langle u_i \mid \eta\rangle$, $\langle N \mid \eta\rangle$, $\langle u_i'' Y_\alpha'' \mid \eta\rangle$ and $\langle W_\alpha \mid \eta\rangle$, for which several different models are available in the literature [6, 71].

CMC models have been widely used for the simulation of several turbulent flames with big success. Specially important is the capability of predicting auto-ignition and other unsteady effects impossible to capture employing one-step chemical reaction mechanisms. Currently, formulations for turbulent spray flames are available in the literature [61, 62, 63]. A rigorous derivation of the CMC equations for spray flames is given by Mortensen and Bilger [61]

$$\begin{aligned}\frac{\partial Q_\alpha}{\partial t} &+ \langle u_i \mid \eta\rangle \frac{\partial Q_\alpha}{\partial x_i} = \langle N \mid \eta\rangle \frac{\partial^2 Q_\alpha}{\partial \eta^2} + \langle W_\alpha \mid \eta\rangle \\ &- \frac{1}{\langle\theta\rangle\rho_\eta \tilde{P}(\eta)} \frac{\partial \langle\theta\rangle\rho_\eta \tilde{P}(\eta)\langle u_i'' Y_\alpha'' \mid \eta\rangle}{\partial x_i} \\ &+ \left[Q_{1,\alpha} - Q_\alpha - (1-\eta)\frac{\partial Q_\alpha}{\partial \eta}\right] \frac{\langle \Pi \mid \eta\rangle}{\langle\theta\rangle} \\ &- \frac{1}{\langle\theta\rangle\rho_\eta \tilde{P}(\eta)} \frac{\partial (1-\eta)\rho_\eta \tilde{P}(\eta)\langle Y_\alpha'' \Pi'' \mid \eta\rangle}{\partial \eta},\end{aligned} \tag{2.32}$$

where Π denotes mass evaporation rate, $Q_{1,\alpha}$ is the mass fraction of species α in the liquid droplets and $\langle\theta\rangle$ is the gas volume fraction. Compared with the CMC equations for gas flames, Eqs. (2.32), new unclosed terms appear in the formulation for spray flames. These new unclosed terms are $\langle \Pi \mid \eta\rangle$ and $\langle Y_\alpha'' \Pi'' \mid \eta\rangle$, and closure models have been proposed for them recently [62, 63].

Despite having a low computational cost when compared with DNS and transported PDF methods, CMC models are still expensive when compared with flamelet models. A review of CMC methods has been published by Klimenko and Bilger [71].

2.1.4 Transported Probability Density Function Models

Transported probability density function methods represent a very convenient alternative for determining the chemical structure in turbulent reacting flows considering detailed chemical reaction mechanisms and it appears to be a powerful approach for the modeling of a wide range of combustion processes including local extinction, reignition and pollutant formation [72, 73]. These methods consist in the derivation of a transport equation for the joint PDF of the variables of interests and in its numerical resolution [72, 73]. The description starts with the description of a gas mass density function $F(\Psi; \mathbf{x}, t)$, which is defined in terms of the one-point, one-time Eulerian fine-grained joint scalar PDF $f^*(\Psi; \mathbf{x}, t)$

$$f^*(\Psi; \mathbf{x}, t) = \delta(\Phi(\mathbf{x}, t) - \Psi) \equiv \prod_{\alpha=1}^{N_\alpha} \delta(\Phi_\alpha(\mathbf{x}, t) - \Psi_\alpha), \tag{2.33}$$

$$F(\Phi; \mathbf{x}, t) = \rho(\Psi)\langle f^*(\Psi; \mathbf{x}, t)\rangle, \tag{2.34}$$

where δ is the Dirac delta function, Φ is the vector of the characteristic gas variables, and Ψ corresponds to the corresponding sample space. The general form of the transport equation of $F(\Psi; \mathbf{x}, t)$, including the interphase exchange effects can be written as [72, 73]

$$\frac{\partial F}{\partial t} + \frac{\partial(\langle u_i|\Psi\rangle F)}{\partial x_i} - \left\langle \frac{S_\mathrm{v}}{\rho} \middle| \Psi \right\rangle F = -\sum_{\alpha=1}^{N_\alpha} \frac{\partial}{\partial \Psi_\alpha} \left(\left\langle \frac{\mathrm{d}\Phi_\alpha}{\mathrm{d}t} \middle| \Psi \right\rangle F \right), \tag{2.35}$$

where u_i is the convection flow velocity. S_v is the spray evaporation effect on gas mass, and ρ the density. "$\langle|\rangle$" represents the conditional expectations and N_α is the number of characteristic gas variables Φ_α. Velocity-composition joint PDFs are commonly considered when reacting flows are under study, this method, however, is not limited to this particular choice and transport equations can be derived for several other variables such as enthalpy, velocities, mixture fraction, progress variable, etc. Typically, transported PDF methods are employed for the calculation of the probability density function of the mixture fraction, which is then used in other models for the determination of the flame structure. PDF methods are very attractive, since the chemical source term appears in closed form in the transport equation, and, therefore, no model is needed for it and it can be treated in an exact way. Another attractive feature is that PDF methods are general and not specifically designed for strict combustion regimes. Thus, the same model can be employed for the simulation of different combustion situations. However, closure models are required for some terms. Different closure models are currently available in the literature. Very comprehensive reviews have been given by Pope [72] and Haworth [73].

Although PDF methods are perceived to be very accurate, they still have a very high computational cost. More details about PDF methods can be found in [72, 73].

2.1.5 Intrinsic Low Dimensional Manifold Method

A different approach, employed for gas flames, is the reduction of the size of the chemical reaction mechanism to be employed. Advanced reduction techniques are based on the observation that a typical combustion system contains many different time scales. In general, time scales associated with fluid mechanical processes cover a smaller range of the spectrum than chemical time scales. Thus, there are chemical processes much faster than any physical process and that can be decoupled by assuming them to be in local equilibrium [74]. This leads to a reduction of the stiffness of the system of equations to be solved and thus, to a lower computational cost of the entire simulation. The Intrinsic Low Dimensional Manifold (ILDM) method, for instance, identifies the fast processes using an analysis of the eigenvalues of the governing equations [75,

76]. The chemical species with a short characteristic time are assumed to be in local equilibrium and the chemical species with long characteristic chemical times are employed as control parameters for the construction of low-dimensional tabulations of chemical structures [75, 76]. The major problem of ILDM is that poor predictions are obtained in low temperature regions, which require very high dimensional manifolds for their proper characterization, since only slow processes take place there. To overcome this problem, ILDM treats these regions by using linear interpolations between a non-burning solution and the last available low-dimensional manifold. Although this improves the performance of the method, it has been shown that simple interpolation is not an appropriate approach [48]. Gicquel et al. proposed an extension of ILDM for overcoming these deficiencies [48]. In the so called Flame Prolongation of ILDM (FPI), ILDM manifolds are used for high temperatures regions and one-dimensional premixed laminar flame structures are employed for low temperatures regions, instead of a simple linear prolongation [48]. More recently, a different extension of ILDM for low temperature regions has been proposed [77].

2.2 Flamelet Models

Flamelet models are a very promising approach for including detailed chemical reaction mechanisms in the simulation of turbulent flames. They are based on the assumption that a turbulent flame can be seen as an ensemble of very thin stretched laminar flames, which can be a-priori generated and tabulated as a function of appropriate characteristic parameters [40]. These thin stretched flames are commonly referred as flamelets and their tabulations as flamelet libraries. This idea was proposed in 1970 in the field of chemical engineering [78] and in 1972 in the field of combustion [79] and it implies that it is not necessary to directly solve the chemical structure during the simulation of a turbulent flame, but instead of this, a-priori tabulated flamelet structures can be included in the computations by means of a probability density function to account for turbulent fluctuations. By doing this, the number of equations to be solved and the computational cost of the simulations are dramatically reduced.

Crucial points for the successful implementation of flamelet models are the selection of appropriate laminar structures for the construction of the flamelet library and the consideration of proper parameters for their unique characterization [44, 80, 45, 46]. Typically, laminar counterflow flame structures are considered the basic structure composing complex turbulent flames. This choice has been made based on experimental results showing that these structures are very similar to the ones formed in turbulent mixing layers [40]. Figure 2.1 shows a schematic representation of a counterflow flame, where fuel droplets carried by air are injected from the left side of the configuration

and directed against an air stream injected from the right side of the configuration. In Fig. 2.1, the generated gas stagnation plane is easily recognized. The counterflow configuration has several advantages, such as the steadiness of the flow, a well-defined flow field, and the ease to vary boundary conditions such as strain rate, temperatures, and composition of the feed streams [54, 56, 82, 83]. This is particularly important in the frame of flamelet models, since the generation of a library requires the consideration of structures under different levels of stretch, which is characterized by the strain rate, a, defined as

$$a = [1 + \alpha]\frac{\partial u}{\partial y}, \tag{2.36}$$

with u denoting the flow axial velocity and y the axial coordinate. α is a constant with a value of 0 for planar counterflow flames and unity for axi-symmetric counterflow flames. Evidently, this value is not unique and it changes along the flame structure. Typically, its value at one of the injection points or at the stagnation plane is considered. During the selection of the boundary and initial conditions for the computations of the laminar flamelets is of vital importance to ensure that they match the specific conditions of the turbulent flame of interest. Specially relevant is that the flamelet structures must correspond to the combustion regime of the turbulent flame to be simulated, since it has been shown that non-premixed, premixed and evaporation dominated flames strongly differ in terms of structure and characteristic parameters required for their unique characterization. For this reason is that different flamelet models exist, which are especially formulated for different combustion regimes.

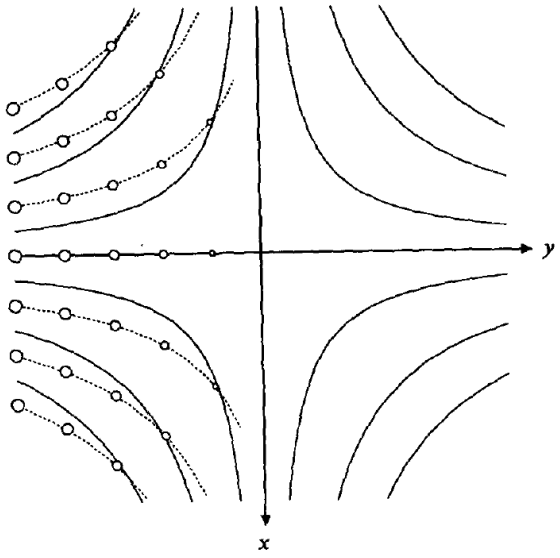

Figure 2.1: Schematic representation of a counterflow flame [81].

Several flamelet models are available for gas combustion, which have been successfully applied to the simulation of non-premixed [40, 47] or premixed turbulent flames [48, 49]. However, strict assumptions regarding the combustion regime that can take place in a turbulent flame are made during the formulation of these models and therefore, they are only valid in the specific combustion regime for which they were developed. Bradley and coworkers have reported simulations of non-premixed turbulent flames by means of look-up tables based on premixed flamelet structures [84, 85, 86] and several authors have reported simulations of non-premixed turbulent spray flames by means of libraries based on non-premixed gas flamelets [50, 51, 52, 53]. However, a systematic test of the accuracy of such attempts has shown that, in general, they lead to poor predictions, which confirms that different combustion regime require different flamelet libraries [41, 44]. This is particularly important when real technical spray flames are considered, in which pure combustion regimes rarely take place and typically non-premixed, premixed and evaporation-dominated combustion regimes may coexist and interact. Thus, single-regime gas flamelet models are not appropriate for the simulation of turbulent spray flames, since they do not take into account their inherent multi-regime nature. Unfortunately, the formulation of a multi-regime flamelet model able to describe all combustion modes present in turbulent spray flames is a very challenging task. Therefore, no such comprehensible model is currently available. However, some attempts have been recently made to extend classical mono-regime gas flamelet formulations to more complex situations, where at least two combustion regime coexist, specifically, for partially premixed gas flames [45, 65, 46] and non-premixed spray flames [42, 59].

The selection of the characteristic parameters is also made according to the particular combustion regime under consideration. For example, since non-premixed flames are mixing controlled, a variable indicating the local state of the mixture between fuel and oxidizer is introduced for this kind of flames, which is commonly referred as the mixture fraction, ξ. This variable and its scalar dissipation rate, $\chi_\xi = 2D\left(\frac{\partial \xi}{\partial x_i}\right)^2$, are employed for the characterization of non-premixed gas flames [40]. For premixed gas flames, on the other hand, the use of the mixture fraction is not appropriate, since its value is constant in perfectly premixed flames. For this reason, a different variable indicating the local state of advancement of the chemical reactions is employed. This variable, commonly denoted as the reaction progress variable, C, and its scalar dissipation rate $\chi_C = 2D\left(\frac{\partial C}{\partial x_i}\right)^2$ are normally employed for the characterization of premixed gas flamelets. The scalar dissipation rates, either of the mixture fraction or of the progress variables can be interpreted as indicators of the local stretch acting on the flame [40]. For non-premixed spray flames, it has been found that the use of the mixture fraction and its scalar dissipation rate are not enough and that three additional

parameters are required (initial droplet radius, droplet size and equivalence ratio) [42]. More specific definitions of all these variables will be given in the remainder of this thesis, as they are required.

Flamelet models are valid for situations where chemical reactions are very fast compared with flow effects. In turbulent flames, this relation is characterized by the Damköhler number, which is defined as

$$Da = t_t/t_c, \tag{2.37}$$

where t_t and t_c are the characteristic turbulent and chemical times, respectively. Thus, flamelet models are valid for high Damköhler numbers, which is fulfilled in most technical applications. A more detailed explanation of the situations under which the flamelet assumption is valid can be found in the work of Borghi [87] for premixed flames, and in its extension for non-premixed flames presented by Peters [88].

In the next subsection, the general formulation of flamelet models is given. Specific classical flamelet formulations and equations for gas non-premixed and gas premixed turbulent flames are reviewed in subsection 2.2.2.1 and 2.2.2.2, respectively. Two-regime flamelet models for partially premixed and spray flames are presented in the subsection 2.2.2.3 and 2.2.3.

2.2.1 General Formulation

When S characteristic parameters (Ξ_1,...,Ξ_s,...,Ξ_S) are employed for the characterization of the flamelet structures (for example, the mixture fraction, a reaction progress variable, etc.), each scalar ϕ defining the flame structure (such as species mass fractions, temperature, etc) can be expressed and tabulated in a flamelet library as [40, 47, 48, 49]

$$\phi = f(\Xi_1, ..., \Xi_s, ..., \Xi_S). \tag{2.38}$$

During the simulation of a turbulent flame, these structures can be averaged employing the joint probability density function of all characteristic parameters. For instance, for the determination of the Favre-averaged mean value of a scalar ϕ, $\tilde{\phi}$, the flamelet structures can be weighted as [40, 47, 48, 49]

$$\tilde{\phi} = \int_{\Xi_{1,Min}}^{\Xi_{1,Max}} ... \int_{\Xi_{S,Min}}^{\Xi_{S,Max}} \phi\left(\Xi_1, ..., \Xi_s, ..., \Xi_M\right)\ \tilde{P}\left(\Xi_1, ..., \Xi_s, ..., \Xi_S\right)\ \mathrm{d}\Xi_1 ... \ \mathrm{d}\Xi_S, \tag{2.39}$$

where, $\tilde{P}\left(\Xi_1, ..., \Xi_s, ..., \Xi_S\right)$ is a Favre joint probability density function.

Although the specific details regarding the considered laminar structures and characteristic parameters differ from model to model, the general strategy followed in their implementation is very similar for all the formulations existing and consists in the following steps [40, 47, 48, 49]

- A-priori generation and tabulation of laminar flamelet structures following Eq. (2.38).
- Determination of a joint PDF, $\tilde{P}\left(\Xi_1, ..., \Xi_s, ..., \Xi_S\right)$, in the entire domain during the simulation of a turbulent flame
- Calculation of the average value of the scalars, $\tilde{\phi}$, by means of Eq. (2.39).

For the generation of the required flamelet structures, two different approaches can be used, namely the consideration of counterflow flame structures [41, 42, 43] or the use of the so called flamelet equations, which describe the flame structure in a one-dimensional framework [40]. The exact form of the flamelet equations and the specific coordinate system in which they are formulated are also chosen depending on the particular combustion regime considered. These topics are discussed in more detail in the next subsections.

For the final inclusion of the flamelet library into the simulation of turbulent flames, the joint PDF of the characteristic parameters employed is needed. In general, two different possible approaches for determining this PDF exist, namely transported PDF methods and presumed PDF methods. In transported PDF methods, a transport equation of the joint PDF is solved [72, 73]. By doing this, the shape of the PDF can be determined in the entire domain for each instant of time. Transported methods have proved to be very accurate [72, 73]. Unfortunately, the computational cost associated with them is very high. In presumed PDF methods, on the other hand, the shape of the joint PDF is presumed. Further simplifications are introduced by assuming statistical independence of the characteristic parameters, which allows the decomposition of any joint PDF, $\tilde{P}(\Xi_1, ..., \Xi_s, ..., \Xi_S)$, into a product of single variable PDFs

$$\tilde{P}(\Xi_1, ..., \Xi_s, ..., \Xi_S) = \prod_{n=1}^{S} \tilde{P}(\Xi_s). \tag{2.40}$$

This transforms the problem of finding a joint PDF into a much simpler one consisting in finding single variable PDFs. For this, means for determining the mean value of the characteristic parameters are required, which can be done by solving appropriate transport equations. Currently, big confidence exists in the accuracy of transport equations of mixture fraction and reaction progress variables, but transport equations of their scalar dissipation rate are not as well established. This could be attributed to the complexity of these equations, which, when averaged for inclusion in the simulation of turbulent flames, present several unclosed terms requiring modeling. Thus, although transport equations for the scalar dissipation rate have been derived and applied before for premixed [89, 90, 91, 92], non-premixed [93, 94] and spray flames [95], they have not been formally tested and evaluated for use in laminar spray flames. This evaluation is required, since several assumptions are adopted for their derivation.

In the next subsections, a review of the main different flamelet models found in the literature is given. Specifically, the classical formulations for pure non-premixed gas flames and pure premixed gas flames are presented in section 2.2.2.1 and 2.2.2.2, respectively. The formulations existing for partially premixed and spray combustion are reviewed in sections 2.2.2.3 and 2.2.3.

2.2.2 Gas Flamelet Models

In this subsection, flamelet models available for non-premixed and premixed gas combustion are reviewed in subsections 2.2.2.1 and 2.2.2.2, respectively. Additionally, partially premixed gas flamelet models are reviewed in subsection 2.2.2.3. These partially premixed gas flamelet models are appropriate for situations where non-premixed and premixed combustion regimes coexist and interact.

2.2.2.1 Non-premixed Gas Flamelet Models

The first complete formulation of a flamelet model was presented for non-premixed gas flames [40]. Peters used the fact that in non-premixed flames the flamelet structure varies with the local mixture state, which is characterized by the mixture fraction, to introduce a coordinate system based on this variable, where all scalar variables can be expressed as

$$Y_k = f_k\left(\xi, \tau\right). \tag{2.41}$$

Thus, each scalar Y_k is considered a function of the mixture fraction and the transformed time τ [40]. Moreover, it is considered that combustion takes place in a very thin layer, i.e. flamelet, in the vicinity of the surface of stoichiometric mixture fraction, ξ_{st} [40],

$$\xi(x_i, t) = \xi_{\text{st}}, \tag{2.42}$$

and the structure of the flamelets is taken to vary only in a direction normal to this surface [40]. Thus, the transport equations of chemical species are transformed from physical space and time t, (x_1, x_2, x_3, t), into a new system of coordinates in the mixture fraction space and transformed time τ, (ξ, τ) [40]. Under the assumption of unity Lewis number and adopting Fick's diffusion law, the non-premixed flamelet equations yield [40]

$$\rho\frac{\partial Y_k}{\partial \tau} = \rho\frac{\chi_\xi}{2}\frac{\partial^2 Y_k}{\partial \xi^2} + \dot{\omega}_k, \tag{2.43}$$

where Y_k is the mass fraction of species k, ρ is the gas density, τ is time and $\dot{\omega}_k$ is the mass source of species k associated with chemical reactions. Note that although Eq. (2.43) mathematically describes the flamelet structure in a one-dimensional way,

three dimensional flames are actually described, since the iso-mixture fraction surfaces are three-dimensional in physical space.

In Eq. (2.43), the scalar dissipation rate, χ_ξ, defined as

$$\chi_\xi = 2D\left(\frac{\partial \xi}{\partial x_i}\right)^2, \tag{2.44}$$

is the only term containing information from the physical space and it comprises all the flow information. The scalar dissipation rate of the mixture fraction is a very important quantity in non-premixed flamelet models, which can be interpreted as the inverse of the characteristic diffusion time [40]

$$t_d = \frac{1}{\chi_\xi}. \tag{2.45}$$

In a burning flamelet, an increase in the local value of the scalar dissipation rate leads to a local reduction of the residence time, which can lead to local extinction or even to the complete extinction of the flame [40]. Thus, the scalar dissipation rate at extinction can be seen as a measurement of the stability of flames [40].

Equation (2.43) has been successfully applied in several numerical simulations. However, the negligence of differential diffusion effects can lead to inappropriate predictions under some conditions. Differential diffusion effects can be included in the generation of the flamelet libraries by employing counterflow flame structures directly instead of considering Eq. (2.43). Another alternative has been proposed by Pitsch and Peters [47], who presented an extension of Eq. (2.43), which considers differential diffusion. After applying the transformation rules proposed by Peters [40], the non-premixed flamelet equations considering differential diffusion and non-constant mean molecular weight of the mixture can be written as [47]

$$\begin{aligned}
\rho\frac{\partial Y_k}{\partial \tau} = {} & \frac{\rho\chi_\xi}{2}\frac{\mathrm{Le}_\xi}{\mathrm{Le}_k}\frac{\partial^2 Y_k}{\partial \xi^2} + \dot{\omega}_k + \frac{\rho\chi_\xi}{2}\frac{\mathrm{Le}_\xi}{\mathrm{Le}_k}\frac{Y_k}{\overline{\overline{M}}}\frac{\partial^2 \overline{M}}{\partial \xi^2} \\
& + \left[\left(\frac{\mathrm{Le}_\xi}{\mathrm{Le}_k} - 1\right)\left(\frac{\partial(\rho\chi_\xi)}{\partial \xi} + \rho\chi_\xi \mathrm{Le}_\xi \frac{C_p}{\lambda}\frac{\partial}{\partial \xi}\left(\frac{\lambda}{C_p \mathrm{Le}_\xi}\right)\right)\right]\frac{\partial Y_K}{\partial \xi} \\
& + \left[\frac{\mathrm{Le}_\xi}{\mathrm{Le}_k}\left(\frac{\partial}{\partial \xi}\left(\rho\chi_\xi \frac{Y_k}{\overline{\overline{M}}}\right) + \rho\chi_\xi \mathrm{Le}_\xi \frac{C_p}{\lambda}\frac{\partial}{\partial \xi}\left(\frac{\lambda}{C_p \mathrm{Le}_\xi}\frac{\mathrm{Y_k}}{\overline{\overline{\mathrm{M}}}}\right)\right)\right]\frac{\partial \overline{M}}{\partial \xi} \\
& + \frac{1}{4}\left[2\rho\chi_\xi \frac{Y_k}{\overline{\overline{M}}}\frac{\partial}{\partial \xi}\left(\frac{\mathrm{Le}_\xi}{\mathrm{Le}_k}\right)\right]\frac{\partial \overline{M}}{\partial \xi} + \frac{1}{4}\left[2\rho\chi_\xi \frac{\partial}{\partial \xi}\left(\frac{\mathrm{Le}_\xi}{\mathrm{Le}_k}\right)\right]\frac{\partial Y_K}{\partial \xi},
\end{aligned} \tag{2.46}$$

where the Lewis number of species k, $\mathrm{Le_k}$ is defined as

$$\mathrm{Le}_k = \frac{\lambda}{D_k \rho C_p}, \tag{2.47}$$

where λ is the thermal conductivity of the mixture, D_k the diffusion coefficient of species k and C_p is the specific heat capacity of the mixture at constant pressure.

Compared with Eq. (2.43), Eq. (2.46) contains additional terms taking into account the spatial changes in the mean molecular weight, $\overline{M}$. Under the assumption of unity Lewis number for the mixture fraction, a constant but not unity Lewis number for chemical species and constant molecular weight of the mixture, Eq. (2.46) can be rewritten as [47]

$$\rho\frac{\partial Y_k}{\partial \tau} - \frac{\rho\chi_\xi}{2\mathrm{Le}_k}\frac{\partial^2 Y_k}{\partial \xi^2} - \dot{\omega}_k + \frac{1}{4}\left(1 - \frac{1}{\mathrm{Le}_k}\right)\frac{\partial(\rho\chi_\xi)}{\partial \xi}\frac{\partial Y_k}{\partial \xi} = 0. \tag{2.48}$$

Here, the only difference in comparison with the original formulation of Peters is the convection term describing the flux of species k in the mixture fraction space. It has been shown for laminar counterflow gas flames, that although the extra terms contained in Eq. (2.48) are not always dominant, they can be important under some situations [47]. It is important to note that Eq. (2.43) can be recovered from Eq. (2.48) if the Lewis number of all chemical species is taken to be unity.

In order to solve Eq. (2.43) or Eq. (2.48), the profile of the scalar dissipation rate as a function of the mixture fraction is required. In general two different approaches exist for this. In the steady flamelet models, an analytical expression for $\chi_\xi(\xi)$ is derived under some assumptions and used then to close the system of equations, which is solved neglecting unsteady effects. These simplifications allow for solving the flamelet equations and tabulating the results in a step anterior to the simulation of the turbulent flame. In the unsteady approach on the other hand, unsteady terms are retained and the scalar dissipation rate profile is directly obtained from the computation of a turbulent flame. In this approach, the flamelet equations are solved in-situ and interactively in parallel with the turbulent flame computations. A more detailed explanation of both approaches is given below.

In the steady flamelet model, the steady form of Eq. (2.43) is solved for the generation of the required flamelet structures. The boundary conditions are fixed excepting the strain rate, which is constantly increased until extinction is reached [40]. This procedure requires an a-priori knowledge of χ_ξ as a function of ξ. For gas flames, an analytical expression can be obtained by assuming that flamelets in turbulent diffusion flames behave in the same way as a one-dimensional laminar mixing layer [40]. The scalar dissipation rate in the counterflow configuration as a function of the mixture fraction can then be estimated as [40]

$$\chi_\xi(\xi) = 4a_s\xi^2\left[\mathrm{erfc}^{-1}(2\xi)\right]^2, \tag{2.49}$$

where a_s is the stagnation-plane strain rate and erfc^{-1} is the inverse of the complementary error function. In this formulation, the only parameter that is varied for the generation of the different flamelet structures is a_s. Note that for $a_s = 0$, $\chi_\xi = 0$ in the entire domain, which corresponds to the equilibrium limit, i.e. no diffusion takes

place since the chemistry is infinitely fast compared with the characteristic diffusion time, t_d. By increasing the value of the parameter a_s, different structures are obtained till the quenching scalar dissipation rate, $\chi_{\xi,q}$, is reached. At this point, the flame is extinguished and a cold solution is obtained [40].

The flamelet structures generated by means of Eq. (2.43) are tabulated as a function of ξ and χ_ξ, and they are later included in the simulation of turbulent flames by means of Eq. (2.39), which requires an appropriate joint PDF of these characteristic parameters, $\tilde{P}(\xi, \chi_\xi)$. Under the assumption of statistical independence, this PDF can be decomposed into a product of two single variables PDFs as (see Eq. (2.40))

$$\tilde{P}(\xi, \chi_\xi) = \tilde{P}(\xi)\tilde{P}(\chi_\xi). \tag{2.50}$$

The mixture fraction is commonly assumed to follow a β distribution [96] of the form

$$\tilde{P}(\xi) = \frac{\Gamma(a+b)}{\Gamma(a)\Gamma(b)}\xi^{a-1}\left(1-\xi\right)^{b-1}, \tag{2.51}$$

where Γ corresponds to the gamma function and the parameters a and b are determined as [96]

$$a = \tilde{\xi}\left[\frac{\tilde{\xi}(1-\tilde{\xi})}{\widetilde{\xi''^2}} - 1\right], \tag{2.52}$$

and [96]

$$b = (1-\tilde{\xi})\left[\frac{\tilde{\xi}(1-\tilde{\xi})}{\widetilde{\xi''^2}} - 1\right], \tag{2.53}$$

respectively, where the mean value of the mixture fraction, $\tilde{\xi}$, and its fluctuations, $\widetilde{\xi''^2}$ are obtained by means of appropriate transport equations [39, 68, 74].

The scalar dissipation rate of the mixture fraction is commonly assumed to follow a log-normal distribution of the form [40]

$$\tilde{P}(\chi) = \frac{1}{\sigma\chi\sqrt{2\pi}}\exp\left[-\frac{1}{2\sigma^2}\left(\ln\chi - \mu\right)^2\right], \tag{2.54}$$

where the parameters μ and σ are related to the first and second moment of χ. In principle, two-equation models of turbulence provide the mean value of the scalar dissipation rate, either by algebraically relating it to the scalar fluctuations and the turbulent time scale, or by means of a derived transport equation for $\tilde{\chi}$, which requires closure modeling [89, 90, 91, 92, 93, 94, 95].

In terms of the $\tilde{k}$-$\tilde{\epsilon}$ turbulence model, for example, $\tilde{\chi}$ is commonly expressed as [97]

$$\tilde{\chi} = c_\chi \tilde{\epsilon}/\tilde{k}\widetilde{\xi''^2}, \tag{2.55}$$

where c_χ is a model constant, $\tilde{\epsilon}$ is the mean dissipation rate of turbulent kinetic energy and $\tilde{k}$ is the mean turbulent kinetic energy. A transport equation of the scalar

dissipation rate of the mixture fraction in non-premixed gas flames has been proposed by Cha et al. [93]. In the derivation of this equation, however, a constant diffusion coefficient and a constant density were considered, which is generally not valid in turbulent reacting flows. Additionally, Fick's diffusion law is employed. The validity of these assumptions has not yet been tested. Cha et al. [93] have focused on the use of the derived equation in a doubly-conditional moment closure approach. In this context, it becomes difficult to evaluate the accuracy of the equation and the validity of the assumptions involved in its derivation, since errors are also introduced through other models. Therefore, an evaluation of the equations in a simplified environment is desirable, which is one of the objectives of the present work.

A variation of the non-premixed steady flamelet model of Peters [40] is the Flamelet Progress Variable approach (FPV), which has been proposed by Pierce and Moin [98]. This non-premixed flamelet approach consists in a modification of the parameters employed for the characterization and tabulation of the flamelet structures generated by means of Eq. (2.43). Thus, in the FPV model, a reaction progress variable, C, is employed instead of the scalar dissipation rate of the mixture fraction χ_ξ [98]. It has been reported in the literature, that this small modification leads to major improvements in the prediction of unsteady dynamical effects [98]. The reason why formulations employing χ_ξ do not perform well under these conditions is that the flamelets employed for the tabulations of steady flamelet models are always stable flamelets [98]. In general, multiple solutions exist for certain values of the scalar dissipation rate and any state between the fully burning and the extinguished state in the steady flamelet models will be projected onto one of them [40, 68, 99]. The use of a reaction progress variable instead of the scalar dissipation rate allows the inclusion of more chemical details, which leads to a better performance of the model in unsteady situations [98]. Thus, adopting the FVP flamelet model, the deficiencies of the steady flamelet models can be overcome in a very simple way. Other extensions of the non-premixed flamelet model have been proposed for taking into account heat losses due to radiation [100, 80].

Unsteady flamelet models, on the other hand, are an alternative approach for situations where unsteady effects are expected to be important. In general, unsteady effects are small only in regions where the flame structure is stable and therefore, their negligence leads to inaccurate predictions of phenomena such as local flame extinction, reignition and slow processes such as NO_x formation. Unsteady effects can be included in the simulation of turbulent non-premixed flames employing the so-called unsteady-flamelet model [101]. This approach was proposed by Pitsch et al. [102] and implemented by Pitsch and Steiner [103] in Large Eddy Simulations (LES) of a piloted jet diffusion flame. Here, the transient terms in the flamelet equations are taken into account. This allows to consider the strong decay of the scalar dissipation rate that

takes place downstream in the flow field [101, 102, 103]. Unsteady effects are important when slow physical and chemical processes are to be considered. This is particularly true when characteristic diffusion times of the flow are smaller than the time required by the flow for reaching local steady conditions.

The implementation of the unsteady flamelet model in the simulation of turbulent flames is normally performed in an interactive way. First, the turbulent flame under consideration is simulated employing a steady flamelet library and the results for the flow field are then employed for the calculation of the mean stoichiometric scalar dissipation rate, $\widetilde{\chi_{\xi,st}}$. In order to derive an expression for the determination of $\widetilde{\chi_{\xi,st}}$, it is useful to reconsider the analytical function employed for the calculation of the scalar dissipation rate χ_ξ in steady flamelet models (Eq. (2.49)). Evaluating Eq. (2.49) for the stoichiometric value of the mixture fraction, ξ_{st}, and solving for a_s

$$a_s = \frac{\xi_{st}^2 \left[\mathrm{erfc}^{-1}(2\xi_{st})\right]^2}{4\chi_{\xi,st}}, \tag{2.56}$$

is obtained. Inserting Eq. (2.56) in Eq. (2.49), we obtain

$$\chi_\xi(\xi) = \chi_{\xi,st} \frac{\xi^2 \left[\mathrm{erfc}^{-1}(2\xi)\right]^2}{\xi_{st}^2 \left[\mathrm{erfc}^{-1}(2\xi_{st})\right]^2}. \tag{2.57}$$

Thus, Eq. (2.57) can be expressed as a product of $\chi_{\xi,st}$ and a function of the mixture fraction $\Phi(\xi)$ as [102, 101]

$$\chi_\xi(\xi) = \chi_{\xi,st}\ \Phi(\xi), \tag{2.58}$$

where

$$\Phi(\xi) = \frac{\xi^2 \left[\mathrm{erfc}^{-1}(2\xi)\right]^2}{\xi_{st}^2 \left[\mathrm{erfc}^{-1}(2\xi_{st})\right]^2}. \tag{2.59}$$

Since both $\chi_{\xi,st}$ and $\Phi(\xi)$ are fluctuating quantities, the mean value of $\chi_\xi(\xi)$ can be obtained by averaging over both variables. After assuming statistical independence and reaccommodating terms, the mean value of the scalar dissipation rate can be expressed as [102, 101]

$$\tilde{\chi}_\xi(\xi) = \int_0^1 \Phi(\xi)\ \tilde{P}\,(\xi)\,\mathrm{d}\xi \int_0^\infty \chi_{\xi,st}\ \tilde{P}\,(\chi_{\xi,st})\ \mathrm{d}\chi_{\xi,st}, \tag{2.60}$$

where the second term at the right hand side is the mean scalar dissipation rate at stoichiometric conditions, $\widetilde{\chi_{\xi,st}} = \int_0^\infty \chi_{\xi,st}\ \tilde{P}\,(\chi_{\xi,st})\ \mathrm{d}\chi_{\xi,st}$. It has been suggested to equate the right-hand side of Eq. (2.60) to the algebraic expression commonly employed in turbulent flame for the calculation of $\tilde{\chi}_\xi(\xi)$ in terms of the mean turbulent kinetic energy and the mean dissipation rate of turbulent kinetic energy (Eq. (2.55), which, after solving for the unconditional scalar dissipation rate at stoichiometric conditions, leads [102, 101]

$$\widetilde{\chi_{\xi,st}} = \frac{c_\chi \tilde{\epsilon}/\tilde{k}\widetilde{\xi''^2}}{\int_0^1 \Phi(\xi)\ \tilde{P}\,(\xi)\,\mathrm{d}\xi}. \tag{2.61}$$

This mean stoichiometric scalar dissipation rate is employed to calculate its volume average, which is introduced in Eq.(2.43) for its resolution as a function of mixture fraction and time [101]. The latter is estimated by means of the following expression [101]

$$\tau(z) = \int_0^z \frac{1}{v(z_d, r)} \, \mathrm{d}z_d, \tag{2.62}$$

where r is the radial coordinate, z and v are the axial coordinate and velocity respectively. The unsteady flamelet model has been shown to lead to good predictions for temperature and OH and NO concentrations in the numerical simulation of nitrogen diluted H_2/air jet diffusion flames [101, 103]. However, its application leads to an increase in the computational cost of the simulations.

2.2.2.2 Premixed Gas Flamelet Models

The big success of non-premixed flamelet models in the simulation of turbulent flames motivated the development of equivalent approaches for premixed flames [49, 104]. However, as pointed out before, in premixed flamelet models the use of the mixture fraction as a coordinate to describe the flame structure is not a good choice, since its value remains constant over the entire domain for perfectly premixed flames. The Flamelet Generated Method (FGM) has been proposed as an appropriate flamelet model for premixed flames [105]. In this method, instead of iso-mixture fraction surfaces, curves perpendicular to iso-surfaces of a certain species mass fraction Y_k are considered, which are parameterized by their arc length, s. The evolution of all species mass fractions Y_k can then be described by one-dimensional transport equations in a space characterized by the parameter s as

$$m\frac{\partial Y_k}{\partial s} - \frac{\partial}{\partial s}\left(\frac{\lambda}{\mathrm{Le}_k C_p}\frac{\partial Y_k}{\partial s}\right) = \dot{\omega}_k^+ - \dot{\omega}_k^- + P_k(s,t), \tag{2.63}$$

where m is taken to be a constant mass-flow rate, $\dot{\omega}_k^+$ and $\dot{\omega}_k^-$ are the chemical rate of production and consumption of species k respectively and P_k is a perturbation term. In this equation, effects associated with convection and diffusion phenomena in s direction are accounted by the terms at the left hand side of the equation. Multi-dimensional and unsteady effects, on the other hand, are all contained in the perturbation term $P_k(s,t)$, which includes flame stretch, variations of the mass-flow rate along the curve, and curvature effects [105]. Typically, perturbations are arbitrarily assumed to be small and $P_k(s,t)$ is neglected. In this simplified situation, the premixed flamelet equations are solved treating the system as a freely propagating premixed flame [105]. For this,

the following boundary conditions are imposed [105]

$$s = -\infty : \quad Y_k = Y_{u,k}; \quad h = h_u; \tag{2.64}$$

$$s = \infty : \quad \frac{\partial Y_k}{\partial s} = 0; \quad \frac{\partial h}{\partial s} = 0; \tag{2.65}$$

with $k = 1...N$, and where $Y_{u,k}$ and h_u are prescribed initial conditions. The mass-burning rate m is an eigenvalue of the system.

The final equilibrium state reached by the premixed flamelets is clearly determined by the imposed unburnt conditions, ($Y_{u,k}$, h_u) [105]. The generation of the flamelet structures to be tabulated is performed employing different set of initial conditions, which are selected in such a way that the enthalpy and the element mass fractions are kept constant. This causes all flamelets to end up in the same chemical equilibrium and therefore a single controlling variable is enough for the parametrization of the resulting structures. Commonly, a reaction progress variable, C, is employed, which is defined as a linear combination of some major species such as CO_2 and CO.

In more complex situations, where $P_k(s,t)$ cannot be ignored, the flamelet library has to be extended by including additional control parameters. The exact quantity and the specific control variables required depend on the particular case under investigation. Of course, the computational cost of this approach increases by increasing the number of control parameters and therefore the use of a reduced quantity of them is normally preferred. Perturbations are included by considering different values of the initial enthalpy, which leads to different final equilibrium situations [105].

Other formulations including stretch effects are also available in the literature, where an additional variable representing the flame stretch is considered [86, 106]. In these approaches, premixed counterflow flame structures are employed for the tabulations instead of freely propagating flames. Kolla and Swaminathan [107, 108] proposed the use of a scalar dissipation rate of the progress variable for the characterization of the flame stretch, which is defined as

$$\chi_C = 2D \left(\frac{\partial C}{\partial x_i} \right)^2, \tag{2.66}$$

similarly to the scalar dissipation rate of the mixture fraction defined for non-premixed flamelet models. Although premixed flamelet models have been notoriously improved during the last years, they are typically not considered to be as well developed as non-premixed flamelet models are [107, 108]

Different approaches can be found in the literature for the estimation of the PDF of the progress variable. It has been proposed the use of a β distribution following the approach explained in the previous subsection for the mixture fraction. For this, the mean value of the mixture fraction, $\tilde{\xi}$, and its fluctuations, $\widetilde{\xi''^2}$ are replaced by

corresponding values for the progress variable, $\tilde{C}$ and $\widetilde{C''^2}$ in Eq. (2.51). Thus, considering a β distribution of the progress variable, its probability density function can be expressed as [107, 108]

$$\tilde{P}(C) = \frac{\Gamma(a+b)}{\Gamma(a)\Gamma(b)} C^{a-1} \left(1-C\right)^{b-1}, \tag{2.67}$$

where Γ corresponds to the gamma function and the parameters a and b are determined as

$$a = \widetilde{C} \left[\frac{\tilde{C}(1-\tilde{C})}{\widetilde{C''^2}} - 1 \right], \tag{2.68}$$

and

$$b = (1-\tilde{C}) \left[\frac{\tilde{C}(1-\tilde{C})}{\widetilde{C''^2}} - 1 \right], \tag{2.69}$$

respectively. The mean value of the progress variable, $\tilde{C}$, and its fluctuations, $\widetilde{C''^2}$ are obtained by means of appropriate transport equations. Since the progress variable is not a conserved scalar, an unclosed chemical source term, $\tilde{\dot{\omega}}_C$, appears in its transport equation [107, 108]. This problem is commonly solved including the chemical source term of the progress variable into the laminar flamelet libraries following Eq. (2.38) and averaging them later by means of Eq. (2.39) in the same way as is done for the species mass fractions [107, 108]. An alternative approach for the determination of the PDF of the progress variable consists in the use of a Dirac delta function, δ, with a peak at the mean value, $\tilde{C}$.

The scalar dissipation rate of the progress variable is commonly assumed to follow a log-normal distribution of the form [107, 108]

$$\tilde{P}(C) = \frac{1}{\sigma C \sqrt{2\pi}} \exp\left[-\frac{1}{2\sigma^2} \left(\ln C - \mu \right)^2 \right], \tag{2.70}$$

where the parameters μ and σ are related to the first and second moment of χ. During the last decades, transport equations for the scalar dissipation rate of the reaction progress variable or the mixture fraction have been derived for premixed flames [89, 90, 91, 92]. However, as pointed out before, these transport equations involve several assumptions that have not yet been systematically tested [109].

2.2.2.3 Partially Premixed Gas Flamelet Models

As already pointed out, pure combustion regimes are rare in real flames and typically different combustion regime can coexist and interact in practical flames. In cases where gas non-premixed and gas premixed combustion regimes are found coexisting and interacting, the flame is referred as a partially premixed gas flame. In this situation,

single-regime gas flamelet models are not appropriate. Therefore, partially premixed flamelet models have been developed in recent years [45, 65, 46]. These approaches are based on a combination of premixed and non-premixed single-regime gas flamelet models, which are selectively applied depending on the local dominant combustion regime. Thus, partially premixed flamelet gas flamelet models are composed of two main steps

- Determination of the locally dominant combustion regime.
- Local application of the appropriate single-regime flamelet model.

For the determination of the locally dominant combustion regime, the use of a flame index has been proposed [110]. Different flame index have been proposed in the literature. For instance, Yamashita et al. suggested the use of the following expression [110]

$$\alpha = \frac{\nabla Y_F \cdot \nabla Y_O}{|\nabla Y_F \cdot \nabla Y_O|}. \tag{2.71}$$

The index α can take values of -1 or 1 and it is expected to be positive in locally premixed regions and negative in local non-premixed combustion regimes. The validity of this flame index has been tested by Fiorina et al. [44], who showed that Eq. (2.71) fails in certain regimes of counterflow partially premixed flames. Particularly in those where the gradients of fuel and oxidizer are aligned, but combustion remains diffusion-controlled. For overcoming this problem, a new formulation of the flame index has been proposed [44]. Although the modified index performs better in the counterflow flames analyzed by Fiorina et al. [44], it remains unclear whether the proposed index is adequate for realistic three dimensional flames [45]. Additionally, the use of the gradient of fuel concentration limits the range of application of this kind of index, since in real combustion situations fuels are rapidly dissociated and they typically do not reach the combustion zone [45].

An alternative flame index for partially premixed gas flames has been proposed by Knudsen and Pitsch [45, 46], which employs a two-regime flamelet equation to determine the local relative importance of non-premixed and premixed combustion regimes. In this formulation, the mixture fraction is employed for the characterization of non-premixed like effects and a Reaction Progress Parameter (RPP), Λ, is employed for the characterization of premixed like effects. Since any two-regime flamelet equation has to reduce to the classical formulation of Peters [40] in the limit of pure non-premixed combustion, the RPP selected as second coordinate has to be statistically independent of the mixture fraction. For ensuring the fulfillment of this requirement, Knudsen and Pitsch [45] used the indexing method proposed by Ihme et al. [99]. In this method, non-premixed flamelet structures are characterized by an index and the value of the

index is treated as a variable. Knudsen und Pitsch defined the flame index Λ as [45]

$$\Lambda = C(\xi_{st}, T_{\xi_{st}}). \tag{2.72}$$

Since the temperature at the point of stoichiometric mixture, $T_{\xi_{st}}$, is unique within a given non-premixed steady flamelet, Λ is statistically independent of the mixture fraction and it is constant within a non-premixed flamelet. Additionally, since $T_{\xi_{st}}$ constantly decreases when the strain rate at the stagnation plane is increased, the index Λ can characterize non-premixed gas flamelets uniquely. Thus, following Peters [40], the transport equations of chemical species can be transformed from physical space and time t, (x_1, x_2, x_3, t), into a system of coordinates composed of the mixture fraction, the reaction progress parameter, and a transformed time τ, (ξ, Λ, τ), which yields [45]

$$\begin{aligned} \rho\frac{\partial Y_k}{\partial \tau} &= \frac{\rho\chi_\xi}{2}\frac{\partial^2 Y_k}{\partial^2 \xi} + \dot{\omega}_k - \frac{\partial Y_k}{\partial \Lambda}\left(\rho\frac{\partial \Lambda}{\partial t} + \rho u_j\frac{\partial \Lambda}{\partial x_j} - \frac{\partial}{\partial x_j}\left[\rho D\frac{\partial \Lambda}{\partial x_j}\right]\right) \\ &+ \frac{\rho\chi_\Lambda}{2}\frac{\partial^2 Y_k}{\partial \Lambda^2} + \rho\chi_{\xi,\Lambda}\frac{\partial^2 Y_k}{\partial\xi\partial\Lambda}, \end{aligned} \tag{2.73}$$

where the scalar dissipation rate of the reaction progress parameter and the crossed scalar dissipation rate are defined as [45]

$$\chi_\Lambda = 2D\left(\frac{\partial \Lambda}{\partial x_i}\right)^2, \tag{2.74}$$

and

$$\chi_{\xi,\Lambda} = 2D\frac{\partial \xi}{\partial x_i}\frac{\partial \Lambda}{\partial x_i}, \tag{2.75}$$

respectively. Evaluating Eq. (2.73) for the progress variable C, neglecting unsteady effects and assuming $\chi_{\xi,\Lambda} = 0$, the following equation is obtained [45]

$$\underbrace{\frac{\partial C}{\partial \Lambda}\left(\rho u_j\frac{\partial \Lambda}{\partial x_j} - \frac{\partial}{\partial x_j}\left[\rho D\frac{\partial \Lambda}{\partial x_j}\right]\right) - \frac{\rho\chi_\Lambda}{2}\frac{\partial^2 C}{\partial \Lambda^2}}_{\text{Premixed}} - \underbrace{\frac{\rho\chi_\xi}{2}\frac{\partial^2 C}{\partial^2 \xi}}_{\text{Non-premixed}} = \dot{\omega}_C. \tag{2.76}$$

Based on Eq. (2.76), Knudsen and Pitsch [45] defined the flame index Θ as

$$\Theta = \frac{\frac{\partial C}{\partial \Lambda}\left(\rho u_j\frac{\partial \Lambda}{\partial x_j} - \frac{\partial}{\partial x_j}\left[\rho D\frac{\partial \Lambda}{\partial x_j}\right]\right) - \frac{\rho\chi_\Lambda}{2}\frac{\partial^2 C}{\partial \Lambda^2}}{-\frac{\rho\chi_\xi}{2}\frac{\partial^2 C}{\partial^2 \xi}}, \tag{2.77}$$

which is a comparison of the budget of the terms associated with each combustion regime that balance the chemical source. Unfortunately, the implementation of Eq. (2.77) in the computation of turbulent flames is a very challenging task [45, 46]. Major difficulties are related to the fact that no transport equation is available for Λ and to the evaluation of gradients of Λ in physical space and gradients of the C in the Λ

coordinate [45, 46]. Additionally, the definition of Λ employed in the work of Knudsen and Pitsch [45] is only valid for gas flames and it remains not clear how it could be extended to spray flames [109]. An analysis of limitations and capabilities of multi-regime flamelet models for gas flames has been given by Knudsen and Pitsch [46].

A different set of two-regime flamelet equations has been proposed by Nguyen et al. [65], who derived a set of two-dimensional flamelet equations for the description of partially premixed gas flames, where non-premixed and premixed combustion regimes coexist. This equation is very similar to Eq. (2.76) in many respects. The formulation employs the mixture fraction for the characterization of non-premixed effects and a reaction progress variable, defined as a linear combination of mass fraction of major products including CO_2, H_2O and CO, for the characterization of premixed effects [65]. Unfortunately, the use of this definition of progress variable requires to neglect its statistical dependence on mixture fraction in order to obtain the classical non-premixed gas flamelet equations [40] when pure non-premixed gas flames are considered. Several attempts have been made in order to define a reaction progress variable independent of mixture fraction [111, 112, 99], but, in general, this is not an easy task. Several other sets of flamelet equations in two coordinates have been proposed. A flamelet formulation employing two mixture fractions has been proposed by Hasse et al. [51], which has been extended for the simulation of direct-injection Diesel engines in the context of the so called representative interactive flamelet (RIF) model [52]. Domingo et al. [113] proposed a two-dimensional flamelet equation using the mixture fraction and a measure of the progress of reaction to relate contributions of self-ignition and flame propagation in a vitiated-air lifted flame. Pitsch et al. have derived a set of two-dimensional equations employing the mixture fraction and the scalar dissipation rate at stoichiometric conditions for the characterization of local extinction and reignition phenomena [94].

2.2.3 Spray Flamelet Model

Single-regime gas flamelet models are not adequate for the simulation of turbulent spray flames, since spray flame structures are strongly affected by evaporation effects [54, 56, 59, 42, 57, 55, 58, 60]. The influence of evaporation cannot be captured by gas flamelet structures and therefore spray flamelet structures have to be considered [42, 60]. Hollmann and Gutheil [42] and Gutheil [59] have extended the classical non-premixed gas flamelet model to spray flames, where non-premixed and evaporation-controlled combustion take place simultaneously. This formulation consistently employs a spray flamelet library based on laminar counterflow spray flame structures. However, it is found that the structure of spray flamelets is not only determined by the mixture fraction, ξ, and its scalar dissipation rate (associated with the strain rate), χ_ξ, as in

counterflowing laminar gas diffusion flames [40], but they also depend on the initial droplet size, r_0, the initial droplet velocity, v_0, and the equivalence ratio on the spray side of the configuration, E [81, 82, 59, 42], which is defined as the ratio of the total mass of liquid fuel injected at the left side of the configuration and the fuel mass required for stoichiometric combustion at the specific conditions under consideration. The inclusion of these additional parameters is required in order to characterize laminar spray flamelets. In the spray flamelet model proposed by Hollmann and Gutheil [42], the laminar spray flame structure is computed in physical space [42], and the mass fractions of relevant species are then transformed into mixture fraction space for their inclusion in the turbulent spray code [66, 67]. This procedure is also followed recently by Franzelli et al. [43], although considering gas flamelet structures. The laminar flamelet structures are finally included in the simulations of turbulent flames by means of a joint PDF of the characteristic parameters as [42]

$$\tilde{\phi} = \int_0^\infty \int_0^\infty \int_0^\infty \int_0^\infty \int_0^1 \phi \; \tilde{P}\left(\xi, \chi, E, R_0, v_0\right) \; \mathrm{d}\xi \; \mathrm{d}\chi \; \mathrm{d}E \; \mathrm{d}R_0 \; \mathrm{d}v_0. \tag{2.78}$$

This approach has been successfully applied to the numerical simulation of turbulent methanol/air [42, 66] and ethanol/air [67] spray flames. However, this model includes a high-dimensional flamelet library of the order five for the mixture fraction, its scalar dissipation rate, the equivalence ratio, and the initial droplet size and velocity.

Statistical independence of the parameters is assumed and a dirac delta function is adopted for the initial droplet radius, initial droplet velocity and the equivalence ratio [42]. For the mixture fraction, it has been shown that the use of a two-parameter beta distribution, normally employed in non-premixed gas flames, is not appropriate [114, 115] and the following modified β distribution employing four parameters has been proposed as a better approximation [114]

$$\tilde{P}(\xi) = \frac{\Gamma(a+b)}{\Gamma(a)\Gamma(b)} \left(\xi_{\max} - \xi_{\min}\right)^{1-a-b} \left(\xi - \xi_{\min}\right)^{a-1} \left(\xi_{\max} - \xi\right)^{b-1}, \tag{2.79}$$

where the shape parameters are calculated as

$$a = \frac{\left(\tilde{\xi} - \xi_{\min}\right)}{\left(\xi_{\max} - \xi_{\min}\right)} \left[\frac{\left(\tilde{\xi} - \xi_{\min}\right)\left(\xi_{\max} - \tilde{\xi}\right)}{\widetilde{\xi''^2}} - 1 \right], \tag{2.80}$$

and

$$b = \frac{\left(\xi_{\max} - \tilde{\xi}\right)}{\left(\xi_{\max} - \xi_{\min}\right)} \left[\frac{\left(\tilde{\xi} - \xi_{\min}\right)\left(\xi_{\max} - \tilde{\xi}\right)}{\widetilde{\xi''^2}} - 1 \right], \tag{2.81}$$

respectively. For the determination of the values of $\xi_{\max}$ and $\xi_{\min}$ it has been proposed to assume that the PDF lies in a symmetric domain around the mean value of the

mixture fraction of $2n$ times the standard deviation as

$$\xi_{\min} = \tilde{\xi} - n\sqrt[2]{\widetilde{\xi''^2}}, \tag{2.82}$$

and

$$\xi_{\max} = \tilde{\xi} + n\sqrt[2]{\widetilde{\xi''^2}}, \tag{2.83}$$

where $n \in \mathbb{Z}^+$. However, this assumption would mean that $a = b$, which would lead to an always symmetric probability density function. Luo et al. [115] proposed to adopt $\xi_{\min} = 0$ and $\xi_{\max} = \tilde{\xi} + 2\sqrt[2]{\widetilde{\xi''^2}}$, which can be generalized as

$$\xi_{\min} = 0, \tag{2.84}$$

and

$$\xi_{\max} = \tilde{\xi} + n\sqrt[2]{\widetilde{\xi''^2}}. \tag{2.85}$$

In the next chapter, the mathematical model and the numerical solution scheme employed in the present dissertation are presented.

3. Mathematical Model and Numerical Solution Scheme

In this chapter, the mathematical model and the numerical scheme used for its solution are presented. The general governing equations for the gas and liquid phase are summarized in subsections 3.1.1 and 3.1.2, respectively, where a Eulerian-Lagrangian approach is considered to describe the spray flow. For the numerical simulations, the variables are non-dimensionalized, and the two-dimensional gas phase equations are then transformed into one-dimensional equations through a similarity transformation [81, 82, 59]. This transformation is presented in subsection 3.1.3.

In section 3.2, a multi-regime spray flamelet model to describe all combustion regimes found in spray flames is derived. The derivation consist of two parts. First, transport equations of mixture fraction and its scalar dissipation rate are derived in subsection 3.2.1, which are then transformed by means of the similarity transformation presented in subsection 3.1.3 for their posterior solution. Additionally, a set of multi-regime spray flamelet equations is derived in subsection 3.2.2.

Finally, the discretization scheme used in this work, as well as the solution algorithm employed are presented in section 3.3

3.1 Governing Equations

3.1.1 Gas Phase

The conservation equations of mass, momentum, mass fractions of chemical species, and energy are written as

$$\frac{\partial \rho}{\partial t} + \frac{\partial (\rho u_i)}{\partial x_i} = S_v \tag{3.1}$$

$$\rho \frac{\partial u_j}{\partial t} + \rho u_i \frac{\partial u_j}{\partial x_i} = -\frac{\partial p}{\partial x_j} - \frac{\partial \tau_{ij}}{\partial x_i} - u_j S_v + S_{m,j} \tag{3.2}$$

$$\rho \frac{\partial Y_k}{\partial t} + \rho u_i \frac{\partial Y_k}{\partial x_i} = \frac{\partial V_{k,i}}{\partial x_i} + \dot{\omega}_k + (\delta_{Fk} - Y_k) S_v \tag{3.3}$$

$$\rho C_p \frac{\partial T}{\partial t} + \rho u_i C_p \frac{\partial T}{\partial x_i} = -\sum_{k=1}^{N} h_k \dot{\omega}_k + \frac{\partial p}{\partial t} + u_i \frac{\partial p}{\partial x_i} - \tau_{ij} \frac{\partial u_i}{\partial x_j} + \frac{\partial}{\partial x_i}\left(\lambda \frac{\partial T}{\partial x_i}\right) - \frac{\partial T}{\partial x_i} \sum_{k=1}^{N} C_{p,k} V_{k,i} - S_v \int_{T_0}^{T} C_{p,F} \mathrm{d}T + S_e, \tag{3.4}$$

where the Einstein summation convention is used. In the above equations, ρ is the gas density, u_i is the gas velocity in i direction, Y_k denotes the mass fraction of species k and p is the static pressure. S_v, $\mathbf{S}_m$, S_e are sources of mass, momentum and energy, respectively, accounting for the exchange between the gas and liquid phases. δ is the Kronecker symbol and the subscript F denotes fuel. The viscous tensor τ_{ij} is defined by

$$\tau_{ij} = -\mu \left(\frac{\partial u_i}{\partial x_j} + \frac{\partial u_j}{\partial x_i}\right) + \frac{2}{3}\mu \frac{\partial u_k}{\partial x_k}\delta_{ij} \tag{3.5}$$

neglecting the bulk viscosity. μ, λ and C_p denote the viscosity, heat conductivity and heat capacity at constant pressure of the mixture and are calculated as

$$\mu = \frac{1}{2}\left[\sum_{k=1}^{N} X_k \mu_k + \frac{1}{\sum_{k=1}^{N} \frac{X_k}{\mu_k}}\right], \tag{3.6}$$

$$\lambda = \frac{1}{2}\left[\sum_{k=1}^{N} X_k \lambda_k + \frac{1}{\sum_{k=1}^{N} \frac{X_k}{\lambda_k}}\right], \tag{3.7}$$

and

$$C_p = \sum_{k=1}^{N} C_{p,k} Y_k, \tag{3.8}$$

respectively. Here, N is the total number of chemical species in the system. In Eqs. (3.6) and (3.7), X_k is the molar fraction of species k. The corresponding values of viscosity and heat conductivity of the individual species k, μ_k, λ_k are determined by means of temperature dependent polynomia as [116]

$$\ln(\mu_k) = \sum_{n=1}^{4} a_{\mu,k,n} \left(\ln\left(T\right)\right)^{n-1} \tag{3.9}$$

and

$$\ln(\lambda_k) = \sum_{n=1}^{4} a_{\lambda,k,n} \left(\ln\left(T\right)\right)^{n-1}, \tag{3.10}$$

respectively, where the coefficients $a_{\mu,k,n}$ and $a_{\lambda,k,n}$ are given in tabulated form [116]. Similarly, the heat capacity at constant pressure of species k at constant pressure, $C_{p,k}$, and the enthalpy of species k, h_k, are determined by means of the NASA polynomial tabulations [117] as

$$C_{p,k} = R \sum_{n=1}^{5} a_{C_p,k,n} T^{n-1}, \tag{3.11}$$

and

$$\frac{h_k}{RT} = \sum_{n=1}^{5} a_{h_k,n} T^{n-1} + \frac{a_{h_k,6}}{T}, \tag{3.12}$$

where the coefficients $a_{C_p,k,n}$ and $a_{h_k,n}$ can be obtained of available databases [117]. In Eqs. (3.11) and (3.12), different coefficients are employed for two different ranges of temperatures, namely 300 to 1000 K and 1000 to 4000 K.

In Eq. (3.4), $V_{i,k}$ is the diffusion velocity of species k in i-direction, which is approximated by the Hirschfelder-Curtiss diffusion law as [74, 39]

$$V_{i,k} = -\rho D_k \frac{Y_k}{X_k} \frac{\partial X_k}{\partial x_i} - \frac{D_T}{T} \frac{\partial T}{\partial x_i}, \tag{3.13}$$

where D_T is the thermal diffusion coefficient, which is considered for the light species H and H_2 and D_k is the diffusion coefficient of species k in the mixture and it is calculated as

$$D_k = \frac{1 - Y_k}{\sum_{j \neq k}^{N} \frac{X_k}{D_{kj}}}, \tag{3.14}$$

where the specific diffusion coefficients of species k in species i are also obtained from the polynomial of Kee et al. [116] as

$$\ln(D_{kj}) = \sum_{n=1}^{4} a_{D,k,n} \left(\ln\left(T\right)\right)^{n-1}. \tag{3.15}$$

By using the product law, Eq. (3.13) can be rewritten as

$$V_{k,i} = -\frac{\partial}{\partial x_i}\left(\rho D_k \frac{\partial Y_k}{\partial x_i}\right) - \frac{\partial}{\partial x_i}\left(\rho \frac{D_k Y_k}{\overline{M}} \frac{\partial \overline{M}}{\partial x_i}\right) - \frac{D_T}{T} \frac{\partial T}{\partial x_i}, \tag{3.16}$$

where $\overline{M}$ is the mean molecular weight of the mixture. If the contribution of the last two terms on the right hand side are neglected, Eq. (3.16) reduces to Fick's diffusion law

$$V_{k,i} = -\frac{\partial}{\partial x_i}\left(\rho D_k \frac{\partial Y_k}{\partial x_i}\right). \tag{3.17}$$

A detailed chemical reaction mechanism consisting of N species and M reactions of the form

$$\sum_{k=1}^{N} \nu'_{kj} A_k = \sum_{k=1}^{N} \nu''_{kj} A_k, \tag{3.18}$$

with $j = 1...M$, is considered here. In Eq. (3.18), A_k represents the symbol for species k and ν'_{kj} and ν''_{kj} are the molar stoichiometric coefficients of species k in reaction j, respectively. Based on this reaction mechanism, the specific chemical reaction rate of species k appearing in Eq. (3.3), $\dot{\omega}_k$, is calculated as [74, 39]

$$\dot{\omega}_k = \sum_{j=1}^{M} \dot{\omega}_{k,j}, \tag{3.19}$$

where $\dot{\omega}_{k,j}$ represents the individual contributions made by each reaction j to the net reaction rate of species k. The values of $\dot{\omega}_{k,j}$ can be calculated as [74, 39]

$$\dot{\omega}_{k,j} = M_k \nu_{k,j} K_j \prod_{n=1}^{N} C_k^{\nu'_{kj}}, \tag{3.20}$$

where M_k and C_k are the molecular weight and the concentration of species k, respectively, $\nu_{k,j} = \nu''_{k,j} - \nu'_{k,j}$, and the rate of reaction j, K_j, is given by

$$K_j = A_j T^{\beta_j} \exp\left(-\frac{E_j}{RT}\right), \tag{3.21}$$

where E_j is the activation energy and A_j and β_j are constants. In the present work, a detailed chemical reaction mechanism consisting of 38 species and 337 reactions is employed [118].

The formulation of the spray flamelet equations requires the definition of the mixture fraction. In general, the definition of the mixture fraction based on a chemical element, A, yields

$$\xi_{\mathrm{A}} = \frac{Z_{\mathrm{A}} - Z_{\mathrm{A,min}}}{Z_{\mathrm{A,max}} - Z_{\mathrm{A,min}}}, \tag{3.22}$$

where Z_{A} is the mass fraction of element A, which can be expressed as

$$Z_{\mathrm{A}} = \sum_{k=1}^{N} \left(\frac{a_{k\mathrm{A}} M_{\mathrm{A}}}{M_k}\right) Y_k, \tag{3.23}$$

where $a_{k\mathrm{A}}$ denotes the number of moles of element A in species k, and M_{A} denotes the molecular weight of element A. In combustion processes including hydrocarbons or alcohols, most often the mixture fraction definition is based on the chemical element C, because this formulation fulfills the requirements of monotonicity and boundedness of the mixture fraction between zero and unity [119]. In the remainder of the present thesis, the mixture fraction is based in carbon and simply noted as ξ.

In the next subsection, the governing equations for the liquid phase are presented.

3.1.2 Liquid Phase

The spray is assumed to be dilute and consisting of spherically symmetric droplets, and a Lagrangian approach is used to describe droplet evaporation, heating, and motion. Even though the present study concerns the injection of mono-disperse sprays, the occurrence of droplet reversal and droplet oscillation may lead to local poly-dispersity [82, 83, 59]. The droplet motion of a droplet size group, k, can be expressed as

$$m_k \frac{\mathrm{d}\mathbf{v}_k}{\mathrm{d}t} = \pi R_k^2 \frac{1}{2} \rho_l \left(\mathbf{u} - \mathbf{v}_k\right) \mid \mathbf{u} - \mathbf{v}_k \mid C_{D,k} + m_k \mathbf{g}, \tag{3.24}$$

where $k = 1, \ldots, K$, and K denotes the total number of different groups of droplets. $C_{D,k}$ is the drag coefficient, $\mathbf{v_k}$ and $\mathbf{u}$ denote the droplet and gas velocity, respectively, R_k is the instantaneous droplet radius, and $m_k = \frac{4}{3}\pi R_k^3 \rho_l$ denotes the mass of a droplet with radius R_k, and ρ_l denotes the liquid density. Droplet evaporation is described by Abramzon and Sirignano's convective droplet evaporation model [120]

$$\dot{m}_k = \frac{\mathrm{d}m_k}{\mathrm{d}t} = 2\pi R_k \rho_{f,k} D_{f,k} \widetilde{\mathrm{Sh}}_k \ln(1 + B_{M,k}), \tag{3.25}$$

where $\dot{m}_k$ is the droplet mass vaporization rate of a droplet in size group k, and the subscript f refers to properties in the film around the droplets. Film properties are computed using the 1/3 rule [121]. The modified Sherwood number $\widetilde{\mathrm{Sh}}_k$ accounts for convective droplet evaporation [120]. The Spalding transfer number, $B_{M,k}$ for each droplet size group, k, is $B_{M,k} = (Y_{F\mathrm{s},k} - Y_F)/(1 - Y_{F\mathrm{s},k})$, where Y_F is the mass fraction of the fuel vapor in the bulk of gas surrounding the droplet. $Y_{Fs,k}$ denotes the fuel mass fraction at the droplet surface, which is given by

$$Y_{Fs,k} = \frac{M_F X_{F\mathrm{s},k}}{M_F X_{F\mathrm{s},k} + (1 - X_{F\mathrm{s},k})\overline{M}_\mathrm{s}}. \tag{3.26}$$

$\overline{M}_\mathrm{s}$ is the mean molecular weight of the gas surrounding the droplet surface, and the fuel mole fraction at the surface of the droplets $X_{F\mathrm{s},k}$ is

$$X_{Fs,k} = p_v/p, \tag{3.27}$$

where p_v is the vapor pressure at the droplet surface which is calculated employing the Clausius-Clapeyron equation [122]

$$p_v = p_0 \exp\left(-\frac{C_1}{T_s} + C_2\right), \tag{3.28}$$

where $C_1 = 4827.53$ K and $C_2 = 13.553$ are used for ethanol [122], and p_0 is the atmospheric pressure. Droplet heating is described through the conduction limit model

$$\frac{\partial T_{l,k}}{\partial t} = \alpha_l \frac{1}{r^2}\frac{\partial}{\partial r}\left(r^2 \frac{\partial T_{l,k}}{\partial r}\right). \tag{3.29}$$

Here, $T_{l,k}$ is the temperature of the liquid, and r denotes the radial coordinate of the droplet. Since the spray is assumed to be dilute, droplet–droplet interaction is neglected and the equation for the droplet number density, n_k, of each droplet size group, k yields

$$\frac{\partial n_k}{\partial t} + \frac{\partial\left(n_k\, v_{i,k}\right)}{\partial x_i} = S_{n,k}, \tag{3.30}$$

where, $v_{i,k}$ denotes the droplet velocity of size group k in i-direction. $S_{n,k}$ is a source term to describe the change in droplet number density if a droplet reverses or oscillates.

In this situation, droplets are transferred from one droplet size group into a different one at the same position leading to local poly-dispersity of the spray [82]. This is done in order to avoid that new information overwrites previously calculated data. Thus, the spray source terms for mass, momentum and energy in every grid point, cf. Eqs. (3.1)-(3.4), yield

$$S_v = \sum_{k=1}^{K} n_k \dot{m}_k, \tag{3.31}$$

$$\mathbf{S}_m = \sum_{k=1}^{K} \left[-n_k m_k \frac{\mathrm{d}\mathbf{v}_k}{\mathrm{d}t} + n_k \dot{m}_k \mathbf{v}_k \right], \tag{3.32}$$

and

$$S_e = \sum_{k=1}^{K} \left[-n_k \left[\dot{q}_k + \dot{m}_k L_V(T_{l,k}) \right] + n_k \dot{m}_k \int_{T_0}^{T_{\mathrm{s},k}} C_{p,F} \mathrm{d}T \right], \tag{3.33}$$

where $\dot{q}_k = \dot{m}_k \left[C_{p,F}(T - T_{\mathrm{s},k})/B_{T,k} - L_V(T_{l,k}) \right]$ is the energy transferred to the droplet. $B_{T,k}$ denotes the Spalding heat transfer number, and $L_V(T)$ is the temperature dependent latent heat of vaporization.

3.1.3 Transformed Equations

The conservation equations for mass, momentum, energy, and mass fractions of chemical species are simplified by the adopting the boundary layer assumption and by considering a low Mach number, M (defined as the ratio of the local gas velocity and the sound speed). Additionally, the gas phase equations, as well as the liquid equations for droplet heating, vaporization and motion are non-dimensionalized using appropriate reference values [81, 82]. Then, the following similarity transformation is used for the two-dimensional gas equations [82]:

$$\eta = \int_0^y \rho \, dy \qquad \text{and} \qquad f = \int_0^\eta \frac{u}{x} \, d\eta. \tag{3.34}$$

Here, x and y are radial and axial physical coordinates, respectively, and u and v are the corresponding gas velocities. Using Eq. (3.34), the following set of transformed equations is obtained where the boundary layer approximation is applied [82]:

$$v = -1/\rho \, ([\alpha + 1]f + f_v) \qquad \text{with} \qquad f_v = -\int_0^\eta 1/\rho \; S_v \; d\eta \tag{3.35}$$

$$\frac{d}{d\eta}\left(\rho\mu \frac{df'}{d\eta} \right) + ([\alpha + 1]f + f_v) \, f'' = (f')^2 - \frac{1}{\rho} - \frac{S_m}{\rho x} \tag{3.36}$$

$$\frac{d}{d\eta}\left(\lambda\rho \frac{d\theta}{d\eta} \right) + c_P([\alpha + 1]f + f_v)\frac{d\theta}{d\eta} = \rho \sum_{k=1}^{K} V_{k\eta} C_{p_k} \frac{d\theta}{d\eta} + \frac{1}{\rho} \sum_{k=1}^{K} h_k \dot{w}_k - \frac{1}{\rho} S_e \tag{3.37}$$

$$-\frac{d}{d\eta}(\rho V_{k\eta}) + ([\alpha+1]f + f_v)\frac{dY_k}{d\eta} = -\frac{1}{\rho}\dot{w}_k - (\delta_{Fk} - Y_k)\frac{1}{\rho}S_v, \tag{3.38}$$

where θ is the non-dimensional temperature. In the above equations α equals zero for the planar counterflow configuration and unity for the present axisymmetric counterflow configuration.

This set of equations for the gas phase is completed by the liquid phase equations and the chemical reaction rates $\dot{w}_k$ for species k.

The liquid phase equations are transformed using

$$\zeta = r/R(t); \qquad \zeta_s = R(t)/R_0; \qquad \tau = \frac{1}{t_l^\star}\int_0^t \frac{dz}{\zeta_s}; \tag{3.39}$$

where z is a dummy variable and * denotes reference values [81]. R_0 is the initial droplet radius, T_l and M_l are liquid temperature and liquid mass, respectively.

The transformed equations are written for each droplet size group omitting the indices to identify them for a better transparency of the equations, which yield [82, 59]

$$\frac{d\zeta_s}{d\tau} = -1/9\ c_1\rho_f D_f \widetilde{\mathrm{Sh}}\ \ln(1+B_M) \tag{3.40}$$

$$\frac{\partial\theta_l}{\partial\tau} - \frac{\zeta}{\zeta_s}\frac{d\zeta_s}{d\tau}\frac{\partial\theta_l}{\partial\zeta} = \frac{1}{\zeta_s\zeta^2}\frac{\partial}{\partial\zeta}\left(\zeta^2\frac{\partial\theta_l}{\partial\zeta}\right) \tag{3.41}$$

$$\frac{\partial^2 x_l}{\partial\tau^2} - \frac{1}{\zeta_s}\left(\frac{d\zeta_s}{d\tau} - c_1\mu\right)\frac{dx_l}{d\tau} = c_1c_2\mu\frac{df}{d\eta}x_l + c_2^2\zeta_s^2 g_x \tag{3.42}$$

$$\frac{\partial^2\eta_l}{\partial\tau^2} + \rho\frac{d\rho^{-1}}{d\tau}\frac{d\eta_l}{d\tau} - \frac{1}{\zeta_s}\left(\frac{d\zeta_s}{d\tau} - c_1\mu\right)\frac{d\eta_l}{d\tau} = c_1c_2\mu(-([\alpha+1]f+f_v)) + \rho c_2^2\zeta_s^2 g_\eta. \tag{3.43}$$

In the above equations, $c_1 = 6\pi(M^\star/M_l^\star)(L_l^\star/L^\star)(t_l^\star/t^\star)$ and $c_2 = t_l^\star/t^\star$.

Mass and energy transfer numbers B_M and B_T, respectively, as well as the modified Sherwood number $\widetilde{\mathrm{Sh}}$ are formulated as derived by Abramzon and Sirignano [120]. This formulation includes non-equal mass and energy transfer numbers as well as a Reynolds number correction to account for the slip.

Droplet number density, n, and source terms, S_v, S_m, S_e, of the gas equations are given by

$$n = n_0 s_0 \eta_{l0}'\rho\,/\,(s\eta_l'\rho_0); \qquad \text{with} \quad s = x_l/u_{l0} \tag{3.44}$$

$$\frac{S_v}{\rho} = -\frac{M_l^\star}{M^\star}\ \frac{t^\star}{t_l^\star}\ \frac{n}{\rho}\ 3\ \zeta_s\ \frac{d\zeta_s}{d\tau} \tag{3.45}$$

$$-\frac{S_m}{\rho x} = \frac{M_l^\star}{M^\star}\ \left(\frac{t^\star}{t_l^\star}\right)^2\ \frac{n}{\rho s}\ \left[\zeta_s\frac{d^2 s}{d\tau^2} + 2\ \frac{d\zeta_s}{d\tau}\ \frac{ds}{d\tau} - 3\ \frac{t_l^\star}{t^\star}f' s\ \zeta_s\ \frac{d\zeta_s}{d\tau}\right] \tag{3.46}$$

$$-\frac{S_e}{\rho} = \frac{c_{Pf}}{\bar{c_P}}\ \frac{M_l^\star}{M^\star}\ \frac{t^\star}{t_l^\star}\ \frac{n}{\rho}\ \dot{m}\left(\theta - \frac{T_l^\star}{T^\star}\theta_{ls}\right)\frac{1+B_T}{B_T}, \tag{3.47}$$

where summation over the individual droplet size groups is required to include these source terms, cf. Eqs. (3.31), (3.32), and (3.33).

This closed system of strongly coupled equations is solved numerically [81, 82] to obtain structures of laminar spray flames in the counterflow configuration. These structures are later used for performing studies of the influence of evaporation on the flame structure and for the evaluation of the multi-regime spray flamelet model to be derived in the next section.

3.1.4 Boundary Conditions

In this section, the boundary conditions for the governing equations for the gas and liquid phase are specified. In the cartesian coordinate system, the gas governing equations, Eqs. (3.1-3.4), are subject to the boundary conditions

$$y = -\infty : \quad v = v_{-\infty}; \quad Y_k = Y_{k-\infty}; \quad T = T_{-\infty}; \tag{3.48}$$

$$y = +\infty : \quad v = v_{+\infty}; \quad Y_k = Y_{k+\infty}; \quad T = T_{+\infty}, \tag{3.49}$$

where $-\infty$ and ∞ denote spray and gas side of the counterflow configuration, respectively. In the present thesis, the value of the velocity at the left side of the configuration is fixed to 0.44 m/s, the species mass fraction at both streams, Y_k, are fixed to the corresponding values for pure air and a injection temperature of 300 K is considered at both sides of the configuration in all cases under study. Since a counterflow configuration is considered here, the outer flow is a potential flow and the velocity field can be described by

$$v_{-\infty} = a_{-\infty} y \qquad u_{-\infty} = a_{-\infty} x; \tag{3.50}$$

$$v_{+\infty} = a_{+\infty} y \qquad u_{+\infty} = a_{+\infty} x. \tag{3.51}$$

After the non-dimensionalization of the governing equations, and the application of the similarity transformation introduced in subsection 3.1.3, the boundary conditions have to be transformed accordingly. The boundary values of Y_k remain the same, since they are non-dimensional quantities, whereas the boundary values for the stream function, f, and its derivative, f', can be easily derived from the boundary conditions specified by Eq. (3.49), the definition of f (Eq. (3.34)), and the equation for the axial gas velocity in similarity space (Eq. (3.35)). For f', it becomes evident from Eq. (3.34) that

$$f' = \frac{u}{x} = \frac{ax}{a_{-\infty} x} = \frac{a}{a_{-\infty}}. \tag{3.52}$$

Thus, at the left side of the configuration, $f' = 1$. For the determination of the value of f' at the right side of the configuration, the contribution of the incoming droplets to the dynamic pressure is neglected and, after equating the static pressure at the

stagnation plane for the potential field at both sides of the configuration, the following relation is obtained [81]

$$a_{+\infty} = \sqrt{\frac{\rho_{-\infty}}{\rho_{+\infty}}} a_{-\infty}, \tag{3.53}$$

which can be introduced into Eq. (3.52) to obtain the boundary condition for f' at the right side of the counterflow configuration

$$f' = \sqrt{\frac{\rho_{-\infty}}{\rho_{+\infty}}} \frac{a_{-\infty}}{a_{-\infty}} = \sqrt{\frac{\rho_{-\infty}}{\rho_{+\infty}}}, \tag{3.54}$$

Since the gas temperature, T, is normalized by the injection temperature, which is the same at both sides of the configuration, the non-dimensional gas temperature, θ, has a value of unity at both boundaries. Thus, finally, the set of governing equations for the gas phase is subject of the boundary conditions

$$\eta = -\infty : \qquad f = f_{-\infty}; \qquad f' = 1; \qquad Y_k = Y_{k-\infty}; \qquad \theta = 1; \tag{3.55}$$

$$\eta = +\infty : \qquad f = f_{+\infty}; \qquad f' = \sqrt{\frac{\rho_{-\infty}}{\rho_{+\infty}}}; \qquad Y_k = Y_{k+\infty}; \qquad \theta = 1. \tag{3.56}$$

For the liquid phase, the following boundary conditions are considered for the motion (Eq. (3.24))

$$\mathbf{x}_k(0) = \mathbf{x}_{k0}; \qquad \mathbf{v}_k(0) = \mathbf{v}_{k0}, \tag{3.57}$$

and the energy equation (Eq. (3.29))

$$T_l(r,0) = T_{l0}; \qquad \frac{\partial T_l}{\partial r} \mid_{r=0} = 0; \qquad \frac{\partial T_l}{\partial r} \mid_{r=R(t)} = \frac{\dot{q}}{4\pi R^2 \alpha_l \rho_l C_{pl}}, \tag{3.58}$$

respectively. In the present thesis, the droplet initial velocity and temperature are fixed to the values of the corresponding variables in the gas phase. Thus, the initial droplet velocity is 0.44 m/s for all cases and the initial droplet temperature is 300 K. The initial droplet position is the left side of the counterflow configuration. The boundary conditions presented in Eqs. (3.57) and (3.58) also have to be written in the framework of the similarity transformation presented in subsection 3.1.3. After this is made, the boundary conditions for the liquid phase are

$$\eta_l(0) = \eta_{l0}; \qquad \eta_0'(0) = \eta_{l0}', \tag{3.59}$$

and

$$\zeta_s(0) = 1; \qquad \frac{\partial \theta_l}{\partial \zeta} \mid_{\zeta=0} = 0; \qquad \frac{\partial \theta_l}{\partial \zeta} \mid_{\zeta=1} = \frac{\dot{q}}{3\zeta_s}, \tag{3.60}$$

with

$$\dot{q} = \dot{m} \left[\frac{c_{Pf}}{c_{Pl}} \left(\frac{T^\star}{T_l^\star} \theta - \theta_{ls} \right) / B_T - L_v \right]. \tag{3.61}$$

In the next section, a multi-regime spray flamelet model is presented.

3.2 Flamelet Model

In this section, an exact transport equation of the scalar dissipation rate and a set of multi-regime spray flamelet equations are derived (subsections 3.2.1 and 3.2.2, respectively). Moreover, a set of non-premixed spray flamelet equations, which proportionates the fundamentals for the non-premixed spray flamelet model of Hollmann and Gutheil [42, 59] is introduced. The derivations presented in this section have been published in [60, 109, 123]. Additionally, the meaning of the flamelet model presented in this section, as well as the approach to be used for its implementation in the simulation of turbulent spray flames is discussed in subsection 3.2.3.

3.2.1 Transport Equation of the Scalar Dissipation Rate

In this subsection, a transport equation for the scalar dissipation rate of the mixture fraction, χ_ξ, is derived. For this purpose, an exact transport equation for the mixture fraction is needed, which is first derived. Multiplication of the species transport equation (Eq. (3.3)) with $a_{Ck}M_C/M_k$ and summation over $k = 1, \ldots, N$ yields

$$\begin{aligned} \rho\frac{\partial\xi}{\partial t} + \rho u_i\frac{\partial\xi}{\partial x_i} &= \frac{\partial}{\partial x_i}\left(\frac{M_F}{a_{CF}}\rho\sum_{k=1}^{N}\frac{a_{Ck}}{M_k}D_k\frac{\partial Y_k}{\partial x_i}\right) \\ &+ \frac{\partial}{\partial x_i}\left(\frac{\rho M_F}{a_{CF}\overline{M}}\sum_{k=1}^{N}\frac{a_{Ck}}{M_k}D_kY_k\frac{\partial\overline{M}}{\partial x_i}\right) + S_v(1-\xi), \end{aligned} \tag{3.62}$$

where Hirschfelder-Curtiss diffusion (Eq. (3.13)) and the definition of the mixture fraction, Eq. (3.22) have been employed. Equation (3.62) represents an exact transport equation for ξ. Using the assumption of equal molecular diffusion coefficient for all chemical species, $D_k = D$, Eq. (3.62) can be rewritten as

$$\rho\frac{\partial\xi}{\partial t} + \rho u_i\frac{\partial\xi}{\partial x_i} = \frac{\partial}{\partial x_i}\left(\rho D\frac{\partial\xi}{\partial x_i}\right) + \frac{\partial}{\partial x_i}\left(\rho D\frac{\xi}{\overline{M}}\frac{\partial\overline{M}}{\partial x_i}\right) + S_v(1-\xi). \tag{3.63}$$

If Eq. (3.63) is to be equivalent to Eq. (3.62), the first and second terms of the r.h.s. of these equations have to be equal, which leads to an expression for the appropriate diffusion coefficient that ensures the fulfillment of this condition. This coefficient will be referred as the equivalent diffusion coefficient, D_e, which is calculated as

$$D_\mathrm{e} = \frac{M_F\left(\sum_{k=1}^{N}\frac{a_{Ck}}{M_k}D_k\frac{\partial Y_k}{\partial x_i} + \frac{1}{\overline{M}}\sum_{k=1}^{N}\frac{a_{Ck}}{M_k}D_kY_k\frac{\partial\overline{M}}{\partial x_i}\right)}{a_{CF}\left(\frac{\partial\xi}{\partial x_i} + \frac{\xi}{\overline{M}}\frac{\partial\overline{M}}{\partial x_i}\right)}. \tag{3.64}$$

Application of the operator $\frac{\partial\xi}{\partial x_j}\frac{\partial}{\partial x_j}$ to each term in Eq. (3.63) results in

$$\underbrace{\frac{\partial\xi}{\partial x_j}\frac{\partial}{\partial x_j}\left(\rho\frac{\partial\xi}{\partial t}\right)}_{\mathrm{I}}+\underbrace{\frac{\partial\xi}{\partial x_j}\frac{\partial}{\partial x_j}\left(\rho u_i\frac{\partial\xi}{\partial x_i}\right)}_{\mathrm{II}}=\underbrace{\frac{\partial\xi}{\partial x_j}\frac{\partial}{\partial x_j}\left(\frac{\partial}{\partial x_i}\left[\rho D\frac{\partial\xi}{\partial x_i}\right]\right)}_{\mathrm{III}}$$
$$+\underbrace{\frac{\partial\xi}{\partial x_j}\frac{\partial}{\partial x_j}\left(\frac{\partial}{\partial x_i}\left[\rho D\frac{\xi}{\overline{M}}\frac{\partial\overline{M}}{\partial x_i}\right]\right)}_{\mathrm{IV}}+\underbrace{\frac{\partial\xi}{\partial x_j}\frac{\partial}{\partial x_j}\left(S_v(1-\xi)\right)}_{\mathrm{V}}, \tag{3.65}$$

where term V describes the effects of evaporation, and terms I, II, III and IV may be simplified as follows. Term I is rearranged using the product law to yield

$$\mathrm{I}=\frac{\rho}{4D}\frac{\partial\chi_\xi}{\partial t}+\frac{\rho\chi_\xi}{4}\frac{\partial}{\partial t}\left(\frac{1}{D}\right)+\frac{\partial\xi}{\partial t}\left(\frac{\partial\xi}{\partial x_i}\frac{\partial\rho}{\partial x_i}\right). \tag{3.66}$$

Similarly, term II in Eq. (3.65) is rearranged as

$$\mathrm{II}=\frac{\rho u_i}{4D}\frac{\partial\chi_\xi}{\partial x_i}+\frac{\chi_\xi\rho u_i}{4}\frac{\partial}{\partial x_i}\left(\frac{1}{D}\right)+\rho\frac{\partial\xi}{\partial x_i}\frac{\partial\xi}{\partial x_j}\frac{\partial u_j}{\partial x_i}+\frac{\partial\xi}{\partial x_i}\frac{\partial\xi}{\partial x_j}u_i\frac{\partial\rho}{\partial x_j}. \tag{3.67}$$

The third term, III, is expressed as

$$\mathrm{III}=\frac{\rho}{4}\frac{\partial^2\chi_\xi}{\partial x_i^2}+\frac{\rho D}{4}\frac{\partial\chi_\xi}{\partial x_i}\frac{\partial}{\partial x_i}\left(\frac{1}{D}\right)+\frac{\rho D}{4}\frac{\partial}{\partial x_i}\left(\chi_\xi\frac{\partial}{\partial x_i}\left[\frac{1}{D}\right]\right)-\rho D\left(\frac{\partial^2\xi}{\partial x_i\partial x_j}\right)^2$$
$$+\frac{\partial^2\xi}{\partial x_i^2}\frac{\partial\xi}{\partial x_j}\frac{\partial\left(\rho D\right)}{\partial x_j}+\frac{\partial\xi}{\partial x_i}\frac{\partial}{\partial x_i}\left(\frac{\partial\xi}{\partial x_j}\frac{\partial(\rho D)}{\partial x_j}\right), \tag{3.68}$$

and term IV is written as

$$\mathrm{IV}=\frac{\rho}{4\overline{M}}\frac{\partial\overline{M}}{\partial x_i}\frac{\partial\chi_\xi}{\partial x_i}+\frac{\rho D\chi_\xi}{4\overline{M}}\frac{\partial\overline{M}}{\partial x_i}\frac{\partial}{\partial x_i}\left(\frac{1}{D}\right)+\frac{\rho D}{\overline{M}}\frac{\partial\xi}{\partial x_i}\frac{\partial\xi}{\partial x_j}\frac{\partial^2\overline{M}}{\partial x_i\partial x_j}+\frac{\partial\overline{M}}{\partial x_i}\frac{\partial\xi}{\partial x_i}\frac{\partial\xi}{\partial x_j}\frac{\partial}{\partial x_j}\left(\frac{\rho D}{\overline{M}}\right)$$
$$+\frac{\chi_\xi}{2D}\frac{\partial}{\partial x_i}\left(\frac{\rho D}{\overline{M}}\frac{\partial\overline{M}}{\partial x_i}\right)+\xi\frac{\partial\xi}{\partial x_i}\frac{\partial}{\partial x_i}\left[\frac{\partial}{\partial x_j}\left(\frac{\rho D}{\overline{M}}\frac{\partial\overline{M}}{\partial x_j}\right)\right]. \tag{3.69}$$

Insertion of Eqs. (3.66)–(3.69) into Eq. (3.65), after rearranging terms, yields

$$\frac{\partial\chi_\xi}{\partial t}+u_i\frac{\partial\chi_\xi}{\partial x_i}=D\frac{\partial^2\chi_\xi}{\partial x_i^2}+S_{\chi_\xi,g}+S_{\chi_\xi,v}+S_{\chi_\xi,\overline{M}}. \tag{3.70}$$

The terms $S_{\chi_\xi,g}$ and $S_{\chi_\xi,v}$ appearing in Eq. (3.70) account for sources stemming from the gas and the liquid phase, respectively, and the last term, $S_{\chi_\xi,\overline{M}}$ accounts for variations of the mean molecular weight of the gas mixture. They yield

$$S_{\chi_\xi,g}=-4D\frac{\partial\xi}{\partial x_i}\frac{\partial\xi}{\partial x_j}\frac{\partial u_j}{\partial x_i}-4D^2\left(\frac{\partial^2\xi}{\partial x_i\partial x_j}\right)^2-D\chi_\xi u_i\frac{\partial}{\partial x_i}\left(\frac{1}{D}\right)-\frac{4D}{\rho}\frac{\partial\xi}{\partial x_i}\frac{\partial\xi}{\partial x_j}u_i\frac{\partial\rho}{\partial x_j}$$
$$+2D^2\frac{\partial\chi_\xi}{\partial x_i}\frac{\partial}{\partial x_i}\left(\frac{1}{D}\right)+\frac{4D}{\rho}\frac{\partial^2\xi}{\partial x_i^2}\frac{\partial\xi}{\partial x_j}\frac{\partial\left(\rho D\right)}{\partial x_j}+\frac{4D}{\rho}\frac{\partial\xi}{\partial x_i}\frac{\partial}{\partial x_i}\left(\frac{\partial\xi}{\partial x_j}\frac{\partial\left(\rho D\right)}{\partial x_j}\right) \tag{3.71}$$
$$-D\chi_\xi\frac{\partial}{\partial t}\left(\frac{1}{D}\right)-\frac{4D}{\rho}\frac{\partial\xi}{\partial t}\frac{\partial\xi}{\partial x_j}\frac{\partial\rho}{\partial x_j}+\chi_\xi D^2\frac{\partial^2}{\partial x_i^2}\left(\frac{1}{D}\right),$$

$$S_{\chi_\xi,v} = \frac{4D}{\rho}\frac{\partial\xi}{\partial x_j}\frac{\partial}{\partial x_j}\left[S_v(1-\xi)\right], \tag{3.72}$$

and

$$\begin{aligned} S_{\chi_\xi,\overline{M}} = {} & \frac{D}{\overline{M}}\frac{\partial\overline{M}}{\partial x_i}\frac{\partial\chi_\xi}{\partial x_i} + \frac{4D\xi}{\rho}\frac{\partial\xi}{\partial x_i}\frac{\partial}{\partial x_i}\left[\frac{\partial}{\partial x_j}\left(\frac{\rho D}{\overline{M}}\frac{\partial\overline{M}}{\partial x_j}\right)\right] + \frac{D^2\chi_\xi}{\overline{M}}\frac{\partial\overline{M}}{\partial x_i}\frac{\partial}{\partial x_i}\left(\frac{1}{D}\right) \\ & + \frac{4D^2}{\overline{M}}\frac{\partial\xi}{\partial x_i}\frac{\partial\xi}{\partial x_j}\frac{\partial^2\overline{M}}{\partial x_i\partial x_j} + \frac{4D}{\rho}\frac{\partial\overline{M}}{\partial x_i}\frac{\partial\xi}{\partial x_i}\frac{\partial\xi}{\partial x_j}\frac{\partial}{\partial x_j}\left(\frac{\rho D}{\overline{M}}\right) + \frac{2\chi_\xi}{\rho}\frac{\partial}{\partial x_i}\left(\frac{\rho D}{\overline{M}}\frac{\partial\overline{M}}{\partial x_i}\right). \end{aligned} \tag{3.73}$$

For simplicity, in the remainder of this paper, the scalar dissipation rate of the mixture fraction, χ_ξ will be noted as χ.

Equations (3.63) and (3.70) have to be transformed by means of the similarity transformation presented in the previous section for their inclusion in the code used in the present work. The transformed equations yield

$$\begin{aligned} \rho^2 v\frac{d\xi}{d\eta} &= \rho^3 D\frac{d^2\xi}{d\eta^2} + \rho\frac{d\xi}{d\eta}\frac{d\left(\rho^2 D\right)}{d\eta} + \frac{\rho^3 D}{\overline{M}}\frac{d\overline{M}}{d\eta}\frac{d\xi}{d\eta} \\ &+ \frac{\xi\rho^3 D}{\overline{M}}\frac{d^2\overline{M}}{d\eta^2} + \xi\rho\frac{d\overline{M}}{d\eta}\frac{d}{d\eta}\left(\frac{\rho^2 D}{\overline{M}}\right) + S_v\left(1-\xi\right), \end{aligned} \tag{3.74}$$

and

$$\rho v\frac{d\chi}{d\eta} = D\rho^2\frac{d^2\chi}{d\eta^2} + \rho D\frac{d\chi}{d\eta}\frac{d\rho}{d\eta} + S_{\chi,g,\eta} + S_{\chi,v,\eta} + S_{\chi,\overline{M},\eta}, \tag{3.75}$$

respectively, with

$$\begin{aligned} S_{\chi,g,\eta} = {} & -4D\rho^3\left(\frac{d\xi}{d\eta}\right)^2\frac{dv}{d\eta} - 4D^2\rho^2\frac{d^2\xi}{d\eta^2} - 4D^2\rho\frac{d\xi}{d\eta}\frac{d\rho}{d\eta} \\ & - D\chi v\rho\frac{d}{d\eta}\left(\frac{1}{D}\right) - 4D\rho^2 v\frac{d\rho}{d\eta}\left(\frac{d\xi}{d\eta}\right)^2 + 2D^2\rho^2\frac{d\chi}{d\eta}\frac{d}{d\eta}\left(\frac{1}{D}\right) \\ & + 4D\rho^3\frac{d\xi}{d\eta}\frac{d\left(\rho D\right)}{d\eta}\frac{d^2\xi}{d\eta^2} + 4D\rho^2\left(\frac{d\xi}{d\eta}\right)^2\frac{d\left(\rho D\right)}{d\eta}\frac{d\rho}{d\eta} + 4D\rho^3\left(\frac{d\xi}{d\eta}\right)^2\frac{d^2\left(\rho D\right)}{d\eta^2} \\ & + 4D\rho^2\left(\frac{d\xi}{d\eta}\right)^2\frac{d\left(\rho D\right)}{d\eta}\frac{d\rho}{d\eta} + 4D\rho^3\frac{d\xi}{d\eta}\frac{d\left(\rho D\right)}{d\eta}\frac{d^2\xi}{d\eta^2} + 4D\rho^2\left(\frac{d\xi}{d\eta}\right)^2\frac{d\left(\rho D\right)}{d\eta}\frac{d\rho}{d\eta} \\ & + \chi D^2\rho^2\frac{d^2}{d\eta^2}\left(\frac{1}{D}\right) + \chi D^2\rho\frac{d}{d\eta}\left(\frac{1}{D}\right)\frac{d\rho}{d\eta}, \end{aligned} \tag{3.76}$$

$$S_{\chi,v,\eta} = 4D\rho\frac{d\xi}{d\eta}\frac{d}{d\eta}\left(Sv\left[1-\xi\right]\right), \tag{3.77}$$

and

$$
\begin{aligned}
S_{\chi,\overline{M},\eta} = & \frac{D\rho^2}{\overline{M}}\frac{d\overline{M}}{d\eta}\frac{d\chi}{d\eta} + 4D\xi\rho\frac{d\xi}{d\eta}\frac{d}{d\eta}\left(\frac{\rho^3 D}{\overline{M}}\frac{d^2\overline{M}}{d\eta^2}\right) + 4D\xi\rho^2\frac{d\xi}{d\eta}\frac{d\overline{M}}{d\eta}\frac{d^2}{d\eta^2}\left(\frac{\rho^2 D}{\overline{M}}\right) \\
& + 4D\xi\rho\frac{d\overline{M}}{d\eta}\frac{d\rho}{d\eta}\frac{d}{d\eta}\left(\frac{\rho^2 D}{\overline{M}}\right) + 4D\xi\rho^2\frac{d\xi}{d\eta}\frac{d}{d\eta}\left(\frac{\rho^2 D}{\overline{M}}\frac{d^2\overline{M}}{d\eta^2}\right) \\
& + \frac{D^2\chi\rho^2}{\overline{M}}\frac{d\overline{M}}{d\eta}\frac{d}{d\eta}\left(\frac{1}{D}\right) + \frac{4D^2\rho^4}{\overline{M}}\left(\frac{d\xi}{d\eta}\right)^2\frac{d^2\overline{M}}{d\eta^2} + \frac{4D^2\rho^3}{\overline{M}}\frac{d\overline{M}}{d\eta}\frac{d\rho}{d\eta} \\
& + 4D\rho^3\frac{d\overline{M}}{d\eta}\left(\frac{d\xi}{d\eta}\right)^2\frac{d}{d\eta}\left(\frac{\rho D}{\overline{M}}\right) + \frac{2\chi\rho^2 D}{\overline{M}}\frac{d^2\overline{M}}{d\eta^2} + 2\chi\frac{d\overline{M}}{d\eta}\frac{d}{d\eta}\left(\frac{\rho^2 D}{\overline{M}}\right).
\end{aligned}
\tag{3.78}
$$

If a spatially uniform molecular weight of the mixture is assumed (equivalent to the adoption of Fick's diffusion law), the terms including $\partial\overline{M}/\partial x_i$ vanish, and the transport equations of ξ and χ reduce to

$$
\rho^2 v\frac{d\xi}{d\eta} = \rho^3 D\frac{d^2\xi}{d\eta^2} + \rho\frac{d\xi}{d\eta}\frac{d\left(\rho^2 D\right)}{d\eta} + S_v\left(1-\xi\right), \tag{3.79}
$$

and

$$
\rho v\frac{d\chi}{d\eta} = D\rho^2\frac{d^2\chi}{d\eta^2} + \rho D\frac{d\chi}{d\eta}\frac{d\rho}{d\eta} + S_{\chi,g,\eta} + S_{\chi,v,\eta}, \tag{3.80}
$$

respectively. In the results' section, the following evaluation is made.

- All species transport equations (Eqs. (3.3)) are solved and the results are employed to calculate the value of the mixture fraction and its scalar dissipation rate by definition. The results obtained are denoted as ξ_e and χ_e, where the subscript e refers to "exact".

- The full transport equations of the mixture fraction and its scalar dissipation rate (Eqs. (3.74) and (3.75)) are solved. For this purpose, the diffusion coefficient, D, must be determined, which is done through the use of a mass averaged diffusion coefficient of the mixture, i.e. $D = \sum_{k=1}^{N} Y_k D_k$. The results are denoted as $\xi_{D,M}$ and $\chi_{D,M}$.

- The simplified transport equations of the mixture fraction and its scalar dissipation rate, which do not consider spatial variations of the mean molecular weight are solved (Eqs. (3.79) and (3.80)). The diffusion coefficient, D is determined either through use of the average diffusion coefficient of the mixture, i.e. $D = \sum_{k=1}^{N} Y_k D_k$, or with the assumption of Lewis number of unity, leading to $D = \lambda/(\rho C_p)$. The results are denoted by ξ_D and χ_D, and ξ_{Le} and χ_{Le}, respectively.

The boundary conditions considered are $\xi = \chi = 0$ at both side of the configuration. The different values of ξ and χ obtained are finally compared in order to evaluate the

effect of the different assumptions involved. Additionally, the value of D_e is compared with the ones obtained by means of the average diffusion coefficient of the mixture and with the assumption of Lewis number of unity in order to determine which of them is the most appropriate approximation. The results of these evaluations can be employed for the simplification of the transport equation of the scalar dissipation rate, which would simplify its implementation in the simulation of turbulent spray flames.

3.2.2 Spray Flamelet Equations

In this subsection, the derivation of a set of multi-regime spray flamelet equations to describe all combustion regimes found in spray flames, and which provides a common framework for several flamelet formulations existing in the literature [42, 60, 45, 65], is presented. This set of equations is then used for the derivation of a set of non-premixed spray flamelet equations, which provides the fundamentals for the non-premixed spray flamelet model of Hollmann and Gutheil [42, 59]. The starting point of the derivation is the transport equation of the mass fraction of chemical species, Y_k, cf. Eq. (3.3). Thermal diffusion is neglected in the present derivation, since it is only relevant for light species, H and H_2. Following the derivation of Nguyen et al. [65] for gas flames, it is assumed that a set of P independent variables ζ_p, and a time-like variable, τ, exist, which constitute a proper coordinate system in which the evolution of any species mass fraction can be described. With the introduction of these $P+1$ variables, a change of coordinates of Eq. (3.3) from the physical space (x_1, x_2, x_3) into the new set of coordinates $(\zeta_1, .., \zeta_p, .., \zeta_P, \tau)$ is performed. The use of the transformation rules

$$\frac{\partial}{\partial t} = \frac{\partial}{\partial \tau} + \frac{\partial \zeta_p}{\partial t}\,\frac{\partial}{\partial \zeta_p} \quad \text{and} \quad \frac{\partial}{\partial x_i} = \frac{\partial \zeta_p}{\partial x_i}\,\frac{\partial}{\partial \zeta_p}, \tag{3.81}$$

in the transport equations of mass fractions of chemical species, Eqs. (3.3), results in [109]

$$\begin{aligned} \rho\frac{\partial Y_k}{\partial \tau} &= -\frac{\partial Y_k}{\partial \zeta_p}\left(\rho\frac{\partial \zeta_p}{\partial t} + \rho u_i\frac{\partial \zeta_p}{\partial x_i} - \frac{\partial}{\partial x_i}\left[\rho D_k\frac{\partial \zeta_p}{\partial x_i}\right]\right) + \rho D_k\frac{\partial \zeta_p}{\partial x_i}\frac{\partial \zeta_l}{\partial x_i}\frac{\partial^2 Y_k}{\partial \zeta_p \partial \zeta_l} \\ &+ \rho\frac{D_k Y_k}{\overline{M}}\frac{\partial \zeta_p}{\partial x_i}\frac{\partial \zeta_l}{\partial x_i}\frac{\partial^2 \overline{M}}{\partial \zeta_p \partial \zeta_l} + \frac{\partial \overline{M}}{\partial \zeta_p}\frac{\partial \zeta_l}{\partial x_i}\frac{\partial}{\partial \zeta_l}\left(\rho\frac{D_k Y_k}{\overline{M}}\frac{\partial \zeta_p}{\partial x_i}\right) + S_v\left(\delta_{Fk} - Y_k\right) + \dot{\omega}_k. \end{aligned} \tag{3.82}$$

However, the consideration of $P+1$ variables is not possible in practical cases, and a simplified set must be selected if Eq. (3.82) is to be evaluated. Equation (3.82) must reduce to the non-premixed flamelet equations [40] in the non-premixed limit, so that the mixture fraction must be chosen as one of the independent variables. Moreover, at least a second coordinate is required in order to characterize the premixed limit [65, 45, 46].

The definition of an adequate second variable for the description of the premixed combustion regime represents a major difficulty, since any variable employed has to be statistically independent of the mixture fraction. Typically, pure premixed combustion is characterized by a reaction progress variable defined as a combination of species mass fractions of major species such as CO_2 and H_2O. However, this definition statistically depends on the mixture fraction and it is therefore not adequate for the present case. This can be better seen in the case of pure non-premixed gas flame structures, which can be described by the non-premixed gas flamelet equations of Peters [40]. When such a flame is considered, the value of the second variable has to be constant, because it is known that non-premixed flamelet structures can be described using the mixture fraction as single coordinate. However, the progress variable defined as a combination of species mass fractions changes along a non-premixed flame and it is therefore not an adequate choice. Because of these difficulties associated with the definition of an adequate progress variable, no exact definition is used in the present work, and a general derivation is performed. Thus, it is assumed that a progress variable Λ exists, which is statistically independent of the mixture fraction ξ. Using ξ and Λ as independent variables and neglecting effects in other directions, the following formulation of Eq. (3.82) is obtained [109]

$$
\begin{aligned}
\rho\frac{\partial Y_k}{\partial \tau} &= \underbrace{-\frac{\partial Y_k}{\partial \xi}\left(\rho\frac{\partial \xi}{\partial t}+\rho u_i\frac{\partial \xi}{\partial x_i}-\frac{\partial}{\partial x_i}\left[\rho D_k\frac{\partial \xi}{\partial x_i}\right]\right)}_{\text{Terms in } \xi \text{ direction}} \\
&+ \underbrace{\frac{\partial \xi}{\partial x_i}\frac{\partial \overline{M}}{\partial \xi}\frac{\partial}{\partial \xi}\left(\frac{\rho D_k Y_k}{\overline{M}}\frac{\partial \xi}{\partial x_i}\right)+\frac{\rho\chi_\xi}{2}\left(\frac{\partial^2 Y_k}{\partial \xi^2}+\frac{Y_k}{\overline{M}}\frac{\partial^2 \overline{M}}{\partial \xi^2}\right)}_{\text{Terms in } \xi \text{ direction}} \\
&- \underbrace{\frac{\partial Y_k}{\partial \Lambda}\left(\rho\frac{\partial \Lambda}{\partial t}+\rho u_i\frac{\partial \Lambda}{\partial x_i}-\frac{\partial}{\partial x_i}\left[\rho D_k\frac{\partial \Lambda}{\partial x_i}\right]\right)}_{\text{Terms in } \Lambda \text{ direction}} \\
&+ \underbrace{\frac{\partial \Lambda}{\partial x_i}\frac{\partial \overline{M}}{\partial \Lambda}\frac{\partial}{\partial \Lambda}\left(\frac{\rho D_k Y_k}{\overline{M}}\frac{\partial \Lambda}{\partial x_i}\right)+\frac{\rho\chi_\Lambda}{2}\left(\frac{\partial^2 Y_k}{\partial \Lambda^2}+\frac{Y_k}{\overline{M}}\frac{\partial^2 \overline{M}}{\partial \Lambda^2}\right)}_{\text{Terms in } \Lambda \text{ direction}} \\
&+ \underbrace{\rho\chi_{\xi\Lambda}\left(\frac{\partial^2 Y_k}{\partial \xi\partial \Lambda}+\frac{Y_k}{2\overline{M}}\frac{\partial^2 \overline{M}}{\partial \xi\partial \Lambda}\right)+\frac{\partial \overline{M}}{\partial \xi}\frac{\partial \Lambda}{\partial x_i}\frac{\partial}{\partial \Lambda}\left(\frac{\rho D_k Y_k}{\overline{M}}\frac{\partial \xi}{\partial x_i}\right)}_{\text{Crossed terms}} \\
&+ \underbrace{+\frac{\partial \overline{M}}{\partial \Lambda}\frac{\partial \xi}{\partial x_i}\frac{\partial}{\partial \xi}\left(\frac{\rho D_k Y_k}{\overline{M}}\frac{\partial \Lambda}{\partial x_i}\right)}_{\text{Crossed terms}}+\dot{\omega}_k+S_v\left(\delta_{Fk}-Y_k\right),
\end{aligned}
\tag{3.83}
$$

where $\chi_\xi = 2D(\frac{\partial \xi}{\partial x_i})^2$, $\chi_\Lambda = 2D(\frac{\partial \Lambda}{\partial x_i})^2$ and $\chi_{\xi\Lambda} = 2D\frac{\partial \xi}{\partial x_i}\frac{\partial \Lambda}{\partial x_i}$ are the scalar dissipation rates of mixture fraction, progress variable and the crossed scalar dissipation rate, respectively. Equation (3.83) describes all combustion regimes found in spray flames.

Note that, provided an adequate definition of Λ is formulated, these equations may be used to define a variable similar to the flame index proposed by Knudsen and Pitsch [45, 46] (see Eq. (2.77)) and to determine the locally dominant combustion regime in spray flames. In fact, the new formulation comprises the flamelet equations proposed by Knudsen and Pitsch [45, 46] for partially premixed gas flames, if the same definition of Λ [45, 46] employed by these authors is considered. Since the gas flamelet equations of Knudsen and Pitsch [45, 46] reduce to the classical formulation of Peters [40] when only non-premixed effects are considered, Eqs. (3.83) also comprise the non-premixed gas flamelet equations [40].

Even though no adequate definition of Λ is currently available for spray flames, Eqs. (3.83) can be indirectly used to evaluate the relative importance of different combustion regimes under various conditions. In particular, changes across Λ are negligible in flames where only non-premixed and evaporation effects are relevant and thus, in those situations, the flame structure can be describe by means of the mixture fraction ξ as sole independent variable. Thus, Eq. (3.83) may be rewritten to yield

$$\begin{aligned}\rho\frac{\partial Y_k}{\partial \tau} &+ \frac{\partial Y_k}{\partial \xi}\left(\rho\frac{\partial \xi}{\partial t} + \rho u_i\frac{\partial \xi}{\partial x_i} - \frac{\partial}{\partial x_i}\left[\rho D_k\frac{\partial \xi}{\partial x_i}\right]\right) - \frac{\partial \xi}{\partial x_i}\frac{\partial \overline{M}}{\partial \xi}\frac{\partial}{\partial \xi}\left(\frac{\rho D_k Y_k}{\overline{M}}\frac{\partial \xi}{\partial x_i}\right)\\ &- \frac{\rho\chi_\xi}{2}\left(\frac{\partial^2 Y_k}{\partial \xi^2} + \frac{Y_k}{\overline{M}}\frac{\partial^2 \overline{M}}{\partial \xi^2}\right) = \dot{\omega}_k + S_v\left(\delta_{Fk} - Y_k\right). \end{aligned} \tag{3.84}$$

A comparison of the steady forms of Eqs. (3.84) and the transport equations of the mass fractions of chemical species, Eqs. (3.3), shows that [109],

$$\Omega_P = \Omega_M \tag{3.85}$$

must be satisfied if no premixed effects exist, where [109]

$$\Omega_P = -\rho u_i\frac{\partial Y_k}{\partial x_i} + \frac{\partial}{\partial x_i}\left(\rho D_k\frac{\partial Y_k}{\partial x_i}\right) + \frac{\partial}{\partial x_i}\left(\frac{\rho D_k Y_k}{\overline{M}}\frac{\partial \overline{M}}{\partial x_i}\right) \tag{3.86}$$

and

$$\begin{aligned}\Omega_M = &\frac{\rho\chi_\xi}{2}\left(\frac{\partial^2 Y_k}{\partial \xi^2} + \frac{Y_k}{\overline{M}}\frac{\partial^2 \overline{M}}{\partial \xi^2}\right) + \frac{\partial \xi}{\partial x_i}\frac{\partial \overline{M}}{\partial \xi}\frac{\partial}{\partial \xi}\left(\frac{\rho D_k Y_k}{\overline{M}}\frac{\partial \xi}{\partial x_i}\right)\\ &- \frac{\partial Y_k}{\partial \xi}\left(\rho\frac{\partial \xi}{\partial t} + \rho u_i\frac{\partial \xi}{\partial x_i} - \frac{\partial}{\partial x_i}\left[\rho D_k\frac{\partial \xi}{\partial x_i}\right]\right). \end{aligned} \tag{3.87}$$

Equations (3.86) and (3.87) present the terms balancing the chemical source in the physical and mixture fraction space, respectively. Hollmann and Gutheil [42] neglected premixed-like effects in laminar spray flames if all fuel is injected in liquid form, and this assumption will be confirmed in the results' section by means of the evaluation and comparison of Ω_P and Ω_M for different situations.

Neglecting gradients of $\overline{M}$ and assuming equal diffusion coefficients for all species, Eq. (3.84) can be rewritten as [60]

$$\rho\frac{\partial Y_k}{\partial \tau} = \underbrace{\rho\frac{\chi_\xi}{2}\frac{\partial^2 Y_k}{\partial \xi^2}}_{\text{Dissipation}} + \dot{\omega}_k + \underbrace{S_v\left(\xi-1\right)\frac{\partial Y_k}{\partial \xi}}_{\text{Mixing/Evaporation}} + \underbrace{S_v\left(\delta_{Fk}-Y_k\right)}_{\text{Evaporation}}, \tag{3.88}$$

where the transport equation of the mixture fraction, Eq. (3.63, has been employed.

Equation (3.88) presents the flamelet equation for laminar non-premixed spray flames [60, 123]. The first three terms are identical to the flamelet equation for gas flames, Eq. (2.43), whereas the last two terms containing the spray evaporation mass source term, S_v, are new, and they represent the effect of evaporation on the flamelet structure. When no evaporation takes place, $S_v = 0$ and Eq. (3.88) reduces to the non-premixed flamelet equations of Peters (see Eq. (2.43)). Thus, it can be concluded that the flamelet formulation for spray flames does not only depend on the mixture fraction and its scalar dissipation rate, but additionally on the spray evaporation source term, S_v.

The derivation of the flamelet equations, Eqs. (3.88), includes two major assumptions, which are usually also made in gas combustion. The first one is the assumption of non-varying mean molecular weight, $\bar{M}$, and the second is the assumption of $\mathrm{Le} = 1$, which is employed for the consideration of a unique diffusion coefficient for all species, $D_k = D = \frac{\rho}{\lambda C_p}$. The validity of these approximations may be studied by comparing terms considering or neglecting relevant contributions. If the second term on the r.h.s. of the definition of the Hirschfelder-Curtiss diffusion law, Eq. (3.16), including $\bar{M}$ [60]

$$\Upsilon_{M,k} = \frac{\partial}{\partial x_i}\left(\rho\frac{D_k Y_k}{\bar{M}}\frac{\partial \bar{M}}{\partial x_i}\right), \tag{3.89}$$

is small, then

$$\Upsilon_{x,k} \approx \Upsilon_{\xi,k}, \tag{3.90}$$

must be satisfied, where

$$\Upsilon_{x,k} = -\rho\frac{\partial Y_k}{\partial t} - \rho u_i\frac{\partial Y_k}{\partial x_i} + \frac{\partial}{\partial x_i}\left(\rho D_k\frac{\partial Y_k}{\partial x_i}\right) + \frac{\partial}{\partial x_i}\left(\rho\frac{D_k Y_k}{\bar{M}}\frac{\partial \bar{M}}{\partial x_i}\right), \tag{3.91}$$

is the contribution in physical space, and

$$\begin{aligned}\Upsilon_{\xi,k} &= -\rho\frac{\partial Y_k}{\partial \tau} + \rho D_k\left(\frac{\partial \xi}{\partial x_i}\right)^2\frac{\partial^2 Y_k}{\partial \xi^2} \\ &- \left(\rho\frac{\partial \xi}{\partial t} + \rho u_i\frac{\partial \xi}{\partial x_i} - \frac{\partial}{\partial x_i}\left[\rho D_k\frac{\partial \xi}{\partial x_i}\right]\right)\frac{\partial Y_k}{\partial \xi}\end{aligned} \tag{3.92}$$

describes the corresponding term in mixture fraction space, where the variation of $\bar{M}$ is neglected. The validity of Eq. (3.90) will be evaluated in the next section.

The diffusion term in the brackets in the second term on the l.h.s. of Eq. (3.84) can be expressed as [60]

$$\frac{\partial}{\partial x_i}\left(\rho D_k \frac{\partial \xi}{\partial x_i}\right) = \frac{\partial}{\partial x_i}\left(\rho D \frac{\partial \xi}{\partial x_i}\right) + \frac{\partial}{\partial x_i}\left(\rho (D_k - D) \frac{\partial \xi}{\partial x_i}\right). \tag{3.93}$$

If Le = 1 is assumed for all chemical species, $D_k = D$, and the last term on the r.h.s. of Eq. (3.93) may be neglected and

$$\Psi_{\xi,k} = -\left(\rho \frac{\partial \xi}{\partial t} + \rho u_i \frac{\partial \xi}{\partial x_i} - \frac{\partial}{\partial x_i}\left(\rho D_k \frac{\partial \xi}{\partial x_i}\right)\right) \frac{\partial Y_k}{\partial \xi} \tag{3.94}$$

can be approximated as

$$\Psi_{k,\mathrm{Le}=1} = S_v(\xi - 1)\frac{\partial Y_k}{\partial \xi}, \tag{3.95}$$

see Eq. (3.84), which implies that the following relation is satisfied

$$\Psi_{\xi,k} \approx \Psi_{k,\mathrm{Le}=1}. \tag{3.96}$$

In the next chapter, the validity of Eq. (3.96) will be evaluated.

3.2.3 Spray Flamelet Modeling of Turbulent Reacting Flows

The flamelet model presented in the previous subsections has several implications for the simulation of turbulent spray flames. Provided an adequate definition of Λ is formulated for spray flames, the multi-regime spray flamelet equations (Eqs. (3.83)) can be used to define a flame index to locally distinguish the dominant combustion regime in turbulent spray flames, similarly to the flame index proposed by Knudsen and Pitsch [45]. This flame index could then be used for the local selection of the adequate flamelet model that should be applied in each flame region.

Since the non-premixed spray flamelet model [42, 59] has been successfully applied to the simulation of several turbulent non-premixed spray flames [42, 66, 67], a multi-regime spray flamelet model could be formulated as a combination of the model of Hollmann and Gutheil [42, 59] and a premixed gas flamelet model. Such a formulation would allow for the description of premixed, non-premixed and evaporation-controlled combustion regimes. The formulation of a flame index appropriate for these multi-regime flamelet model can be obtained by evaluating Eqs. (3.83) for a reaction progress variable, C, defined as a lineal combination of mass fractions of major species and comparing the budget of the terms in the Λ coordinate with the total budget of the terms balancing the chemical source term of the progress variable, $\dot{\omega}_C$. For example,

assuming the crossed scalar dissipation rate to be zero and an uniform mean molecular weight of the mixture, a flame index for spray flames, Θ_s, can be defined as

$$\Theta_s = \frac{\Theta_{pre}}{\Theta_{total}}, \tag{3.97}$$

where

$$\Theta_{pre} = \left| \frac{\partial C}{\partial \Lambda} \left(\rho u_j \frac{\partial \Lambda}{\partial x_j} - \frac{\partial}{\partial x_j} \left[\rho D \frac{\partial \Lambda}{\partial x_j} \right] \right) - \frac{\rho \chi_\Lambda}{2} \frac{\partial^2 C}{\partial \Lambda^2} \right| \tag{3.98}$$

and

$$\begin{aligned} \Theta_{total} &= \left| \frac{\partial C}{\partial \Lambda} \left(\rho u_j \frac{\partial \Lambda}{\partial x_j} - \frac{\partial}{\partial x_j} \left[\rho D \frac{\partial \Lambda}{\partial x_j} \right] \right) - \frac{\rho \chi_\Lambda}{2} \frac{\partial^2 C}{\partial \Lambda^2} \right| \\ &+ \left| -\frac{\rho \chi_\xi}{2} \frac{\partial^2 C}{\partial \xi^2} + S_v \left[C + (1 - \xi) \frac{\partial C}{\partial \xi} \right] \right| \end{aligned} \tag{3.99}$$

are the absolute values of the sum of the terms associated with premixed effects in Eq. (3.83) and the sum of the absolute values of the different terms balancing the chemical source, respectively. In Eq. (3.97) the use of absolute values is required to keep the value of the index Θ_s between zero and one. Thus, Θ_s can be used to locally distinguish the dominant combustion regime, where $\Theta_s = 0$ indicates a locally non-premixed spray flame and $\Theta_s = 1$ a locally perfectly premixed flame. Based on this evaluation, the appropriate flamelet model can be used for the computation of the Favre-averaged mean value of the variables of interest (for example the mass fraction of chemical species). For zones where $0 < \Theta_s < 1$, values of $\tilde{\phi}$ obtained by the use of premixed and non-premixed spray flamelet models can be weighted by

$$\tilde{\phi} = \Theta_s \ \tilde{\phi}_{pre} + (1 - \Theta_s) \ \tilde{\phi}_{spray}, \tag{3.100}$$

where $\tilde{\phi}_{pre}$ and $\tilde{\phi}_{spray}$ are the Favre-averaged values of the variable ϕ using the premixed flamelet model and the non-premixed spray flamelet model respectively.

Additionally, Eq. (3.88) suggests that spray flamelet structures can be characterized by the use of the mixture fraction, its scalar dissipation rate and the evaporation rate. This is consistent with the findings of Hollmann and Gutheil [42], who found that the initial droplet radius, r_0, the initial droplet velocity v_0 and the initial equivalence ratio at the spray side of the configuration where required additional to the mixture fraction and its scalar dissipation rate. These three parameters are of vital importance on the definition of the spray evaporation mass rate S_v, and, therefore, the use of S_v instead of r_0,v_0 and E should be equivalent. Thus, these results suggest that the non-premixed spray flamelet formulation of Hollmann and Gutheil [42] given as

$$\tilde{\phi} = \int_0^\infty \int_0^\infty \int_0^\infty \int_0^\infty \int_0^1 \phi \ \tilde{P}\left(\xi, \chi, E, R_0, v_0\right) \ \mathrm{d}\xi \ \mathrm{d}\chi \ \mathrm{d}E \ \mathrm{d}R_0 \ \mathrm{d}v_0, \tag{3.101}$$

may be replaced by the formulation

$$\tilde{\phi} = \int_{-\infty}^{\infty} \int_{0}^{\infty} \int_{0}^{1} \phi \; \tilde{P}\left(\xi, \chi, S_v\right) \; \mathrm{d}\xi \; \mathrm{d}\chi \; \mathrm{d}S_v. \tag{3.102}$$

The use of Eq. (3.102) has the advantage of reducing the dimensionality of the probability density function required for the implementation of the spray flamelet model (from five variables to three). However, the equivalence ratio, initial droplet size and velocity might be more straight forward parameters to be determined a priori for the computations of the flamelet library. The major difference between both formulations is that the former formulation requires consideration of input parameters into the laminar flame computation, whereas the evaporation rate in the new formulation is a result from the laminar flame simulation.

A second problem that arise with the newly proposed spray flamelet model (Eq. (3.102)) is the need of the determination of a means for calculating the joint PDF of the characteristic parameters, $\tilde{P}\left(\xi, \chi, S_v\right)$. As a first approach, the procedure described in the previous studies [42, 66, 67] may be followed. This includes the assumption of statistical independence of the three dependent variables of the PDF, and the use of a (generalized) β function [42, 114] for the mixture fraction and a log normal distribution [40, 42] for the scalar dissipation rate with a constant value of the variance, $\sigma_\chi^2 = 2$ [40]. The PDF of the mass evaporation rate, S_v, is still unclear, but a diract delta function at the mean value of the evaporation rate, $\tilde{S}_v$ could be employed.

In the next section, the numerical solution scheme employed in the present dissertation is presented.

3.3 Numerical Solution Scheme

3.3.1 Discretization Method

The ordinary differential equations introduced in the previous sections can be expressed in the following general form

$$A\frac{d^2\phi}{d\eta^2} + B\frac{d\phi}{d\eta} + C\phi = D, \tag{3.103}$$

where A, B and C are constants. Eq. (3.103) can be transformed into a set of discrete algebraic equations by means of a discretization scheme [124]. In the present work, a cental finite difference scheme is employed, which can be derived by considering an expansion in Taylor series of the value of ϕ in a point η in the vicinity of a point η_0.

This expansion yields [124]

$$\begin{aligned}\phi(\eta) &= \sum_{n=0}^{\infty} \frac{1}{n!} \frac{d^n \phi(\eta_0)}{d\eta^n} (\eta - \eta_0)^n \\ &= \phi(\eta_0) + \frac{d\phi(\eta_0)}{d\eta}(\eta - \eta_0) + H,\end{aligned} \tag{3.104}$$

where H represents higher order terms. Defining a grid over the one-dimensional domain determined by the η-coordinate presented in the previous section, three consecutive points can be expressed as, η_{i-1}, η_i and η_{i+1}. After H is neglected, Eq. (3.104) can be evaluated for the points $\eta_{i+1} = \eta_i + \Delta\eta_i$ and $\eta_{i-1} = \eta_i - \Delta\eta_{i-1}$, which yields [124]

$$\begin{aligned}\phi(\eta_{i+1}) - \phi(\eta_i) &= \frac{d\phi(\eta_i)}{d\eta}(\eta_i + \Delta\eta_i - \eta_i) \\ &= \frac{d\phi(\eta_i)}{d\eta}\Delta\eta_i,\end{aligned} \tag{3.105}$$

and

$$\begin{aligned}\phi(\eta_{i-1}) - \phi(\eta_i) &= \frac{d\phi(\eta_i)}{d\eta}(\eta - \Delta\eta_{i-1} - \eta_i) \\ &= -\frac{d\phi(\eta_i)}{d\eta}\Delta\eta_{i-1}\end{aligned} \tag{3.106}$$

respectively. Substracting Eq. (3.106) from Eq. (3.105) yields [124]

$$\phi(\eta_{i+1}) - \phi(\eta_{i-1}) = \frac{d\phi(\eta_i)}{d\eta}\Delta\eta_{i+1} + \frac{d\phi(\eta_i)}{d\eta}\Delta\eta_{i-1}, \tag{3.107}$$

which can be rewritten as

$$\frac{d\phi(\eta_i)}{d\eta} = \frac{\phi(\eta_{i+1}) - \phi(\eta_{i-1})}{\Delta\eta_{i+1} + \Delta\eta_{i-1}}. \tag{3.108}$$

In this work, an equidistant grid is employed, which implies [124]

$$\Delta\eta_{i+1} = \Delta\eta_{i-1} = \Delta\eta. \tag{3.109}$$

Thus, Eq. (3.108) can be simplified as [124]

$$\frac{d\phi(\eta_i)}{d\eta} = \frac{\phi(\eta_{i+1}) - \phi(\eta_{i-1})}{2\Delta\eta}. \tag{3.110}$$

An expression for the second derivative of $\phi(\eta_i)$ can be obtained from Eq. (3.110) by considering [124]

$$\phi(\eta_i) = \frac{d\phi(\eta_i)}{d\eta}, \tag{3.111}$$

with a step of $\Delta\eta/2$. This yields [124]

$$\begin{aligned}\frac{d^2\phi(\eta_i)}{d\eta^2} &= \frac{\frac{d\phi\left(\eta_i+\frac{\Delta\eta}{2}\right)}{d\eta} - \frac{d\phi\left(\eta_i-\frac{\Delta\eta}{2}\right)}{d\eta}}{\Delta\eta} \\ &= \frac{\frac{\phi(\eta_i+\Delta\eta)-\phi(\eta_i)}{\Delta\eta} - \left[\frac{\phi(\eta_i)-\phi(\eta_i-\Delta\eta)}{\Delta\eta}\right]}{\Delta\eta} \\ &= \frac{\phi(\eta_i+\Delta\eta)+\phi(\eta_i-\Delta\eta)-2\phi(\eta_i)}{\Delta\eta^2}.\end{aligned} \tag{3.112}$$

The discretization scheme specified by Eqs. (3.110) and (3.112) is the central finite difference scheme [124], which is employed in the present thesis.

3.3.2 Solution Algorithm

After the governing differential equations have been discretized, a set of algebraic equations is obtained, which can be written as follow [125]

$$\begin{array}{cccccccc}
\phi_1 & & & & & & & = d_1 \\
a_2\phi_1 & +b_2\phi_2 & +c_2\phi_3 & & & & & = d_2 \\
 & a_3\phi_2 & +b_3\phi_3 & +c_3\phi_4 & & & & = d_3 \\
 & & . & . & . & & & = . \\
 & & & . & . & . & & = . \\
 & & & & . & . & . & = . \\
 & & & & a_{R-1}\phi_{R-2} & +b_{R-1}\phi_{R-1} & +c_{R-1}\phi_R & = d_{R-1} \\
 & & & & & & \phi_R & = d_R
\end{array}$$

where R is the total number of grid points and ϕ_1 and ϕ_R are boundary conditions. Tridiagonal systems of this kind can be solved by means of the Thomas algorithm, which is also known as the Tri-Diagonal Matrix Algorithm (TDMA). For this purpose, each equation is first expressed in the following general way [125]

$$a_j\phi_{j-1} + b_j\phi_j + c_j\phi_{j+1} = d_j, \tag{3.113}$$

with $j = 2, ..., R-1$. Considering the particular equation corresponding to $j = 2$ we have [125]

$$\phi_2 = \frac{d_2 - a_2\phi_1}{b_2} - \frac{c_2}{b_2}\phi_3. \tag{3.114}$$

Defining the variables A_2 and B_2 as [125]

$$A_2 = \frac{d_2 - a_2\phi_1}{b_2} \tag{3.115}$$

and

$$B_2 = \frac{c_2}{b_2} \tag{3.116}$$

respectively, Eq. (3.114) can be rewritten as [125]

$$\phi_2 = A_2 - B_2\phi_3. \tag{3.117}$$

For $j = 3$ we can write

$$\phi_3 = \frac{d_3 - a_3\phi_2}{b_3} - \frac{c_3}{b_3}\phi_4. \tag{3.118}$$

Replacing Eq. (3.114) in Eq. (3.118), and making use of Eqs. (3.115) and (3.116) yields [125]

$$\begin{aligned} \phi_3 &= \frac{d_3 - a_3\left[A_2 - B_2\phi_3\right]}{b_3} - \frac{c_3}{b_3}\phi_4 \\ &= \frac{d_3 - a_3A_2}{b_3} + \frac{a_3B_2\phi_3}{b_3} - \frac{c_3}{b_3}\phi_4, \end{aligned} \tag{3.119}$$

which can be solved for ϕ_3 as [125]

$$\phi_3 = \frac{d_3 - a_3A_2}{b_3 + a_3B_2} - \frac{c_3}{b_3 + a_3B_2}\phi_4. \tag{3.120}$$

Repeating the process employed to obtain Eq. (3.120), it is straightforward to show that the following expression can be obtained for ϕ_4 [125]

$$\phi_4 = \frac{d_4 - a_4A_3}{b_4 + a_4B_3} - \frac{c_4}{b_4 + a_4B_3}\phi_5. \tag{3.121}$$

Thus, for $j = 3, ..., R-1$, variables A_j and B_j can be defined as [125]

$$A_j = \frac{d_j - a_jA_{j-1}}{b_j + a_jB_{j-1}} \tag{3.122}$$

and

$$B_j = \frac{c_j}{b_j + a_jB_{j-1}}, \tag{3.123}$$

respectively and the general equation corresponding to ϕ_j can be written as [125]

$$\phi_j = A_j - B_j\phi_{j+1}. \tag{3.124}$$

Since the coefficients A_j and B_j are known for all j. The system of equations can be solved backwards, starting from the boundary condition ϕ_R [125].

The governing equations are finally solved as follows. At the beginning of each simulation, a grid is defined in the η space and initial estimations for the value of each variable in every node are adopted. Typically, these initial estimations are taken from previous computations, when they are available. In the following step, governing equations for motion, evaporation and energy of the liquid phase are solved using a Lagrangian approach and the results are employed for calculating the source terms

of mass, momentum and energy required for the gas phase computations (Eqs. (3.31)-(3.33). After this, the governing gas phase equations for momentum, energy and species mass fractions are solved. Due to the non-linear nature of the equations, unknowns appear in the coefficients calculated in the TDMA, which means that an iterative approach has to be applied. In general, 100 iterations are performed for the gas phase before convergence is checked by means of the following criterion

$$\frac{\sum_{i=2}^{R-1}\left(f_i^{t+\Delta t}-f_i^t\right)}{f_1^t} < e_{\max}, \tag{3.125}$$

where $e_{\max}$ is the maximum acceptable error imposed by the user. For the computations presented in this thesis, an error of 10^{-5} was commonly enough. In Eq. (3.125), f_i^t is the value of the stream function f in the grid point i for the previous iteration, $f_i^{t+\Delta t}$ the corresponding value of for the current iteration and f_1^t is the value of the boundary condition imposed on f. In case converge is not yet reached, a new iteration of the entire algorithm is started, employing the results of the latest iteration as initial approximations. If convergence is reached, the code is stopped. Depending on the initial values used and the particular conditions to be simulated, the entire process can take between 100 and 500 iterations to converge.

After convergence has been reached, the transport equations of mixture fraction and its scalar dissipation rate are solved. The Thomas algorithm is also employed for these variables. First, the equation for ξ, Eq. (3.74), is solved and the results are employed for calculating the source term appearing in Eq. (3.75) The convergence criterion used here is similar to Eq. (3.125), but employing values of ξ and χ at the current and previous iterations instead of the stream function.

In the next chapter, numerical simulations of laminar mono-disperse ethanol/aur counterflow spray flames are presented and discussed.

4. Results and Discussion

This chapter presents numerical results for laminar mono-disperse ethanol/air counterflow spray flames, where a Eulerian/Lagragnian formulation is employed for the description of the spray flow. The numerical setup employed has been already shown in Fig. 2.1. The ethanol spray with carrier gas air is injected from the left side of the configuration and directed against an opposed air flow.

It is important to note that, although the gas flow field considered here is steady, the Lagragnian description of the droplets is unsteady. Therefore, in the present chapter, evaporation profiles are very oft discussed in terms of time, even when the gas flow field is steady.

In all cases considered in this chapter, both air streams, as well as the liquid fuel, are at atmospheric temperature (300 K). Moreover, the initial droplet velocity always matches the gas velocity at the left side of the configuration, which has a fixed value of 0.44 m/s. On the other hand, the values of the equivalence ratio and strain rate at the spray side of the configuration, as well as the initial droplet radii are different for different cases considered. The specific boundary and initial conditions taken into account in each case studied are explained in the respective sections and subsections when required.

The results presented in this chapter can be roughly classified in the following three categories

- Evaluation of the importance of evaporation effects on the flame structure.
- Evaluation of the importance of premixed and non-premixed combustion regimes.
- Evaluation of the validity of assumptions made during the derivation of the transport equations of mixture fraction and its scalar dissipation rate.

The chapter is divided in two sections, which present results in physical and mixture fraction spaces (sections 4.1 and 4.2, respectively).

In subsection 4.1.1, the key role of evaporation is emphasized. Counterflow spray flame structures with different initial and boundary conditions are analyzed. A parametric study of the effects of changing the initial droplet radius and strain rate at the spray side of the configurations is carried out and the effects of evaporation on the definition of the outer flame structure are analyzed and discussed.

In subsection 4.1.2, the non-premixed spray flamelet equations (Eq. (3.84)) are employed to evaluate the relative importance of non-premixed and premixed combustion regimes in counterflow spray flames. This is done in order to determine whether a formulation considering non-premixed and evaporation effects only [42] is enough for describing the flame structure in counterflow spray flames or if the inclusion of premixed effects is required.

The evaluation of the different assumptions made during the derivation of the transport equation of the scalar dissipation rate is carried out in subsection 4.1.3.

Finally, in section 4.2 the effects of evaporation on spray flamelet structures in mixture fraction space is performed. These structures are obtained from projecting the counterflow flame structures into the mixture fraction space [60].

4.1 Spray Flame Structures in Physical Space

In this section, laminar spray counterflow structures are presented and discussed. In subsection 4.1.1, the effects of evaporation on the flame structure is emphasized at low and high strain rate situations. In subsection 4.1.2, the dominant combustion regime in the counterflow flames under consideration is evaluated. The objective of this evaluation is the validation of the non-premixed spray flamelet model [42], which assumes premixed effects are negligible in these flames. Finally, the assumptions adopted during the derivation of the transport equations of mixture fraction and its scalar dissipation rate for spray flames are evaluated in subsection 4.1.3.

4.1.1 Influence of Evaporation

In this subsection, the effects of evaporation on the flame structure are studied in physical space. In general, flame structures strongly depend on strain. In spray flames, this relation is even more important, since the strain rate imposed does not only affect the gas flow field, but also how and where the fuel droplets are evaporated [54, 56, 59, 42, 57, 55, 58, 60].

Figure 4.1 exemplarily shows the velocity profiles of the gas and liquid phases, v_g and v_d, the gas temperature, T_g, and the normalized droplet radius R/R_0, for the basic standard situation considered in the next subsections. A strain rate of 55/s on the spray side of the configuration, an initial droplet radius of 25 µm and an equivalence ratio of unity at the left side of the configuration are considered. At this low strain rate situation, the liquid droplets, injected from the left side of the configuration, penetrate into the flame front and evaporate before they reach the gas stagnation plane, located at an axial position $x = 0$ mm. Two reaction zones are generated, which are separated

by a low temperature region generated by the energy transfer from the gas phase to the liquid phase required for the droplets evaporation. Flames structures are highly sensible to variations of the gas temperature, since this strongly affects chemical reactions. This situation is a clear example of the influence of evaporation on the flame structure. It is also clear from Fig. 4.1 that changes in the initial and boundary conditions will move the evaporation region and, therefore, modify the outer flame structure. Thus, strain rate, the initial droplet radius and droplet velocity and the initial equivalence ratio are very important parameters. In the remainder of this section, a more complete analysis of the influence of evaporation on the flame structure and of the effects of changing strain rate and the initial droplet radius is performed.

4.1.1.1 Low Strain Rate

In the present subsection, the influence of evaporation on the outer flame structure of laminar ethanol/air spray flames at low strain rates is analyzed. Figure 4.2a and 4.2b give a survey of the different cases that are presented and discussed. Figure 4.2a displays the gas temperature profiles (lines without symbols) and the normalized droplet radius (lines with symbols) for different initial droplet radii between 5 and 50 µm, and Fig. 4.2b shows corresponding profiles for initial droplet radii between 50 and 125 µm.

For an initial droplet radius of 5 µm, the droplets enter the hot temperature region of

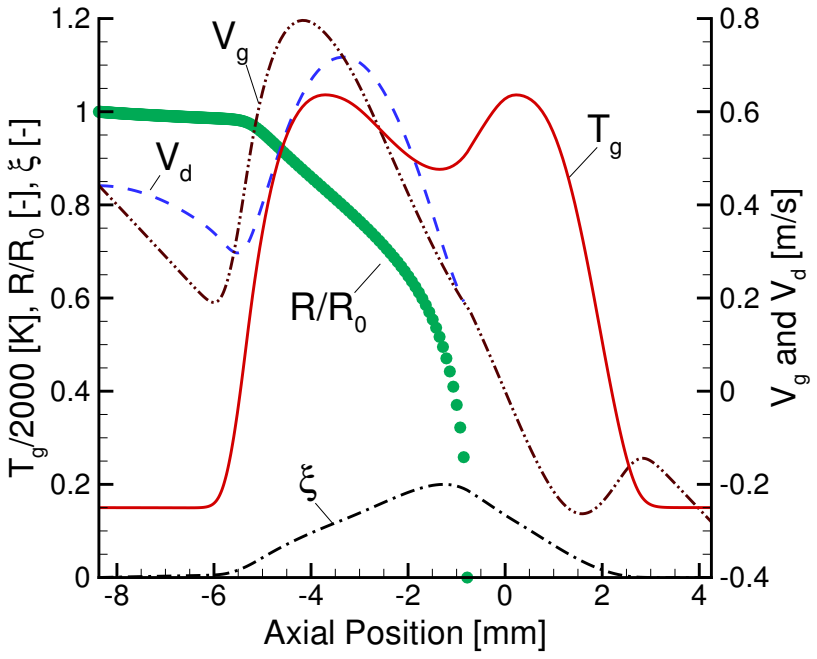

Figure 4.1: Example of gas and droplet velocity profiles

the gas, and they quickly evaporate in an zone extending over 2 mm, providing the fuel vapor for chemical reactions to take place over a wide region of 14 mm (see Fig. 4.2a). The maximum flame temperature is 2.215 K, and the reaction zone is mainly located at the left side of the configuration. A progressive increase of the initial droplet radius retards the evaporation of the droplets, since a longer time is needed for their heating. This leads to a progressive displacement of the evaporation zone to the right side of the configuration, and a decrease of the width of the reaction zone until a minimum value is reached for an initial radius of around $R_0 = 50$ μm, situation for which the droplets slightly cross the gas stagnation plane. After this, any further increment of the initial droplet radius leads to an enhancement of the penetration of the droplets into the gas side of the configuration. This allows the droplets to evaporate in regions where no fuel could be found before, extending the reaction zone to these regions. At high initial droplet sizes, the droplets deeply penetrate into the gas side of the configuration and the droplets are decelerated by the opposed air flow till the droplet movement is reversed, generating a polydisperse spray flame. For sufficiently high initial droplet radius, the droplet can cross back the gas stagnation plane, penetrating again into the left side of the configuration. This can lead to droplet oscillation around the gas stagnation plane, see Fig. 4.2b. This phenomenon is not new and it has been studied in more detail in [54, 59, 82, 83].

For droplet radii higher than 125 μm, it appears that the droplet oscillation becomes so large, that the zone of evaporation is wider than the reaction zone, and the droplets reside outside of the reaction zone on the gas side of the configuration. This leads to a flame instability in such a way that the spray evaporation cannot be achieved any more through the heat release of the chemical reactions, which eventually break down due to energy consumption of the evaporation process. The flame with largest droplet size that could be obtained has an initial droplet radius of 128 μm. This extinction process is novel in the sense that the spray flame does not extinguish due to increased gas strain rate, but to increased need of energy from the gas phase for spray evaporation. The strain that leads to extinction in this situation is imposed by the droplet motion through droplet drag. This interesting mechanism requires more study in future and it has not been identified in the literature so far.

Figure 4.3 shows the maximum gas and spray sided reaction zone temperatures as a function of the initial droplet radius. Two reaction zones develop at about 15 μm. For this initial droplet radius, the spray completely evaporates at an axial position near to -4 mm (see Fig. 4.2), where the local minimum in the gas temperature profile resides. At an initial radius of 25 μm, the two peaks attain about the same flame temperature, see Fig. 4.3. Between an initial droplet radius of 25 and 100 μm, the spray sided flame is hotter than the gas side flame, see Fig. 4.3. This situation occurs

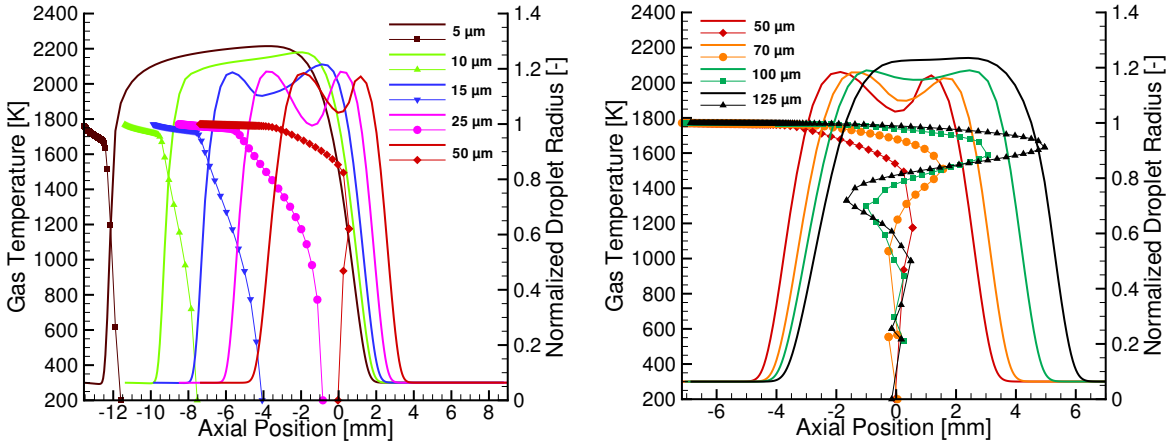

(a) (b)

Figure 4.2: Gas temperature and normalized droplet radius for: (a) initial droplet radii from 5 to 50 µm and (b) from 50 to 125 µm, $a = 55/\text{s}$ [123]

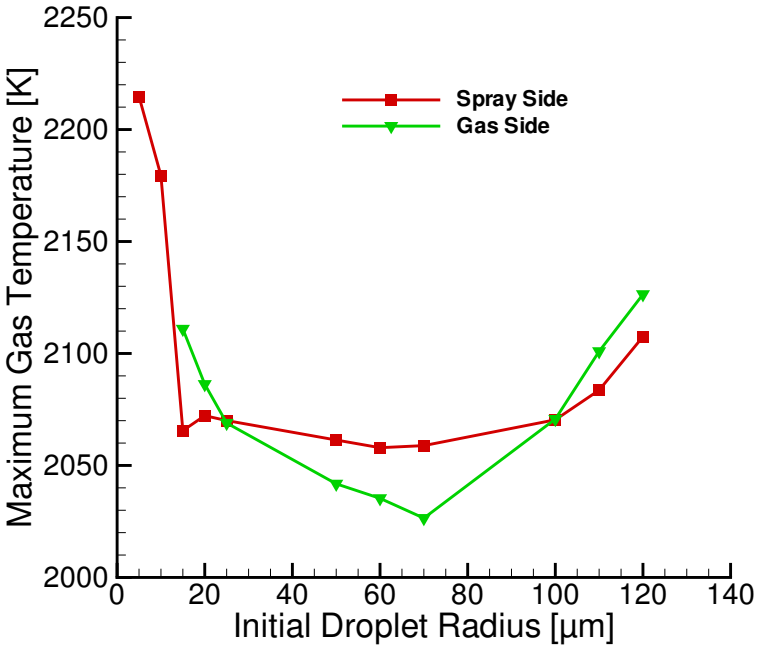

Figure 4.3: Maximum gas temperature versus initial droplet radius for the spray and air sided flame [123]

because of the progressive displacement of the evaporation zone to the right side of the configuration and it is reversed at higher initial droplet sizes (beyond 100 µm), since the penetration of the reversed droplets into the spray side is enhanced. This re-entry

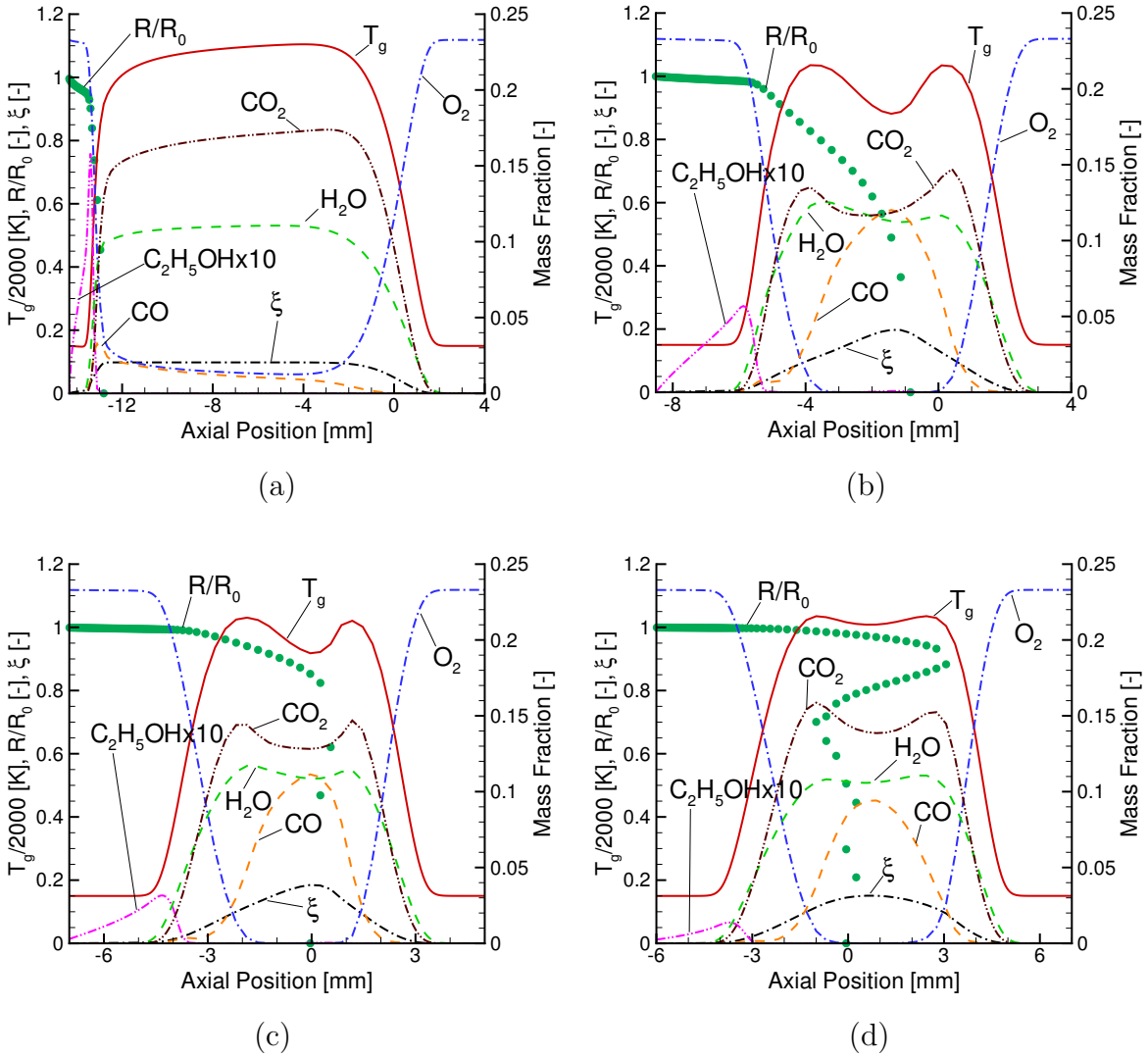

Figure 4.4: Outer ethanol/air flame structure, $a = 55/\text{s}$, $E = 1$, (a) $R_0 = 5$ µm; (b) $R_0 = 25$ µm; (c) $R_0 = 50$ µm and (d) $R_0 = 100$ µm [123]

of the droplets enhances combustion, and therefore, the flame temperatures increase again after a local minimum is reached. The latter increase is typical for spray flames with droplet reversal [59, 83]. For radii higher than 125 µm, the double reaction zone disappears, and a single reaction zone is found again. This single reaction zone is a spray flame and evaporation occurs over its entire extension.

Figure 4.4 shows the outer flame structure for four selected cases. These cases correspond to initial droplet radii of $R_0 = 5$ µm, $R_0 = 25$ µm, $R_0 = 50$ µm and $R_0 = 100$ µm. In the next paragraphs, a detailed study of these selected spray flames is presented.

Considering the profiles of the chemical species shown in Fig. 4.4, typical features of

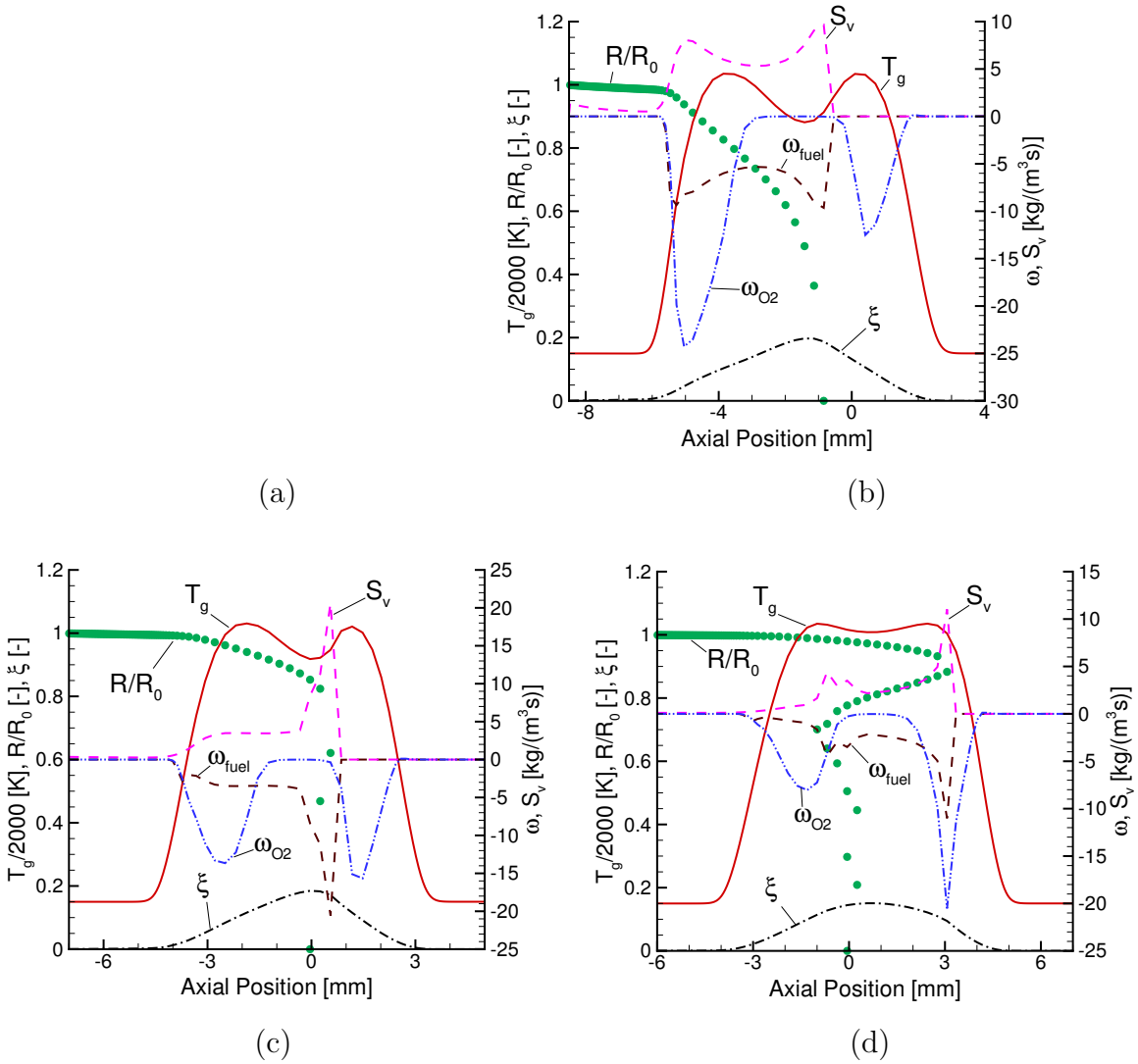

Figure 4.5: Profile of evaporation rate and chemical reaction rate, $a = 55/\mathrm{s}$, $E = 1$, (a) $R_0 = 5$ µm; (b) $R_0 = 25$ µm; (c) $R_0 = 50$ µm and (d) $R_0 = 100$ µm [123]

gas phase chemistry such as formation of CO prior to CO_2 are observed. The principal profiles of H_2O and CO_2 follow the shape of gas temperature whereas the profile of CO attains a maximum value in the area of local minimum of the gas temperature for high initial droplet sizes. Figure 4.5 shows both the mass evaporation rate, S_v, and the specific reaction rates, $\dot{\omega}_k$ of oxygen and ethanol vapor. For $R_0 = 5$ µm (Figure 4.5a), spray evaporation occurs very fast as the spray enters the reaction zone, here a peak of the mass evaporation rate, S_v, is found. At this location, the absolute value of the specific chemical reaction rate of the ethanol vapor is higher than the evaporation rate of liquid ethanol (see Fig. 4.5a), indicating that molecular diffusion is important in this zone as also can be seen from the profile of the fuel vapor. Diffusion is caused by

the accumulation of vapor fuel outside of the chemical reaction zone (see the fuel mass fraction profile in Fig. 4.4a). The specific reaction rate of oxygen is also displayed, and its absolute value is about double the value of fuel vapor which is associated with the stoichiometry of ethanol/air combustion.

For $R_0 = 25$ μm, the spray penetrates deep into the reaction zone and two peaks in the profile of the spray evaporation source term are found. In the situation under consideration, the oxygen chemical reaction rate presents two peak values. One of them occurs near the first peak of spray evaporation (from left to right), whereas the second one is placed at the air side of the flame, and it does not coincide with the the local extremum of fuel consumption. This second peak corresponds to a diffusion flame on the gas side of the counterflow configuration, see Fig. 4.5b.

For a spray with $R_0 = 50$ μm, Fig. 4.5c, it is observed that evaporation is delayed and the evaporation rate at the entrance of the spray into the chemical reaction zone is considerably reduced compared with the corresponding profiles for $R_0 = 5$ μm and $R_0 = 25$ μm. A first droplet reversal is found after the droplets crossed the gas stagnation plane. At the position of droplet reversal, droplets move very slowly and the residence time of the droplet is extended and a peak in the evaporation rate is generated, which is much higher than the one found for $R_0 = 25$ μm. This occurs because for $R_0 = 25$ μm the droplets start to evaporate earlier, reducing the liquid fuel mass available for evaporation at the position of low droplet velocity and high residence time. Figure 4.5c shows how evaporation is concentrated in the reversal position for $R_0 = 50$ μm, whereas its distribution is much more uniform for $R_0 = 25$ μm.

For an initial droplet radius of 100 μm, the high initial momentum associated with the increased droplet size leads to droplets oscillation [81, 82]. For this case, several droplet reversal points are found, which are associated with peaks of the profile of the evaporation rate. Moreover, an additional peak of S_v is found at the stagnation plane (see Fig 4.5d).

Figure 4.6 shows the influence of the evaporation on the scalar dissipation rate profile for the four cases considered here. In laminar gas diffusion flames, the profile of the scalar dissipation rate, χ, attains only one maximum value, which is located at the gas stagnation plane. In spray flames, however, the evaporation dominates the profile of the scalar dissipation rate as discussed for methanol/air spray flames [42]. For small droplet sizes ($R_0 = 5$ μm, and $R_0 = 25$ μm), the droplets do not reach the stagnation plane, and the typical peak value of the scalar dissipation rate at the gas stagnation plane is maintained, since evaporation does not affect this region of the flame [59]. However, in the zone where evaporation takes place, the scalar dissipation rate profile strongly differs from the one that is characteristic for gas flames. In general, the evaporation mass source generates different local mixture states leading to considerably

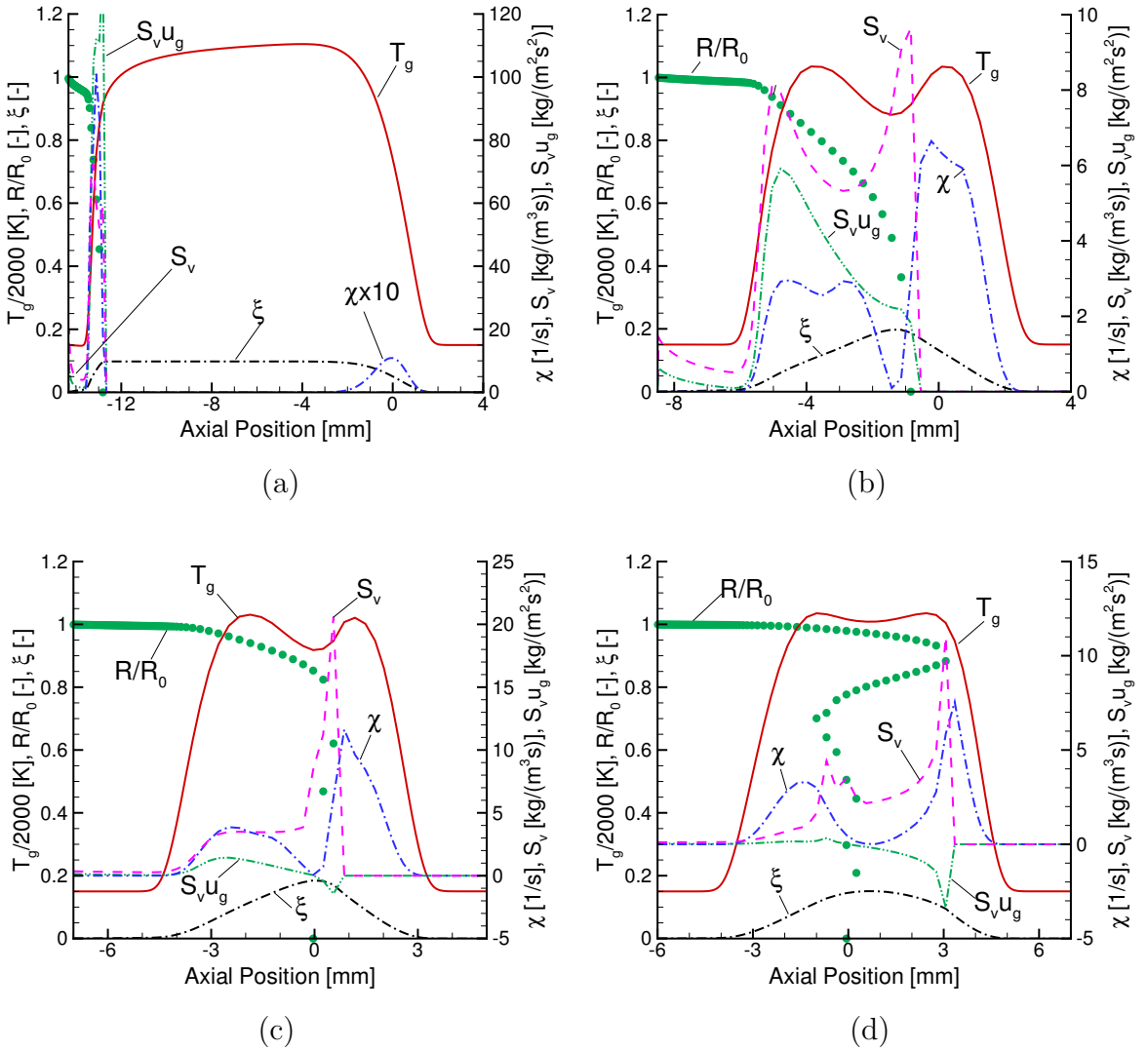

Figure 4.6: Profile of scalar dissipation rate, $a = 55/\text{s}$, $E = 1$, (a) $R_0 = 5$ µm; (b) $R_0 = 25$ µm; (c) $R_0 = 50$ µm and (d) $R_0 = 100$ µm [123]

different values of the gradient of the mixture fraction, where high local values of the scalar dissipation rate are generated. For $R_0 = 5$ µm, see Fig. 4.6a, a peak in the profile of the scalar dissipation rate, additional to the one located at the stagnation plane, is found in the spray zone, whereas for $R_0 = 25$ µm, two extra peaks of the scalar dissipation rate are found in this area (see Fig. 4.6b). When the droplet penetration increases and the droplets cross the stagnation plane, the peak located at the stagnation plane disappear and a new peak of the scalar dissipation rate is generated at the gas side of the configuration, which coincides with the location of the droplet reversal position [42]. For $R_0 = 100$ µm, several droplet reversals occur. The first droplet reversal, generates a peak value at the right side of the configuration, which is very

similar to the one found for the case with $R_0 = 50$ µm. The second reversal point, located at the left side of the configuration coincides with the position of the second peak of the scalar dissipation rate (see Fig. 4.6d). However, the next reversal points do not affect the profile of the scalar dissipation rate. This can be explained by the fact that the further oscillation of the droplets around the gas stagnation plane generates an evaporation profile relatively uniform. This produces a very small gradient of mixture fraction, which leads to a low value of its scalar dissipation rate. The importance of the maximum local values of the evaporation rate generated at the positions of droplet reversal and the associated local maximum of the scalar dissipation rate will be discussed in more detail in the next section. Figure 4.6 shows that the local maximum values of the scalar dissipation rate decrease when the initial droplet radius is increased. This is related to the uniformer profile of mixture fraction observed for cases with large initial droplets.

In the next section, spray flame structures at high strain rates are analyzed. Flame extinction usually occurs with the increase of the gas strain rate, and this strongly affects the flame structure as well as the evaporation effect on the spray flame characteristics discussed so far.

4.1.1.2 High Strain Rate

In this subsection, laminar spray flame structures at different strain rates, from 55/s up to extinction, are presented. Four different initial droplet radius are analyzed, 5 µm, 25 µm, 50 µm and 100 µm.

Figure 4.7 shows the maximum flame temperature versus gas strain rate on the spray side of the counterflow configuration for the different initial droplet sizes under consideration. Non filled symbols show the maximum flame temperatures on the spray side and filled symbols corresponding values on the air side of the configuration, and the lines are drawn for a better visibility of similar conditions. A similar study has been performed in the literature [83], although for conditions different to those studied in the present thesis.

The hottest flame occurs for the smallest initial droplet radius of 5 µm. For low strain, one single reaction zone exists, see Fig. 4.4a, and for strain rates higher than 300/s, a double flame develops where the spray sided flame is always considerably colder than the gas flame on the gas side of the configuration, see Fig. 4.8a. This is due to the evaporation, which takes place at the left side of the configuration over a reduced region of only few millimeters, considerably reducing the gas temperature. At a strain rate of 800/s, extinction occurs for both reaction zones.

For an initial droplet radius of 25 µm, two reaction zones exist at low strain, c.f. Fig. 4.4b, where the gas sided flame is somewhat colder than the flame on the spray

side, which is a consequence of the deep penetration of the spray into the reaction zone. The small difference in the gas temperature at both sides of the configuration is due to the fact that, under these conditions, evaporation takes place in a long region of 8 mm and therefore the energy sink is not concentrated but widely distributed, which leads to a small gas temperature reduction. When the strain rate is increased over 600/s, the reaction zones merge to yield a single one as shown in Fig. 4.7. The flame temperature increases between a strain rate of 600/s and about 1,000/s due to droplet oscillation, and beyond 1,000/s it decreases because of reduced residence time. Extinction of the single reaction zone occurs at 1,035/s. Figure 4.7 shows that the spray flames with an initial droplet radius of 25 µm are most stable compared to the other conditions studied. The spray flames with initial droplet radius of 50 µm behave similar to the 25 µm situation except that the extinction strain rate is much lower (310/s). Figure 4.7 shows that the maximum flame temperature for $R_0 = 100$ µm increases with higher strain rate until extinction is reached at a strain rate of 85/s. This behaviour, which differs from the extinction process of the other flames studied in this section, has been already identified in the literature for other flames [82]. The gas sided flame is somewhat colder than the spray sided flame, which is typical for sprays with large initial droplet radius, which deeply penetrate into the gas sided chemical reaction zone. In summary, it can

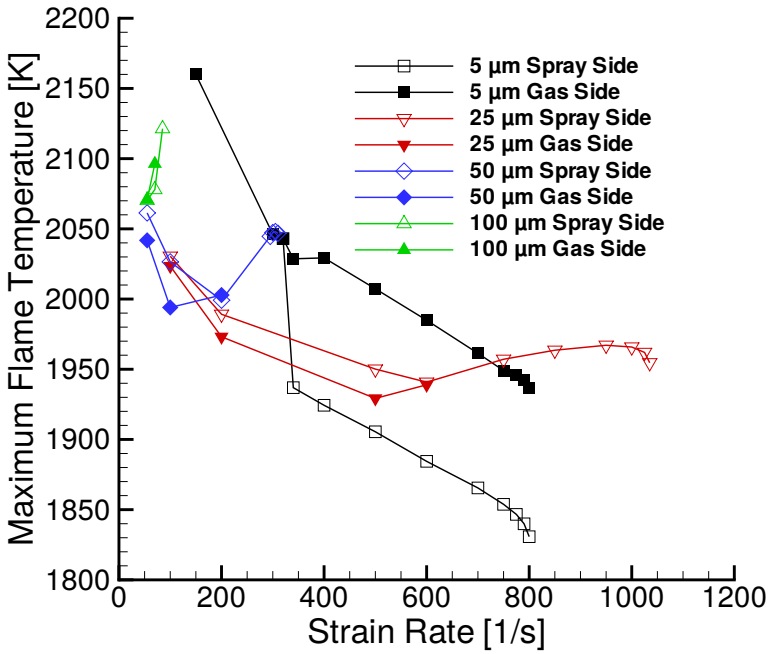

Figure 4.7: Maximum gas temperature versus gas strain rate on the spray side for different initial droplet radii [123]

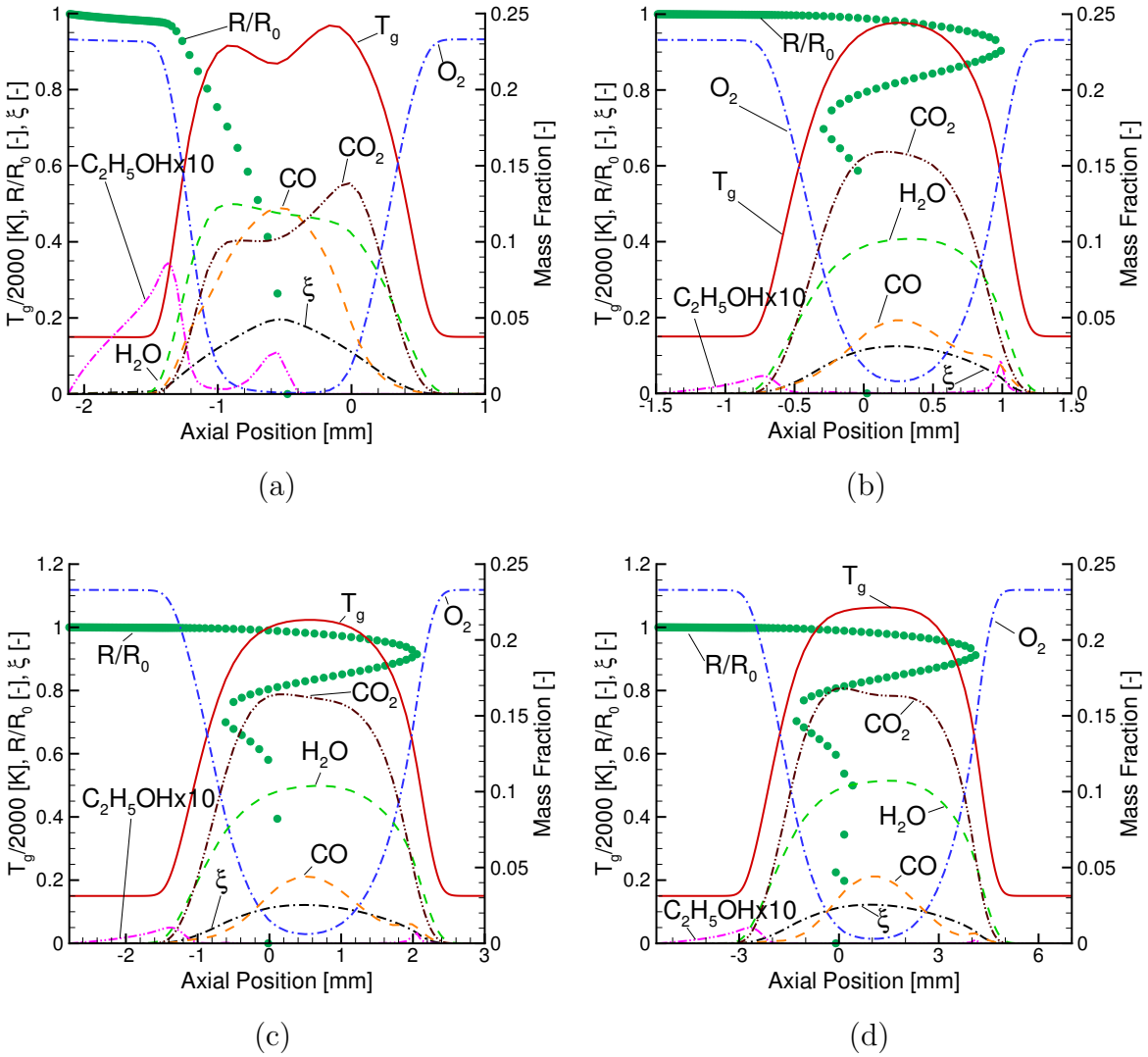

Figure 4.8: Outer ethanol/air flame structure, $E = 1$, (a) $R_0 = 5$ µm, $a = 800$/s; (b) $R_0 = 25$ µm, $a = 1035$/s; (c) $R_0 = 50$ µm, $a = 310$/s and (d) $R_0 = 100$ µm, $a = 85$/s [123]

be seen that the structure of spray flames in the counterflow configuration is greatly dominated by the spray process. In particular, the penetration depth of the spray into the spray sided and the gas sided reactions zones plays a major critical role: the spray penetration depth and possible oscillation determine if the spray or the gas sided flames are hotter and if there are one or two reaction zones in a flame [56, 82].

The outer spray flame structure at extinction for the four different initial droplet radii discussed in this subsection is shown in Fig. 4.8. Figure 4.9 shows the corresponding profiles of evaporation rate and chemical reaction rates, and Fig. 4.10 displays evaporation rates and the scalar dissipation rate. For $R_0 = 5$ µm, a local minimum value

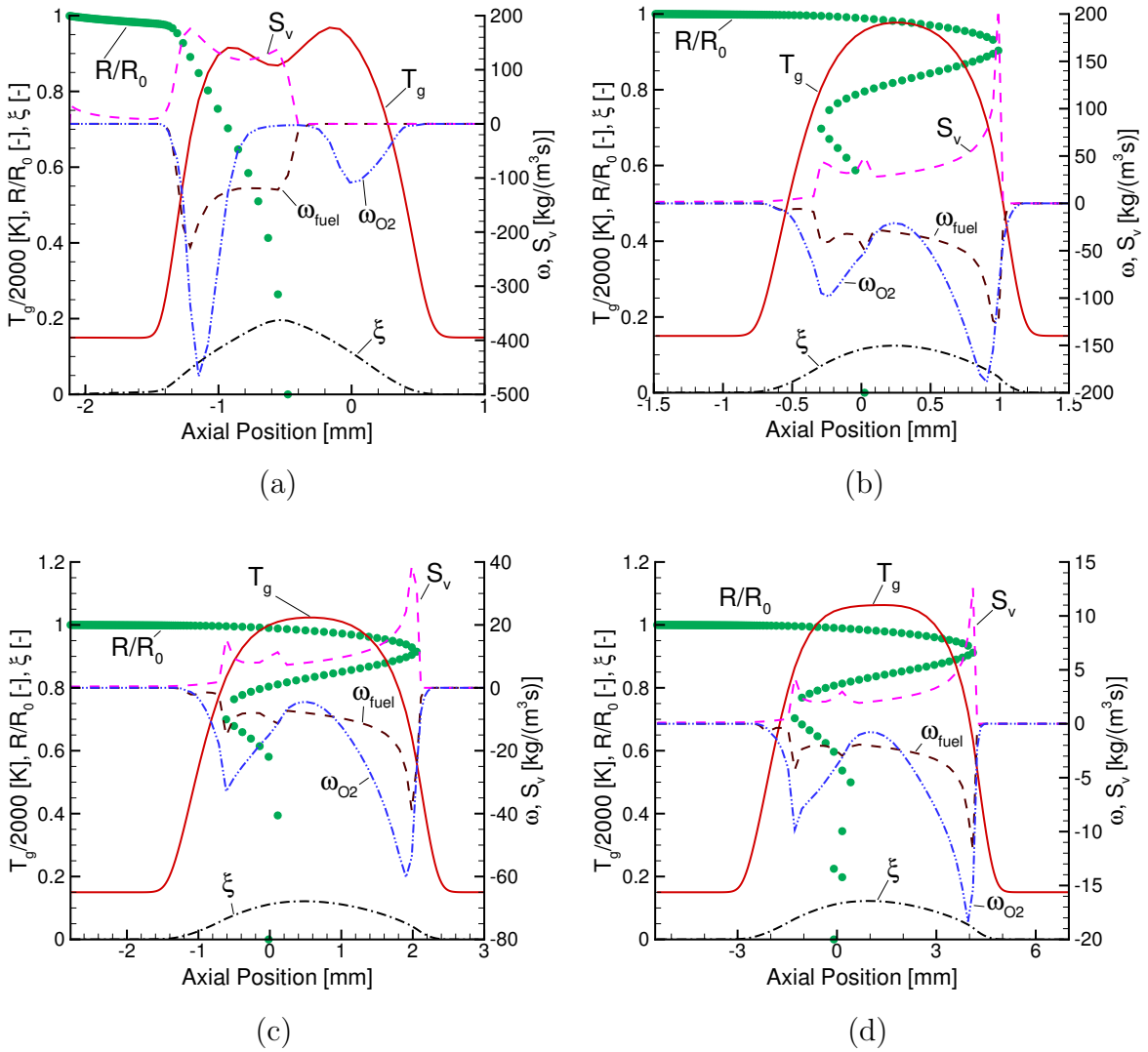

Figure 4.9: Profile of evaporation rate and chemical reaction rate, $E = 1$, (a) $R_0 = 5$ µm, $a = 800$/s; (b) $R_0 = 25$ µm, $a = 1035$/s; (c) $R_0 = 50$ µm, $a = 310$/s and (d) $R_0 = 100$ µm, $a = 85$/s [123]

of the temperature profile is located in the center of the reaction zone, which is similar to the situation for intermediate droplet radii at low strain, c.f. Fig. 4.4b and 4.4c. However, in the low strain results, all fuel vapor is consumed at the left edge of the reaction zone, which differ from the present high strain rate results, where considerable amount of fuel is present. This occurs because chemical reactions are retarded in this region due to the reduced gas temperature, which is also visible in the profile of CO_2, where the first local maximum is much smaller than the second one close to the air side of the configuration, where gas temperature is higher. This retardation is also reflected in the profile of CO, which attains a local maximum where the dip in the gas

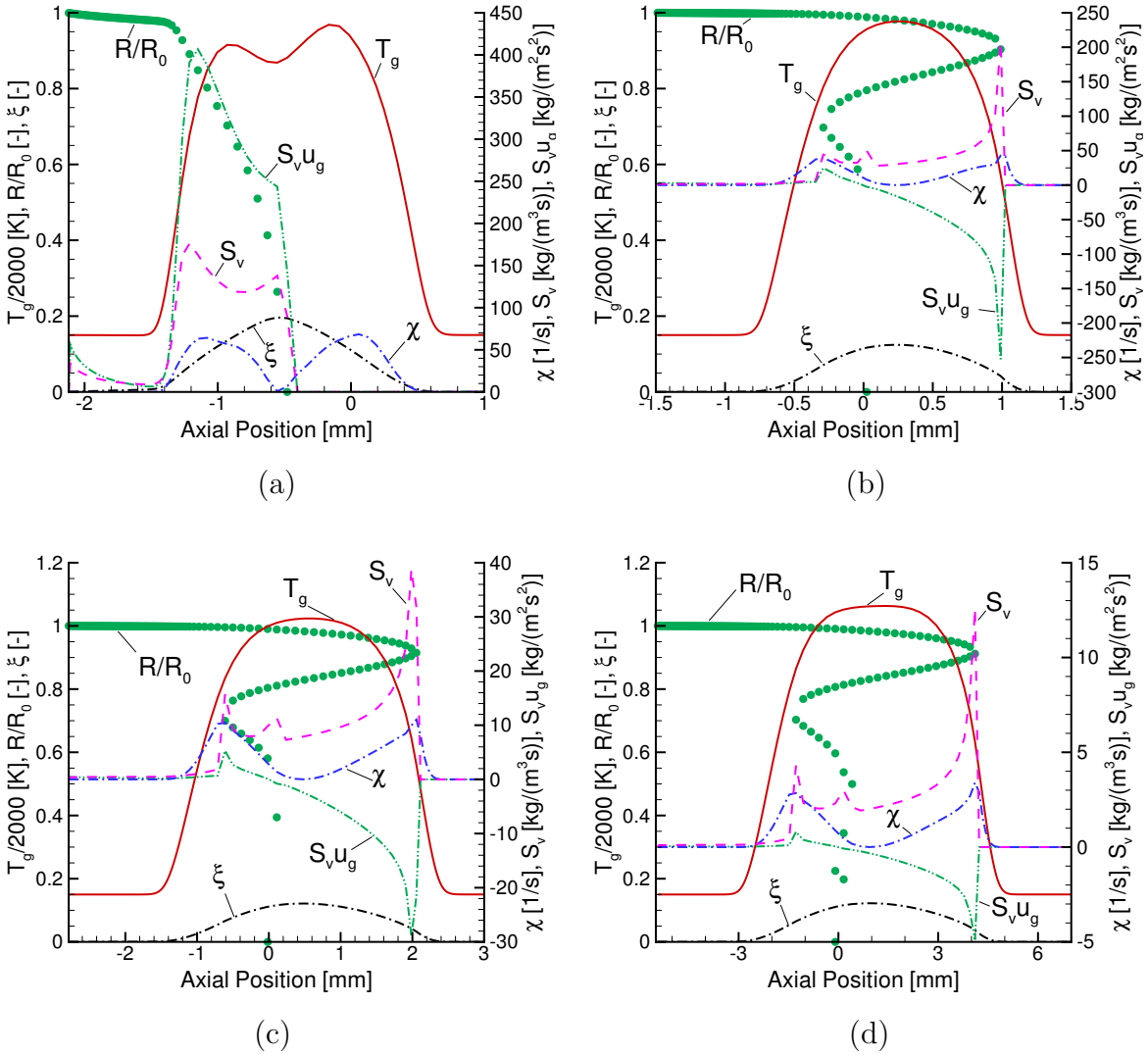

Figure 4.10: Profile of scalar dissipation rate, $E = 1$, (a) $R_0 = 5$ µm, $a = 800$/s; (b) $R_0 = 25$ µm, $a = 1035$/s; (c) $R_0 = 50$ µm, $a = 310$/s and (d) $R_0 = 100$ µm, $a = 85$/s [123]

temperature profile occurs, and here, CO attains higher values than CO_2. As the initial droplet size is increased, spray oscillation occurs and broadens the spray flame, and a single reaction zone is visible, which moves towards the gas side of the configuration.

Figure 4.9 shows the profiles of the chemical reaction rate of the fuel vapor and oxygen, and the evaporation rate for the four cases under consideration. For $R_0 = 5$ µm, the chemical reaction rate of fuel overweights the evaporation at the left edge of the reaction zone (see Fig. 4.9a). This occurs because of the peak of ethanol vapor observed outside of the reaction zone (see Fig. 4.8a). This fuel vapor diffuses into the chemical reaction zone and feeds the flame. In the center of the reaction zone, this

diffusion is not present and therefore the chemical reaction rate of fuel balances the evaporation rate. For $R_0 = 25$ µm, droplet oscillation is found, which generates an extension of the evaporation rate over the entire reaction zone (see Fig. 4.9b). The fuel vapor mass peak located at the left edge of the reaction zone is considerably reduced, due to the delay in the evaporation rate generated by the increased droplet size, which increases the time required for droplet heating and evaporation. For this reason, the fuel diffusion into the main reaction zone is very low compared with the previous situation considered. This can be also observed in the profile of chemical reaction and evaporation rate (see Fig. 4.9b), which show how these two terms balance. This means that all fuel reacting in this flames comes from the local evaporation alone. A second peak of the fuel mass fraction is located at the gas side of the configuration, at the location of the reversal point, see Fig. 4.8b. This peak appears due to the peak of evaporation at this location, which is related with the low droplet velocity at this point. The profile of the reaction rate of oxygen presents two peak values, which coincide with the peak values of the evaporation rate. This occurs because in these regions fuel is feeded in high quantities by evaporation. The radicals coming from the decomposition of the fuel react with oxygen near to the peaks of evaporation. For $R_0 =$ 50 µm and $R_0 = 100$ µm the profiles of chemical reaction rates and evaporation are qualitatively similar to the ones observed for $R_0 = 25$ µm. It is observed, however, that the width of the reaction zone increases when the initial droplet size is increased. This is associated with the increase of the oscillation of the spray, which is attributable to the higher momentum and the already explained delay in evaporation associated with the increased droplet size.

Figure 4.10 shows the scalar dissipation rate profile and the profile of the product $S_v u_g$ for the four different initial droplet radii studied. For $R_0 = 5$ µm two local maxima are found in the profile of the scalar dissipation rate of the mixture fraction. These peaks are located at the left and right side of the configuration, respectively. Under these conditions, the droplets do not reach the stagnation plane, and therefore, the gas sided peak of the scalar dissipation rate is found at the gas stagnation plane, which is typical for gas phase combustion. For bigger initial droplet radii, the scalar dissipation rate presents two peak values, which are associated with the first and second droplet reversal points. It is observed that the local maxima of the profile of the product of the gas velocity, u_g, and the evaporation rate, S_v, coincides with the local maxima of the scalar dissipation rate, χ, which does no longer coincide with the stagnation plane as in gaseous counterflow flames. As already explained, this situation was studied earlier for methanol/air spray flames [42]. The present simulations for the fuel ethanol confirm this finding.

In the next section, the multi-regime spray flamelet equations are employed to

evaluate the contribution of premixed effects to the definition of the flame structure in laminar counterflow spray flames.

4.1.2 Evaluation of the Dominant Combustion Regime

In this section, the derived multi-regime spray flamelet equations are employed to evaluate whether premixed-like effects are negligible in counterflow spray flames, where the fuel is completely injected in liquid phase. The goal of this evaluation is to confirm that the spray flamelet model of Hollmann and Gutheil [42, 59] is appropriate for this kind of flames.

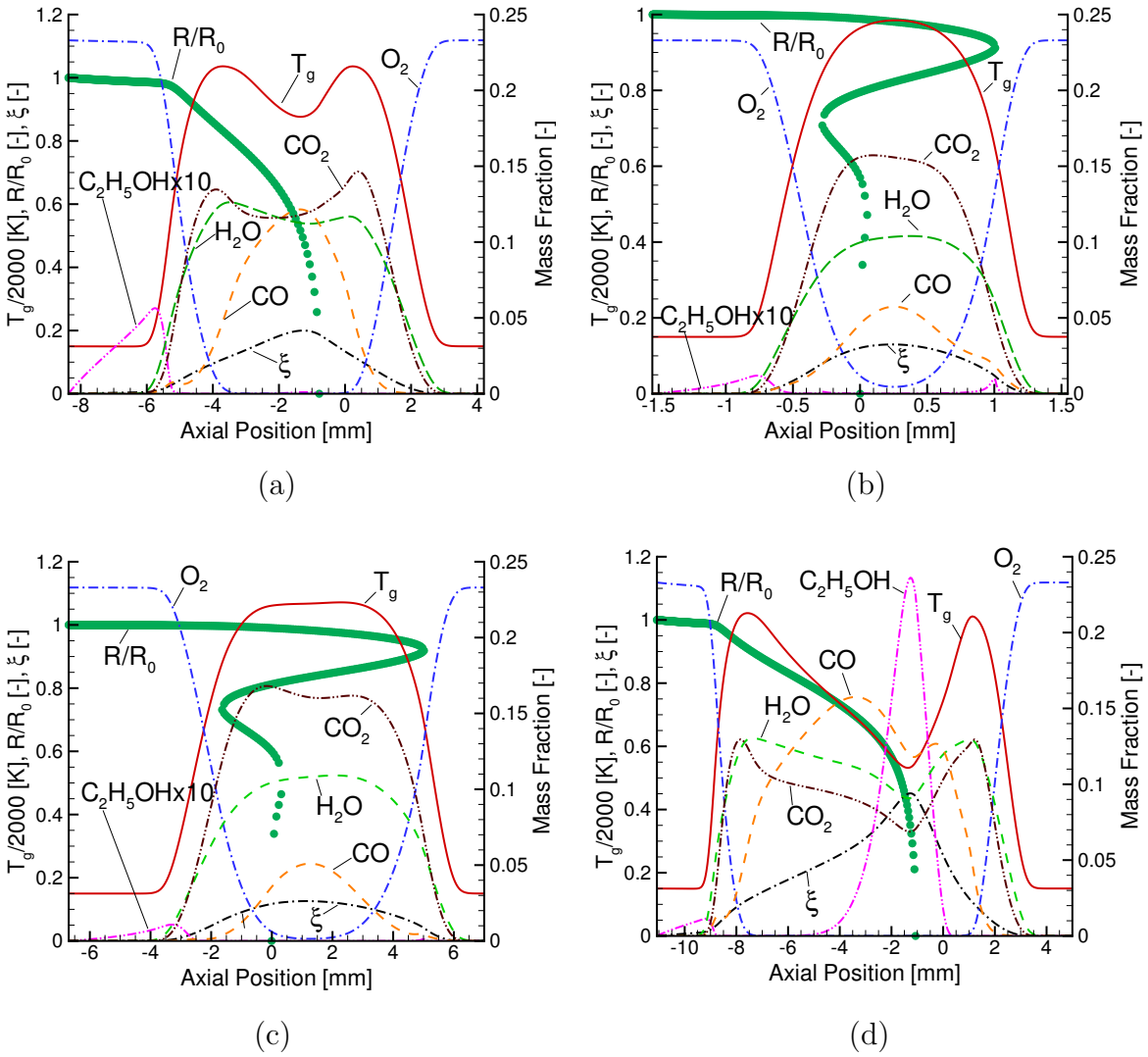

Figure 4.11: Outer ethanol/air flame structure, (a) $R_0 = 25$ µm, $a = 55$/s, $E = 1$; (b) $R_0 = 25$ µm, $a = 950$/s, $E = 1$; (c) $R_0 = 100$ µm, $a = 55$/s, $E = 1$ and (d) $R_0 = 25$ µm, $a = 55$/s, $E = 3$ [109]

Four different combinations of spray-sided strain rates, a, equivalence ratio, E, and initial droplet radius, R_0, are considered for this evaluation. In particular, the situation at $a = 55/\text{s}$, $E = 1$, and $R_0 = 25$ µm presented in the previous section is taken as reference condition, and then one of the parameters is modified to study their influence on the spray flame structure.

Figure 4.11a shows the outer spray flame structure for the reference conditions, whereas Fig. 4.11b shows the corresponding outer spray flame structure when the strain rate is increased to 950/s, which is close to extinction occurring at 1.035/s [60]. Figure 4.11c shows the outer flame structure for an increased initial droplet radius of 120 µm. This condition is close to extinction, which occurs for R_0 =128 µm [123]. As already explained before, this extinction process occurs due to the increased droplet evaporation, leading to flame extinction not due to flame strain but due to reduced flame temperatures caused by enhanced spray evaporation. Finally, Fig. 4.11d shows the corresponding structure for the reference case and an increase of the equivalence ratio to $E = 3$.

The reference flame has been already discussed in the previous section and will not be discussed here again. In the situation with the increased strain rate (Fig. 4.11b), the two reaction zones observed for low strain rate merge [83, 59], and a single reaction zone is found. This situation is very similar to the extinction situation already discussed in the previous section (see Fig. 4.8b), where the droplets cross the stagnation plane, and they are then decelerated by the opposed air stream, leading to droplet oscillation around the stagnation plane, generating local poly-dispersity of the spray [59, 60, 82, 83].

In the situation with increased initial droplet radius (Fig. 4.11c), the very large droplets cause slow evaporation due to the retarded droplet heating [126], and the droplets penetrate the spray flame and exit the reaction zone towards the gas side of the configuration, so that reversal in the colder flame region on the gas side of the configuration occurs, leading to droplet oscillation. Since this case is very similar to the situation with a initial droplet radius of 100 µm explained in the previous section, no detailed analysis of its outer flame structure is given here.

Finally, in the situation with increased equivalence ratio (Fig. 4.11d), all droplets evaporate before reaching the stagnation plane, and a mono-disperse spray prevails throughout the computational domain. Similarly to the reference case, two reaction zones are found for the fuel-rich case under consideration. However, due to the increased equivalence ratio, which implies a higher amount of mass to be evaporated, the energy required for droplet evaporation is much higher than in the reference case and therefore, the minimum temperature between the reaction zones is much lower reaching a value of 1.063 K, which may be compared to 1752 K for the reference case.

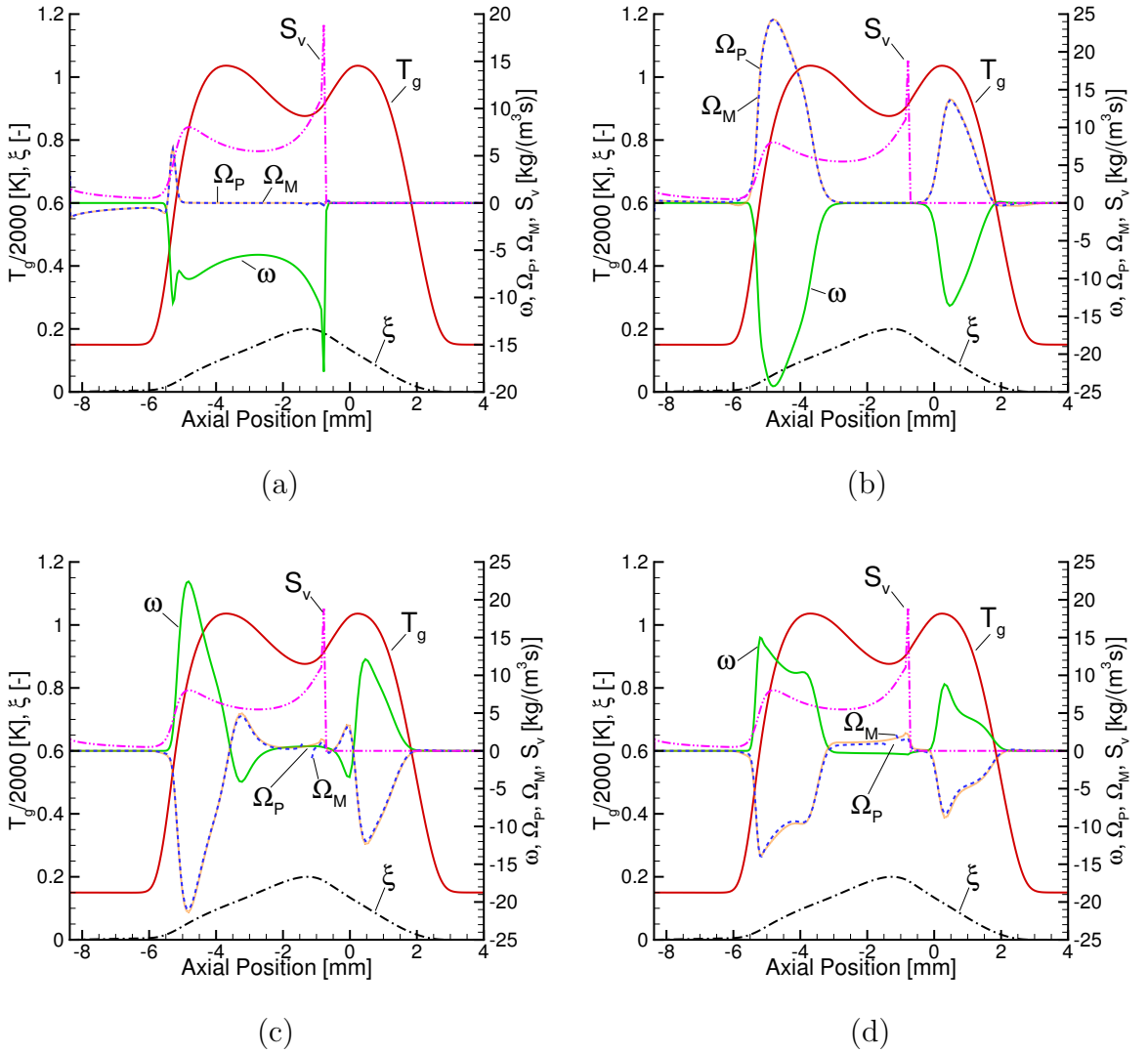

Figure 4.12: Profiles of Ω_P and Ω_M for (a) C_2H_5OH (b) O_2 (c) CO_2 and (d) H_2O, for the reference case, cf. Fig. 4.11a [109]

In the remainder of this subsection, a comparison of the terms Ω_P and Ω_M, defined by Eqs. (3.86) and (3.87), is presented for representative chemical species. For each of the four conditions considered in this section, the chemical species ethanol, oxygen, and the two reaction products, CO_2 and H_2O, are investigated. Figures 4.12-4.15 show the evaluation of Ω_P and Ω_M, cf. Eqs. (3.86) and (3.87), for the relevant species. Additionally, profiles of evaporation rate, S_v and of the specific chemical reaction rate, $\dot{\omega}_k$ are presented as reference. For the present spray flames with pure air on either side of the configuration, the mixture fraction varies from zero to a maximum value, and then it falls to zero again at the air side of the configuration. At the location of the maximum value of the mixture fraction $\partial\xi/\partial y = 0$, and the one-dimensional transformation

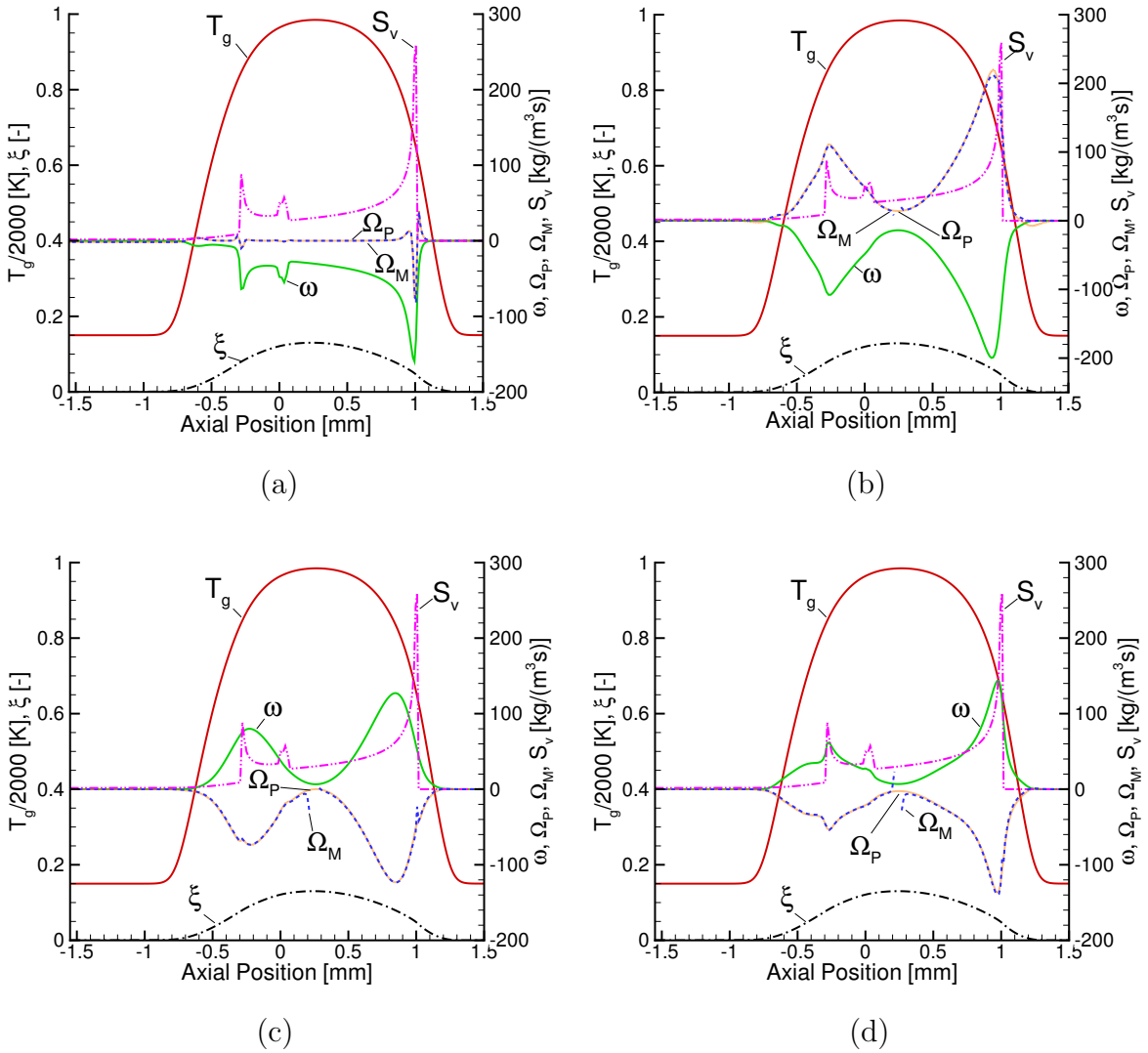

Figure 4.13: Profiles of Ω_P and Ω_M for (a) C_2H_5OH (b) O_2 (c) CO_2 and (d) H_2O, for $a = 950$, cf. Fig. 4.11b [109]

breaks down. However, this occurs only in a single point of the computational domain and therefore, it is not relevant for the global performance of the flamelet equations evaluated in this paper.

Figure 4.12a displays the profiles of $\dot{\omega}_k$, S_v, Ω_P, and Ω_M for ethanol at the reference conditions ($a = 55/\text{s}$, $E = 1$ and $R_0 = 25$ µm). The profiles of both the evaporation rate and the specific reaction rate attain relatively high absolute values over the entire range of the spray flame, where both evaporation and combustion occur simultaneously. Since ethanol is an evaporating species, the chemical source term is mainly balanced by the evaporation term, and only a small contribution of the transformed terms is found. However, the terms Ω_P and Ω_M balance, which means that a one-dimensional flamelet

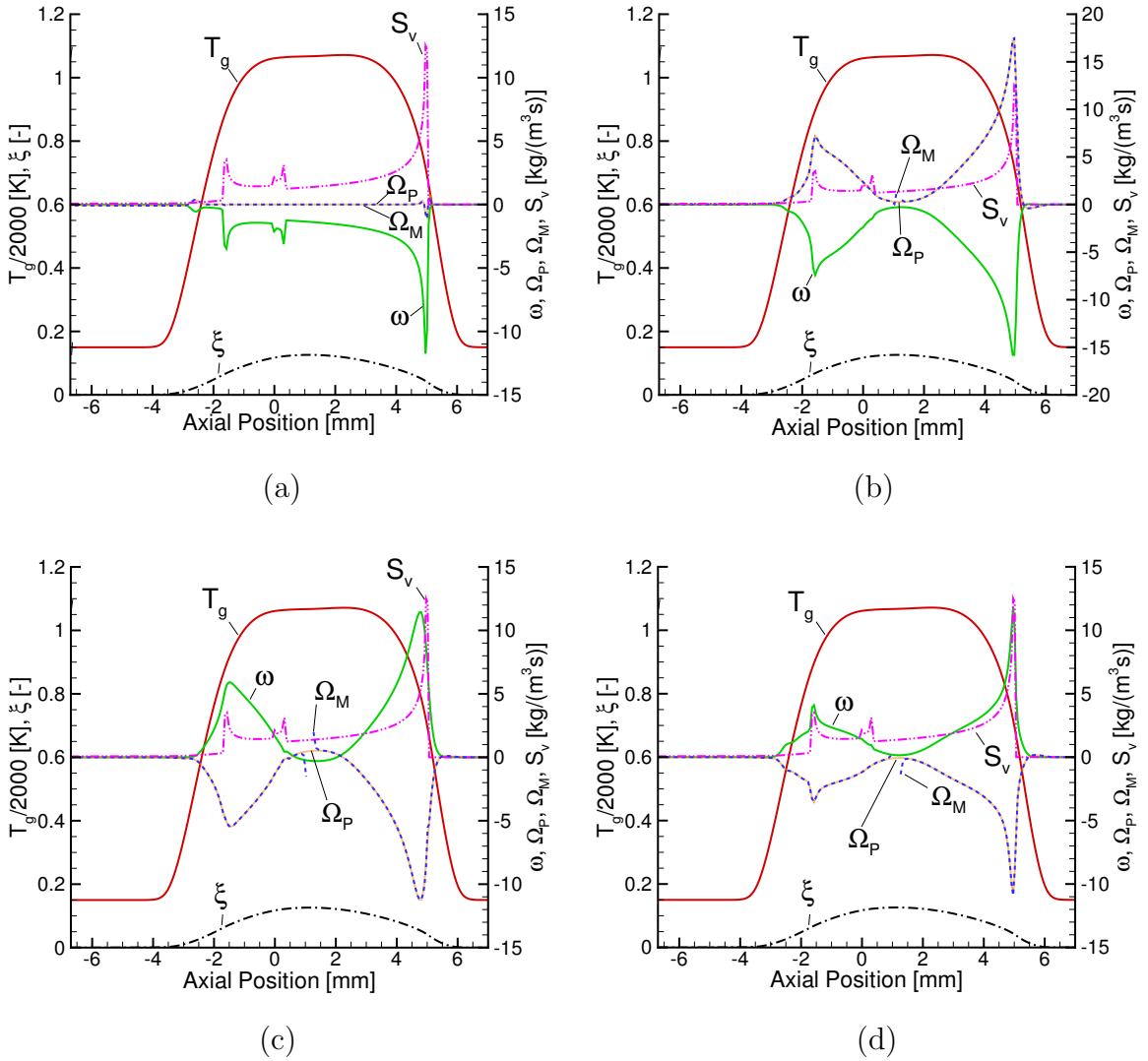

Figure 4.14: Profiles of Ω_P and Ω_M for (a) C_2H_5OH (b) O_2 (c) CO_2 and (d) H_2O, for $R_0 = 100$ μm, cf. Fig. 4.11c [109]

transformation based on the mixture fraction performs very well and thus, premixed-like effects are not relevant for the profiles of ethanol vapor under these conditions.

Figure 4.12b shows corresponding profiles of Ω_P and Ω_M for O_2. Oxygen is not an evaporating species, so that convective and diffusive effects play the important role in balancing the chemical source term $\dot{\omega}_k$, cf. Eq. (3.84), replacing the role of the evaporation rate for the fuel vapor. The figure shows that the transformed terms in mixture fraction space are equivalent to those in physical space over the entire computational domain. The corresponding profiles for CO_2 and H_2O are shown in Figs. 4.12c and 4.12d, respectively. A comparison of these profiles with those of oxygen reveals that the terms are largely the same as for oxygen, except for that they are

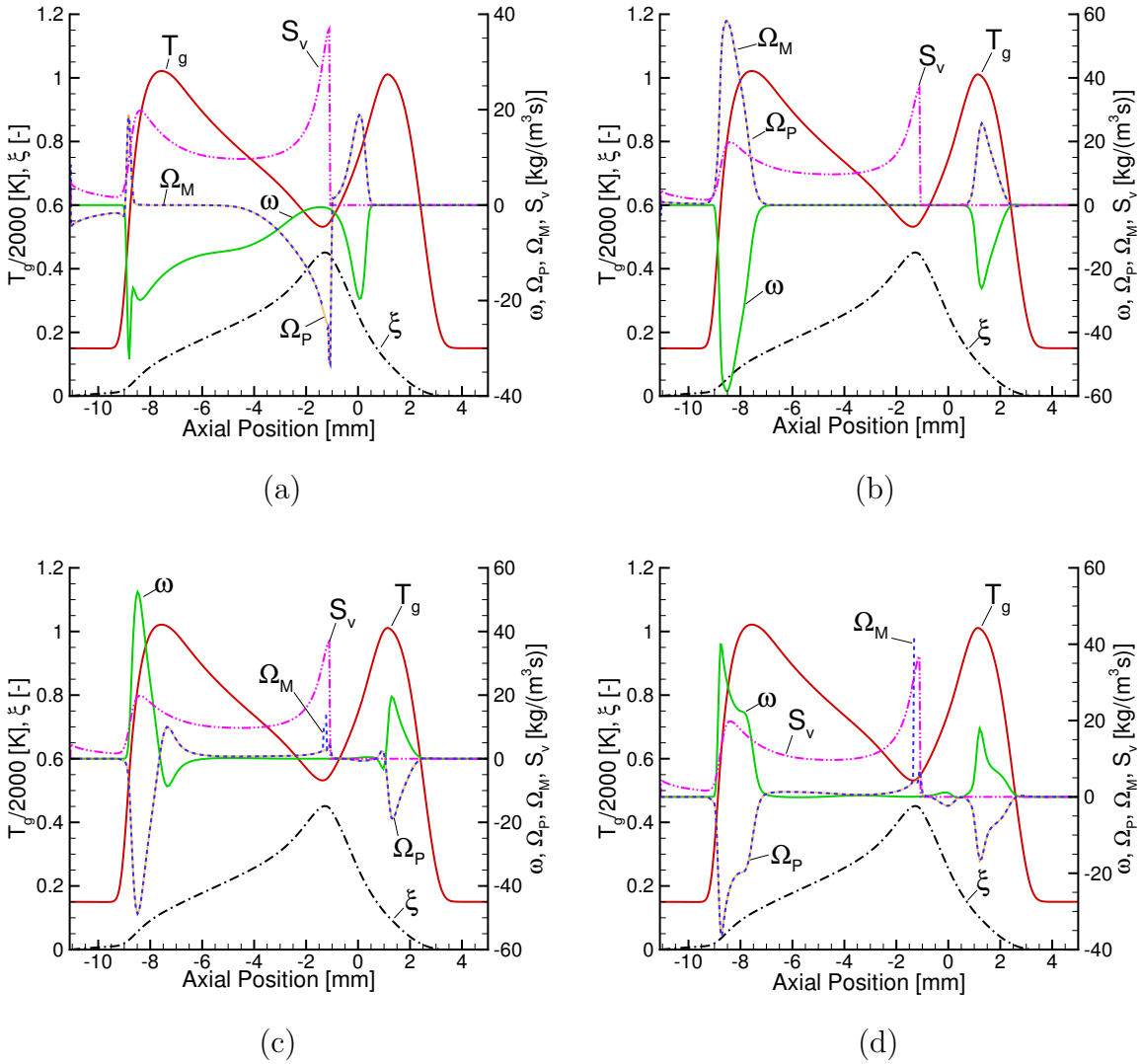

Figure 4.15: Profiles of Ω_P and Ω_M for (a) C_2H_5OH (b) O_2 (c) CO_2 and (d) H_2O, for $E = 3$, cf. Fig. 4.11d [109]

negative since CO_2 and H_2O are reaction products, whereas O_2 is a reactant.

Figure 4.13 displays the evaluation of Ω_P and Ω_M for the high strain rate situation (Fig. 4.11b). The results are qualitatively the same as for the reference situation, which shows that the one-dimensional description of counterflow spray flames is also valid at high strain rate prior to extinction. The corresponding profiles of Ω_P and Ω_M for the situation with increased initial droplet size are displayed in Fig. 4.14. It is found that under these conditions, the terms Ω_P and Ω_M are also equivalent.

Finally, Fig. 4.15 shows the corresponding evaluation for a situation with an increased equivalence ratio of 3. At this condition, two pronounced reaction zones are found, separated by a region of low temperature caused by droplet evaporation. Al-

though this structure seems very similar to the one for the reference case, big qualitatively differences exist in the region of reduced temperature where a high accumulation of fuel vapor is observed. This accumulation is caused by the retardation of chemical reactions due to the low gas temperature due to evaporation. The results obtained for this condition also show the equivalence between Ω_P and Ω_M.

In summary, it is found that evaporation-dominated combustion regimes in monodisperse ethanol/air counterflow spray flames can, in general, be properly described by a set of one-dimensional non-premixed spray flamelet equations in the mixture fraction space. This finding formally confirms the validity of the use of counterflow diffusion spray flames as the basic flamelet structure composing turbulent spray flames when non-premixed and evaporation controlled combustion regime coexist and validates the assumption of small premixed effects adopted by Hollmann and Gutheil [42]

4.1.3 Analysis of the Scalar Dissipation Rate

In this subsection, the evaluation of the different assumptions commonly employed in the literature for the derivation of transport equations of mixture fraction and its scalar dissipation rate is carried out for the counterflow spray flames presented in Figs. 4.11a and 4.11b. The assumptions investigated are the consideration of unity Lewis number, which allows the use of $D = \lambda/(\rho C_p)$ for the calculation of the diffusion coefficient of the mixture, and the assumption of spatial uniformity of the mean molecular weight of the mixture, which implies $\frac{\partial \overline{M}}{\partial x_i} = 0$ and allows great simplifications of the transport equation of the scalar dissipation rate. The evaluation is carried out as follows

- All species transport equations (Eqs. (3.3)) are solved and the results are employed to calculate the value of the mixture fraction and its scalar dissipation rate by definition. The results obtained are denoted as ξ_e and χ_e, and they are the reference values for the present evaluation.

- The transport equations of the mixture fraction and its scalar dissipation rate are simplified by neglecting spatial variations of the mean molecular weight (Eqs. (3.79) and (3.80)), and they are solved. The equations are solved twice, using different approximations for the evaluation of the diffusion coefficient, D. First, the diffusion coefficient is determined through use of the average diffusion coefficient of the mixture, i.e. $D = \sum_{k=1}^{N} Y_k D_k$, and the results are denoted by ξ_D and χ_D. Then, the assumption of Lewis number of unity is adopted, which leads to $D = \lambda/(\rho C_p)$. The results obtained are denoted as ξ_{Le} and χ_{Le}, respectively. A comparison of these results with the reference values ξ_e and χ_e, is presented in Fig. 4.16.

- The value of D_e (see Eq.(3.64)), which is the diffusion coefficient that ensures the exactness of employing an unique diffusion coefficient for all diffusion species, is calculated in the entire domain. The results are compared with the values obtained by using $D = \lambda/(\rho C_p)$ and $D = \sum_{k=1}^{N} Y_k D_k$, in order to determine which of these approximations is a better choice. These comparisons are presented in Figs. 4.17a and 4.17b, for low and high strain rate, respectively.

- Finally, the full transport equations of the mixture fraction and its scalar dissipation rate are solved, which include spatial variations of the mean molecular weight, $\overline{M}$ ((Eqs. (3.74) and (3.75)). For this case, a mass averaged diffusion coefficient of the mixture, i.e. $D = \sum_{k=1}^{N} Y_k D_k$, is employed. The results are denoted as $\xi_{D,M}$ and $\chi_{D,M}$ and they are compared with the results obtained when the same diffusion coefficient is employed, but gradients of the mean molecular weight of the mixture are neglected (ξ_D and χ_D). Additionally, a comparison with the reference values ξ_e and χ_e is performed. The results are displayed in Figs. 4.17c and d.

Figures 4.16a and 4.16 b show profiles of the exact and transported mixture fraction, ξ, and scalar dissipation rate, χ, for $a = 55/\text{s}$. As explained above, the transported values shown in these figures are obtained by means of simplified transport equations (Eqs. (3.74) and (3.75)), which do not consider spatial variations of the mean molecular weight of the mixture. In Fig. 4.16a, Le = 1, i.e. $D = \rho/(\lambda C_p)$ is used, and in 4.16b, the mean average diffusion coefficient, D, of the mixture is employed. A comparison of the profiles of the mixture fraction shows that the differences between transported and exact values is negligible if the average diffusion coefficient is used, but the assumption of Le = 1 results in somewhat higher values for the transported ξ. A comparison of the profiles of the scalar dissipation rates, reveals that the differences between transported and exact values are bigger when compared to the ones obtained for the mixture fraction. This can be attributed to the fact that the gradient of the mixture fraction is involved in the definition of the scalar dissipation rate, leading to a higher sensitivity of the scalar dissipation rate to the errors introduced by the approximations done in the diffusion coefficient. Use of the assumption of Le = 1 results in somewhat lower values of χ. Considering the results presented in Figs. 4.16a and 4.16b, it can be stated that for low strain the mass averaged diffusion coefficient performs better than the diffusion coefficient obtained employing the assumption of unity Lewis number. This is especially true for the profile of the scalar dissipation rate, since the assumption of unity Lewis number tends to under-predict the peak value of the scalar dissipation rate located at the right hand side of the counterflow configuration.

Figures 4.16c and 4.16d show corresponding profiles of ξ and χ at high strain, $a = 950/\text{s}$. Although the results are qualitatively similar to those obtained for the

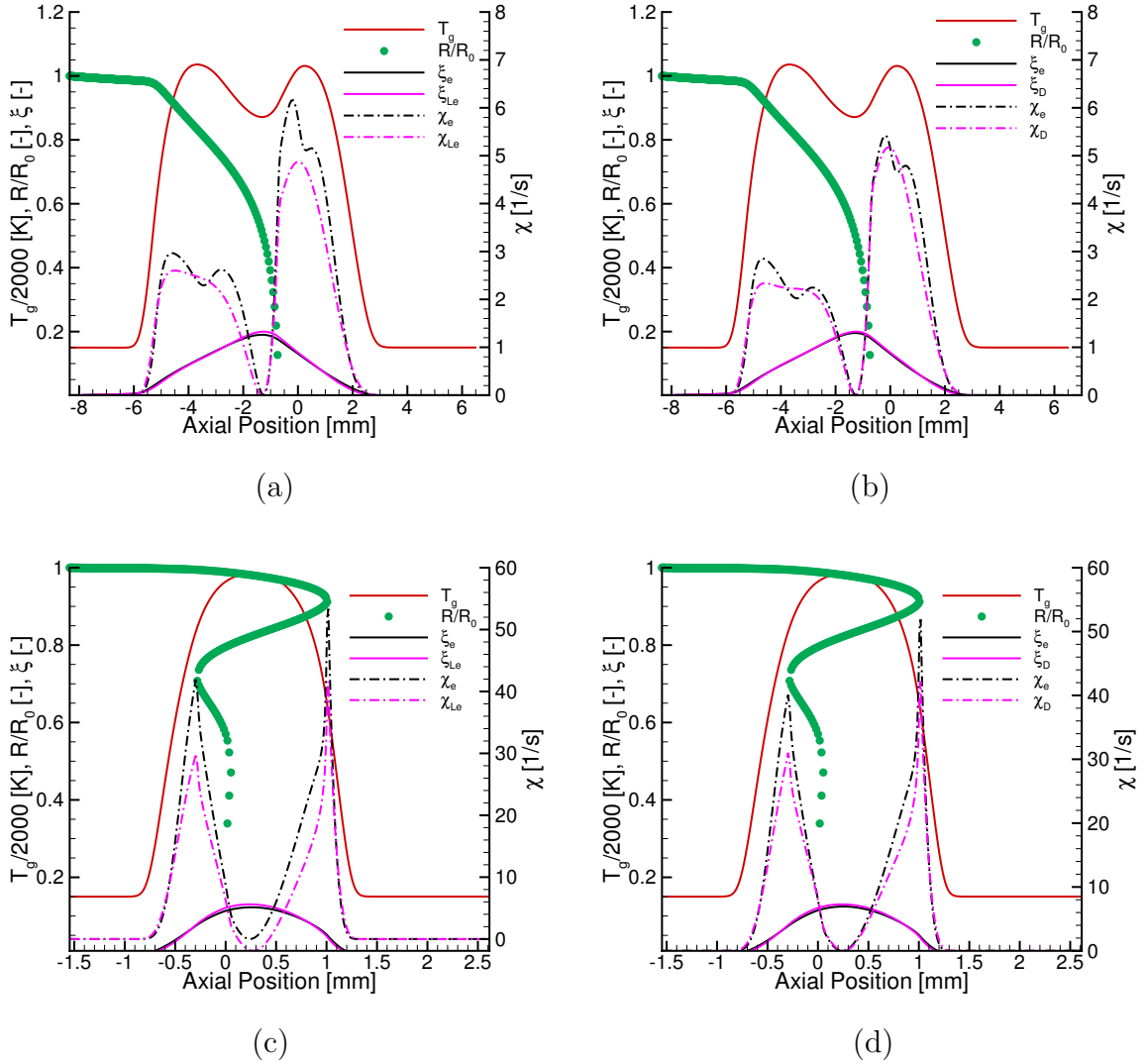

Figure 4.16: Profiles of ξ_e, ξ_{Le}, χ_e and χ_{Le} using (a) $D = \rho/(\lambda C_p)$; (b) averaged diffusion coefficient D, for $a = 55/\text{s}$ and (c) $D = \rho/(\lambda C_p)$ and (d) averaged diffusion coefficient D, for $a = 950/\text{s}$. [109]

low strain rate situation, the assumption of unity Lewis number leads to unphysical results for the scalar dissipation rate χ, predicting a negative value near to the axial position $x = 0$ mm (see Eq. (4.16c)). These results clearly show the inadequacy of the assumption of unity Lewis number in this situation.

Figures 4.17a and 4.17b show profiles of the mass averaged diffusion coefficient, D_{MA}, the diffusion coefficient obtained employing the assumption of unity Lewis number, $D_{\text{Le=1}}$, and the diffusion coefficient that ensures the validity of employing an unique diffusion coefficient for all chemical species, D_{e}, which is calculated using Eq. (3.64). Both, low and high strain rate situations are considered. The profiles of D_{e} show a

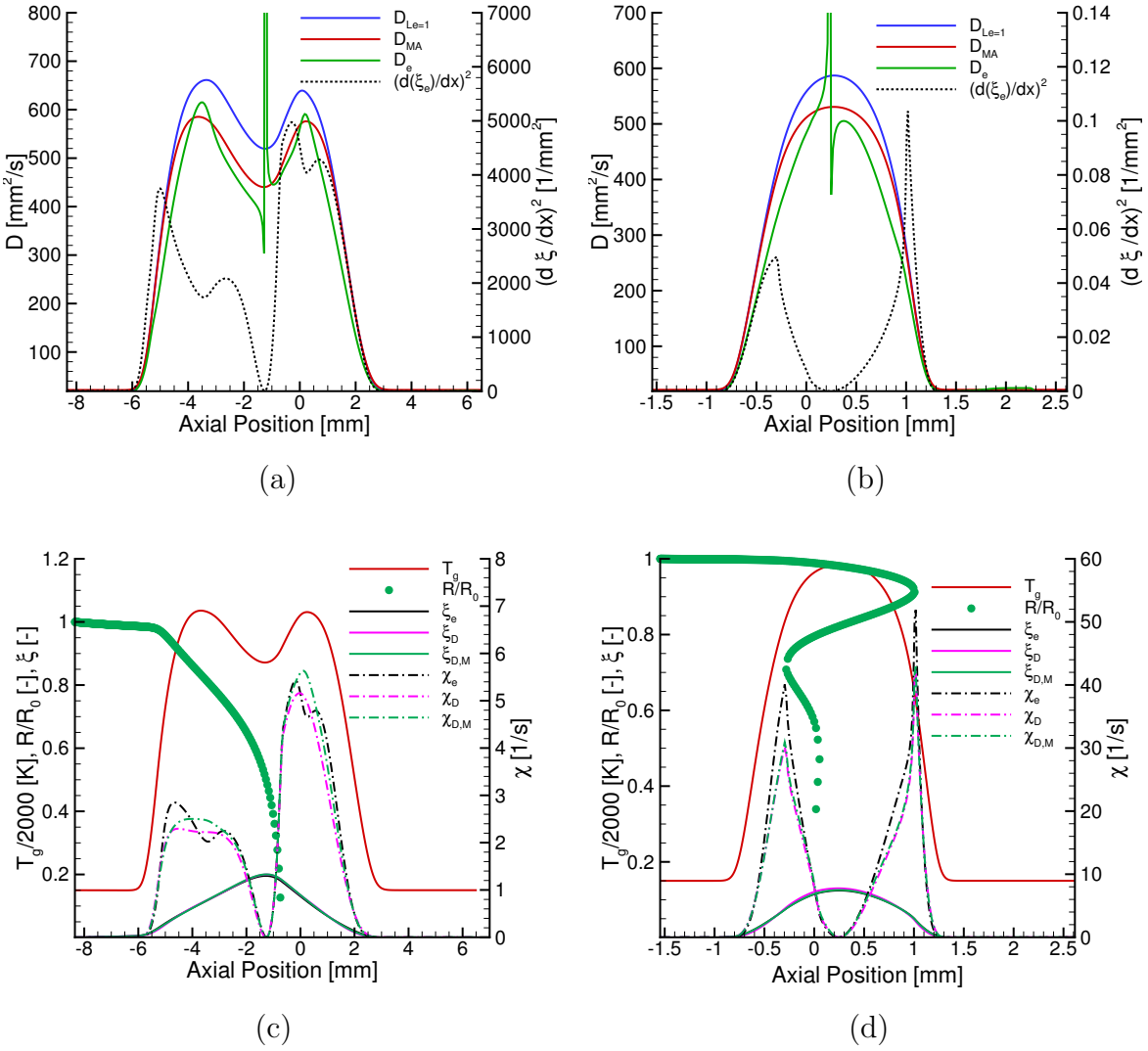

Figure 4.17: Diffusion coefficients of the mixture for (a) $a = 55/\text{s}$; (b) $a = 950/\text{s}$ and profiles of ξ_D, $\xi_{D,M}$, χ_D and $\chi_{D,M}$ for (c) $a = 55/\text{s}$; (d) $a = 950/\text{s}$ [109]

singularity in the point where the gradient of the mixture fraction equals zero, which is related with its definition (the gradient of the mixture fraction appears in the denominator of Eq. (3.64)). It is clear that the use of a mass averaged diffusion coefficient is better than the assumption of unity Lewis number, although none of them perfectly matches the value of D_e.

Profiles of the transported values of ξ and χ obtained by means of the full transport equations of mixture fraction, $\xi_{D,M}$, and its scalar dissipation rate, $\chi_{D,M}$ (Eqs. (3.74) and (3.75)), are shown in Figs. 4.17c and 4.17d for low and high strain rates, respectively. These results are compared with transported values obtained employing the simplified equations for mixture fraction and the scalar dissipation rate, which neglect

gradients of the mean molecular weight (ξ_D and χ_D, which are obtained by means of Eqs. (3.79) and (3.80), respectively). As explained at the beginning of this subsection, a mass averaged diffusion coefficient is employed for the computations presented in these figures. Additionally, the exact values, ξ_e and χ_e are displayed for comparisons.

For the low strain rate situation (see Fig. 4.17c), only small differences between the three different formulations are found for the mixture fraction, which suggests that terms associated with $\frac{\partial \overline{M}}{\partial x}$ are not important for the profiles of mixture fraction. Thus, Eq. (3.79) is an excellent means for determining the value of the mixture fraction [109]. However, the comparison of the profiles of the scalar dissipation rate reveals bigger differences than those observed for the mixture fraction. As already explained, this can be attributed to the fact that gradients of mixture fraction are involved in the definition of χ, leading to a higher sensitivity of its profile to the errors introduced by means of the approximation of the diffusion coefficient. Although the inclusion of effects associated with spatial variations of the mean molecular weight slightly improves the prediction of χ, both formulations, with and without terms containing $\frac{\partial \overline{M}}{\partial x_i}$, do not properly predict the peak values of χ.

Figure 4.17d shows corresponding profiles of ξ and χ for a strain rate of 950/s. It can be seen that at this high strain rate, the results obtained by means of the transport equations with and without considering gradients of the mean molecular weight of the mixture are identical, which implies that terms including $\frac{\partial \overline{M}}{\partial x_i}$ are negligibly small and that the consideration of Fick's diffusion law at high strain rate situations is justified. However, considerable differences between exact and transported values of the mixture fraction and its scalar dissipation rate are found. From the results obtained, it can be concluded that these differences are due to the inadequacy of the diffusion coefficient selected for χ and not to the use of Fick's diffusion law.

In summary, it can be concluded that gradients of the mean molecular weight can be neglected for high strain rate situations, which is normally fulfilled in technical applications. Additionally, efforts should be made for developing an alternative for the determination of the diffusion coefficient of the mixture, since it is found that the currently used approximations are not always adequate. In particular, the assumption of unity Lewis number can lead to unphysical results.

4.2 Spray Flame Structures in Mixture Fraction Space

In this section, the influence of evaporation on the flame structure of spray flames is investigated in mixture fraction space. For this, the relative importance of the different terms of the non-premixed spray flamelet equations derived in the previous

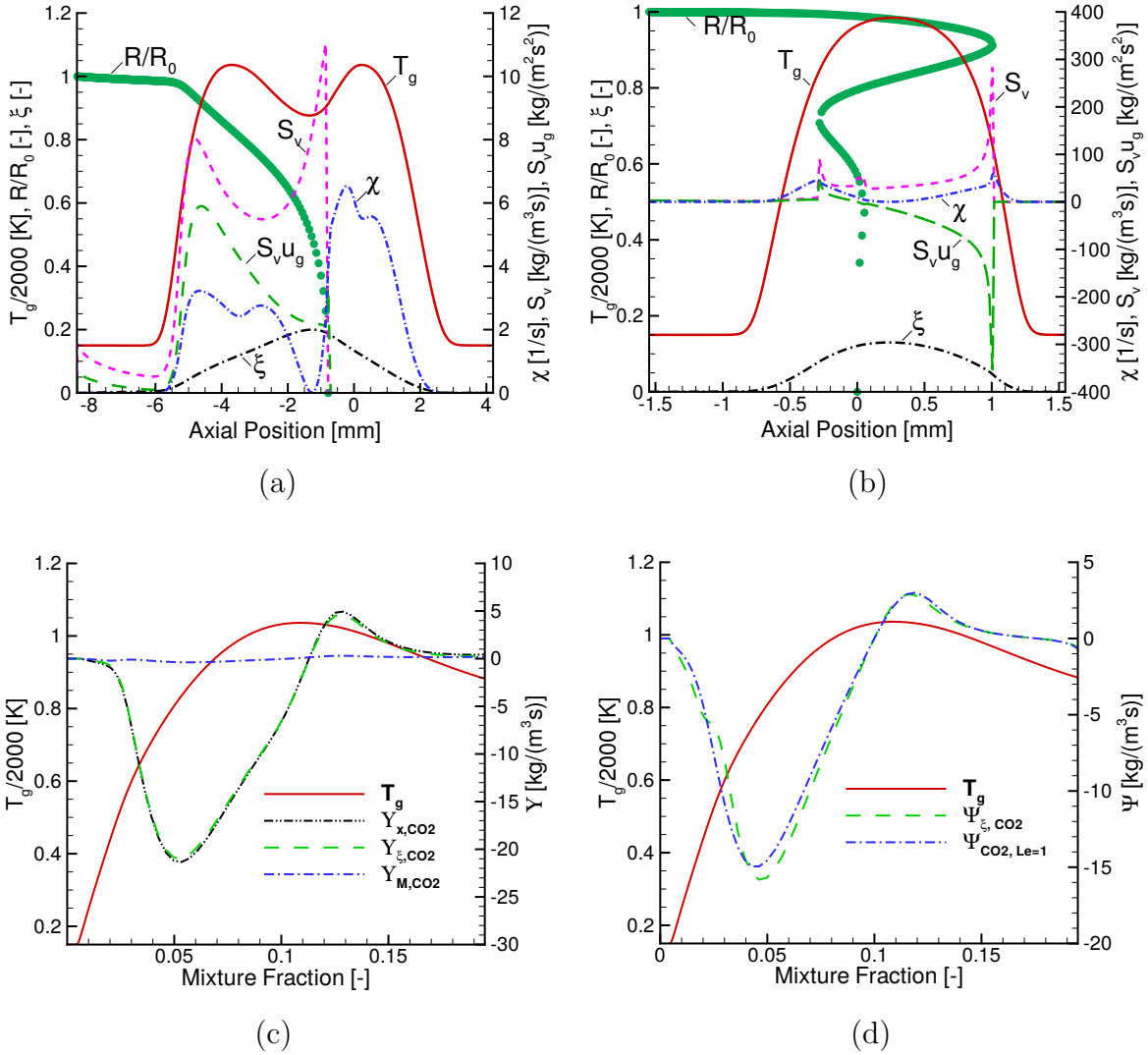

Figure 4.18: Profiles of salar dissipation rate and evaporation rate for conditions of (a) Fig. 4.11a; and (b) Fig. 4.11b; (c) Profile of Υ and (d) Ψ, for conditions of Fig. 4.11a [60]

chapter, c.f. Eqs. (3.88), is evaluated for counterflow spray flame structures. Here, the same low (55/s) and high (950/s) strain rate situations studied in subsection 4.1.3 are considered.

Figures 4.18a and b show profiles of temperature, evaporation rate and scalar dissipation rate for the low and the high strain rate situations, respectively. The profiles for $a = 55/\text{s}$ have been already presented in the previous section (see Fig. 4.6) and they are shown here only to facilitate the understanding of the present discussion. For a complete analysis of these profiles, the reader is referred to subsection 4.1.1.1.

In the high-strain situation (see Fig. 4.18b), the evaporation rate peaks at the loca-

tions of droplet reversal, where the residence time of the droplets increases. associated with the low droplet velocity generated at these locations, and evaporation is therefore enhanced.

Before the spray flamelet equations are evaluated, the assumptions of Lewis number of unity and non-variable mean molecular weight are reconsidered. These assumptions have been already evaluated in the context of the transport equations of mixture fraction and its scalar dissipation rate in the previous section. However, their influence on spray flame structures in mixture fraction space has not yet been tested. Due to the non-monotonicity of mixture fraction with space, see Figs. 4.18a and 4.18b, the flame structure has to be divided in two. For the present analysis, the local maximum of the mixture fraction is used to separate the figures. Therefore, the results shown for the spray side of the configuration exhibit an increasing scale of the mixture fraction, whereas the gas-sided structures display a decrease of mixture fraction on the abscissa. This procedure has already been employed in the literature [42, 59].

Figure 4.18c shows profiles of $\Upsilon_{x,k}$, $\Upsilon_{\xi,k}$ and $\Upsilon_{M,k}$ (see Eqs. (3.92), (3.91) and (3.89)) for CO_2 at low strain rate. CO_2 is selected as a representative species because of its high concentration, which increases $\Upsilon_{M,k}$. $\Upsilon_{x,k}$ and $\Upsilon_{\xi,k}$ match very well, which confirms the validity of Eq. (3.90), which implies that the gradient of the mean molecular weight of the mixture can also be neglected in the non-premixed spray flamelet equations . Figure 4.18d shows the profiles of $\Psi_{\xi,k}$ and $\Psi_{k,\mathrm{Le}=1}$ for CO_2 at low strain rate. Very good agreement is found, confirming that $\Psi_{k,\mathrm{Le}=1}$ is an excellent approximation of $\Psi_{\xi,k}$ for the chemical system under consideration, and $\mathrm{Le} = 1$ will be assumed in the remainder of the section.

In order to investigate the influence of spray evaporation on the flame structure, the different terms in the non-premixed spray flamelet equations (Eq. (3.88)) are evaluated for different species. Figures 4.19a and 4.19b show the contribution of the dissipation, mixing/evaporation and evaporation terms to the flamelet equation of ethanol vapor for the low strain situation, where the left side shows the spray side and the right side the gas side of the configuration. On the spray side of the configuration, see Fig. 4.19a, the dominating term is found to be the pure evaporation term. The dissipation term is relevant at the left side of the evaporation zone. As already explained in the previous section, at the left edge of the reaction zone, a peak of the fuel concentration is found, which generated diffusion into the reaction zone. At higher values of the mixture fraction, the evaporation term dominates the flamelet equation of ethanol. In this region, the mixing/evaporation term plays a minor role, since the gradient of the vapor mass fraction becomes very small in this region (see Eq. (3.88)).

Figure 4.19b displays the same profiles for the gas side of the configuration. The droplet completely evaporated at elevated values of the mixture fraction, which leads

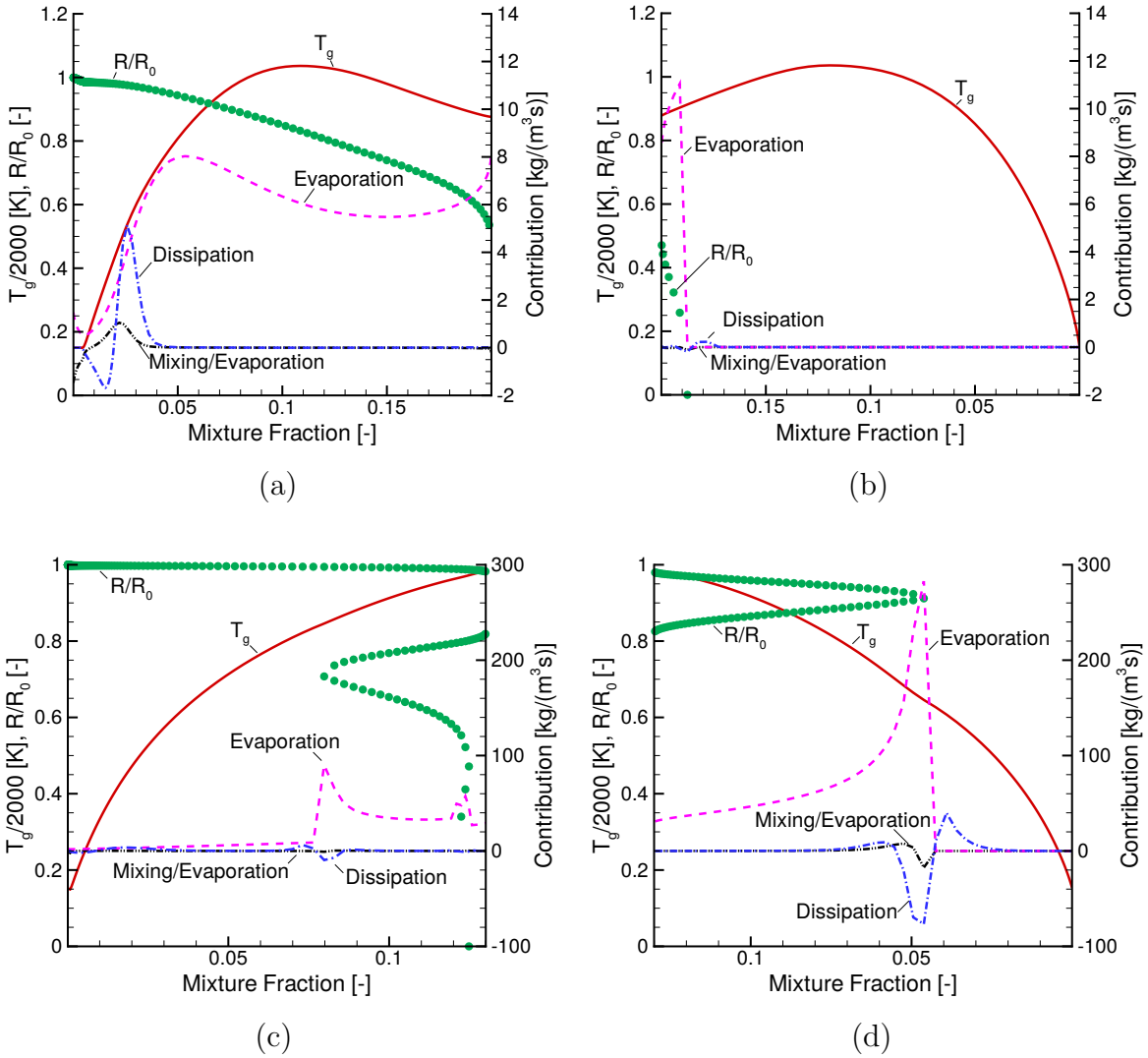

Figure 4.19: Contributions for C_2H_5OH, (a) spray side, a =55/s; (b) gas side, a =55/s; (c) spray side, a =950/s and (d) gas side, a =950/s [60]

to a dominance of the evaporation term just before evaporation is completed. Since there is hardly any evaporated fuel left, all contributions are about zero on the gas side of the configuration. Corresponding profiles at high strain rates are shown in Fig. 4.19c and 4.19d. For this condition, the dissipation term becomes relevant at the first position of droplet reversal, see Fig. 4.19d, but the pure evaporation term strongly dominates the structure. Droplet oscillation changes the relevance of contributions on the gas side of the flame structures as seen in Fig. 4.19d, where the evaporation shows significant influence on the flamelet equation of the mass fraction of fuel vapor, whereas the dissipation and mixing/evaporation terms play a minor role.

In summary, it can be stated that the flamelet equation for the fuel vapor is dom-

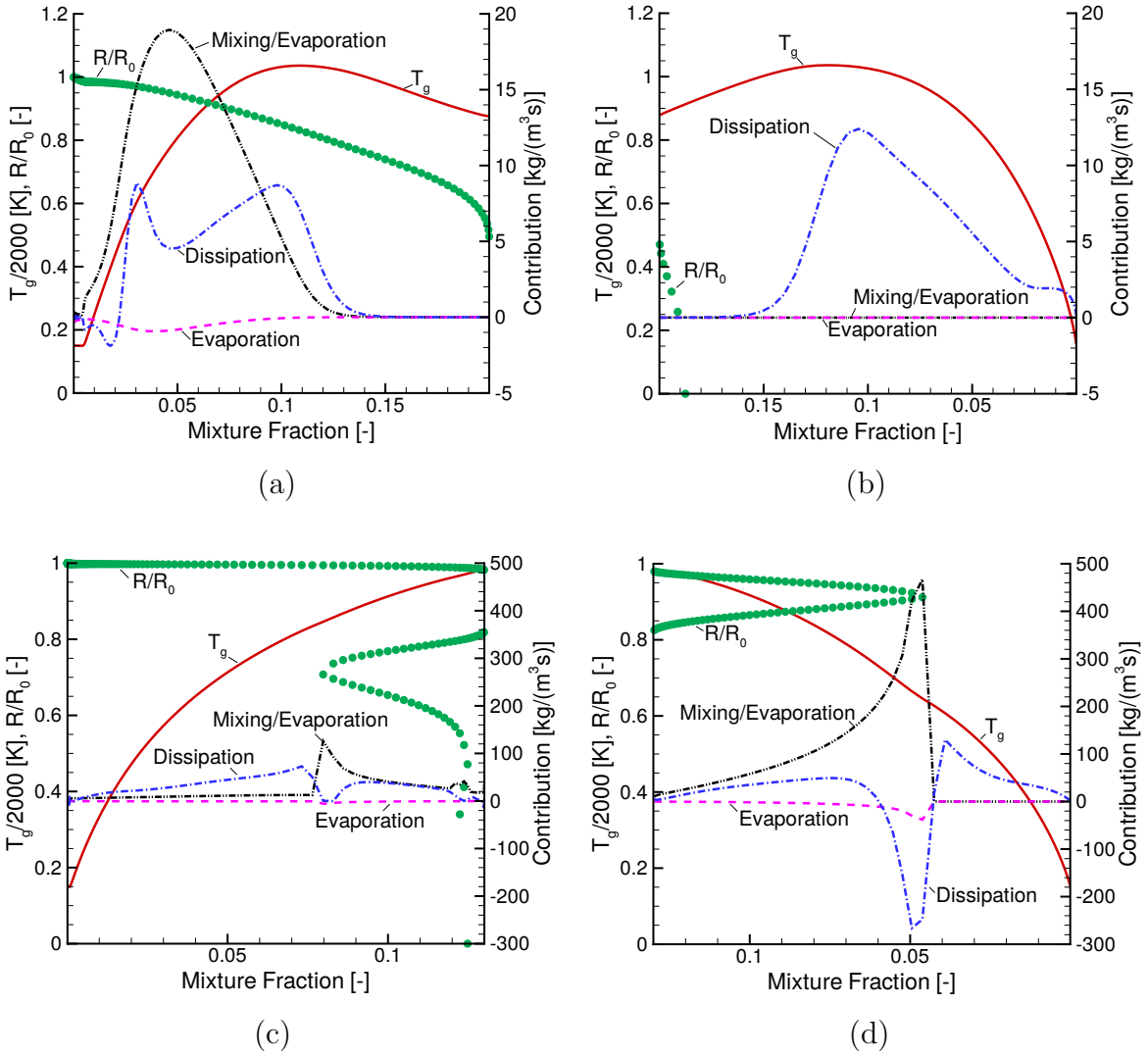

Figure 4.20: Contributions for O_2, (a) spray side, a =55/s; (b) gas side, a =55/s; (c) spray side, a =950/s and (d) gas side, a =950/s [60]

inated by the evaporation term of the flamelet equation, and this explains why approaches neglecting spray evaporation are not suitable to represent the flamelet structure of laminar spray flames with gas flamelet models, and the spray evaporation must be taken into account in spray flamelet computations of turbulent spray flames.

Figures 4.20a and 4.20b show the low strain results for the flamelet equation of O_2 and the corresponding results for the high strain condition are displayed in Figs. 4.20c and 4.20d. In both situations, the mixing/evaporation term dominates the flamelet equation on the spray side of the configuration (left part of the figures), and the dissipation term also shows a considerable contribution. The pure evaporation term is not relevant here, because oxygen is not an evaporating component. Even though this is

the case, it can be seen, that the effect of evaporation on the spray flamelet equation for the mass fraction of oxygen may not be neglected, since it has a pronounced influence through the combined mixing/evaporation term. For the low strain situation (see Figs. 4.20a and 4.20b), the droplets do not cross the stagnation plane, and dissipation determines the flamelet equation of oxygen on the gas side of the configuration. Note that when no evaporation is present, $S_v = 0$ and the non-premixed spray flamelet equation (Eq. 3.88) reduces to the gas flamelet equation of Peters [40]. For increased strain, the droplets cross the stagnation plane, and the mixing/evaporation term again dominates the flamelet equation at both side of the configuration with considerable contribution also of dissipation. Corresponding profiles for the flamelet equation of

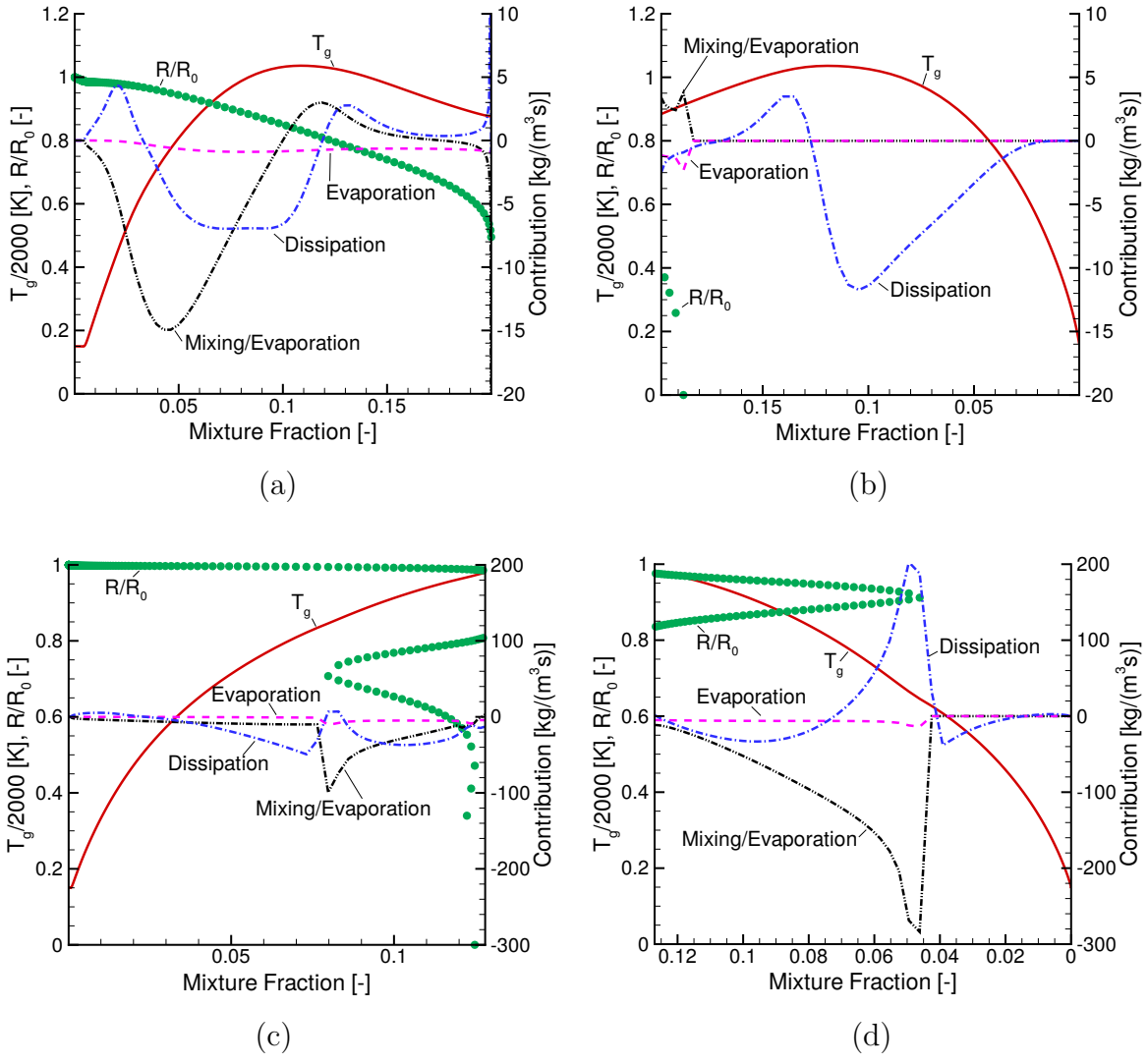

Figure 4.21: Contributions for CO_2, (a) spray side, a =55/s; (b) gas side, a =55/s; (c) spray side, a =950/s and (d) gas side, a =950/s [60]

CO_2, are shown in Fig. 4.21. Since CO_2 is produced whereas O_2 is consumed and both are non-evaporating components, the contributions of the different terms are similar, however, their sign is opposite.

In summary, it is concluded that for the evaporating species, the evaporation term in the flamelet equation is dominating wherever spray evaporation takes place. The flamelet equation of oxygen and carbon dioxide are dominated by the contribution of combined mixing/evaporation, whereas the contributions have opposite signs since oxygen is consumed and carbon dioxide is produced. For low strain rate where the droplets do not cross the stagnation plane, the non-premixed gas flamelet equations [40] are recovered on the gas side of the configuration. This supports the formulation proposed by Gutheil [59], which uses pure gas flamelet formulations for the gas side of spray flames, where all the liquid has evaporated.

The present results show that terms attributable to spray processes are important, and they must be considered whenever spray flames are considered. The non-premixed spray flamelet equations derived in the present thesis are an appropriate extension of the classical flamelet formulation for gas flames to spray flames and they provide the fundamentals for the spray flamelet model of Hollmann and Gutheil [42, 59].

5. Summary and Conclusions

The objective of the present thesis is to advance in the formulation of a comprehensive flamelet model for the inclusion of detailed chemical reaction mechanisms in the simulation of turbulent spray flames. Due to the inherent multi-regime nature of spray flames, the final multi-regime spray flamelet model has to take into account non-premixed, premixed and evaporation-dominated combustion regimes.

Laminar mono-disperse axi-symmetric ethanol/air counterflow spray flames are studied by means of numerical simulations to emphasize the importance of evaporation effects in the definition of spray flame structures. Parametric studies of the influence of the initial droplet radius and strain rate are carried out, which clearly illustrate the influence of evaporation on the flame structure. Typical effects of evaporation, such as the reduction of the local gas temperatures in flame regions with strong evaporation and droplet reversal and oscillations, are observed, which have been widely documented in the literature [54, 55, 56, 57, 58, 42, 59, 60]. A novel extinction mechanism is identified, which takes place due to the increased need of energy from the gas phase for spray evaporation (in contrast to the typical extinction mechanism due to high strain rates). This extinction phenomenon occurs due to the increased initial droplet size, which forces the evaporation front to move outside of the chemical reaction zone. Since the droplets momentum (with fixed injection velocity), the time required for the evaporation of the droplets and, therefore the droplets penetration increase with increased droplet size, a displacement of the main evaporation zone to the right edge of the flame takes place. In this region, spray evaporation cannot be achieved any more through the heat release of the chemical reactions, which eventually break down due to energy consumption of the evaporation process. This extinction mechanism has not been identified in the literature so far and it requires more investigation, which will be carried out in the future.

Exact transport equations for the mixture fraction and its scalar dissipation rate are derived considering the Hirschfelder-Curtiss diffusion law. Compared with the commonly used formulations employing Fick's diffusion law, the present formulations explicitly take into account terms associated with spatial changes of the mean molecular weight of the mixtures, which are commonly neglected. For the simplification of the derived transport equations, an unique diffusion coefficient is adopted for all chemical species. A comparison of the exact and the approximated formulations allows for

the derivation of an expression for determining the value that the diffusion coefficient assumed for all chemical species has to adopt in order to ensure the exact equivalence between both formulations. This value is compared with values of the diffusion coefficient obtained by means of the assumption of unity Lewis number and by mass averaging the diffusion coefficients of the individual chemical species existing in the mixture. The results show that, although perfect agreement is never obtained, the use of a mass averaged diffusion coefficient is a better assumption than the use of unity Lewis number. Additionally, the transport equations of the mixture fraction and its scalar dissipation rate are solved employing either the mass averaged diffusion coefficient or the diffusion coefficient obtained from the assumption of unity Lewis number. The results show that, for high strain rate situations, the assumption of unity Lewis number can lead to unphysical results.

The importance of terms associated with spatial variations of the mean molecular weight of the mixture is evaluated by means of the derived transport equations of mixture fraction and its scalar dissipation rate, which are solved either considering these terms or without considering them. Only small differences between the obtained mixture fraction profiles are found. These results show that the use of Fick's diffusion law is appropriate for the transport equation of the mixture fraction at low and high strain rate situations. However, for the scalar dissipation rate profiles, the differences are more pronounced and, especially at low strain rate situations, the consideration of the Hirschfelder-Curtiss approximation is found to be more appropriate than the use of Fick's diffusion law. The amplification of the small differences found for mixture fraction profiles when scalar dissipation profiles are considered are explained by the definition of the scalar dissipation rate, which involves squared gradients of mixture fraction. Although Fick's diffusion law may not be appropriate for calculating scalar dissipation rate profiles at low strain rate, it was found that for high strain rate situations, this approximation leads to excellent results. Under these conditions, differences between calculated and exact values of the scalar dissipation rate of the mixture fraction are not due to the negligence of effects associate with spatial variations of the mean molecular weight of the mixture, but to the inadequacy of the selected diffusion coefficient of the mixture. Thus, it is concluded that Fick's diffusion law is a good approximation for high strain rate situations. More research is required for the formulation of an alternative definition of the diffusion coefficient of the mixture.

A set of multi-regime spray flamelet equations for the description of premixed, non-premixed and evaporation-dominated combustion is derived. This set of equations comprises the flamelet equations for partially premixed gas flames derived by Knudsen and Pitsch [45, 46] and the classical non-premixed gas flamelet equations of Peters [40]. Thus, the derived multi-regime spray flamelet equations provide a common

framework for the description and combination of several flamelet models available in the literature.

The new multi-regime spray flamelet equations are evaluated for counterflow spray flames under representative conditions. In particular, a situation with a strain rate of 55/s, an initial droplet radius, $r_0 = 25$ μm, an unity equivalence ratio at the left side of the configuration, $E = 1$, and an initial gas and droplet velocity, $v_g = v_d = 0.44$ m/s is taken as a base case. Different situations are generated starting from this base case by the modification of either the strain rate, the initial droplet radius or the equivalence ratio. Thus, profiles with an increased strain rate of 950/s, an increased droplet radius of 120 µm and an increased equivalence ratio of 3 are studied. The results show that premixed effects in those flames are very small, which confirms the assumption made by Hollmann and Gutheil [42] in the derivation of the non-premixed spray flamelet model [42, 59].

The multi-regime spray flamelet equations are simplified by neglecting terms associated with premixed effects. Additionally, unity Lewis numbers for all chemical species are assumed. The resulting non-premixed spray flamelet equations in the mixture fraction space provide the fundamentals for the non-premixed spray flamelet model of Hollmann and Gutheil [42] and the base for a new formulation of the spray-flamelet model, which requires the consideration of only three characteristic parameters (mixture fraction, its scalar dissipation rate and the evaporation rate), instead of the five parameters required by the previous formulation of Hollmann and Gutheil [42] (mixture fraction, its scalar dissipation rate, the initial droplet radius and velocity and the equivalence ration at the spray side of the configuration). Although these results are very promising, more work is required for the determination of a possible shape of this new three-variate probability density function, as well as for the development of techniques and procedures for the elaboration of an appropriate flamelet library. Specially important is the question about how to consider the entire spectrum of possible combinations of the characteristic parameters.

Finally, the non-premixed spray flamelet equations are employed for the evaluation of the relative importance of effects attributable to evaporation on the flamelet structures. For this purpose, the spray flamelet equations for the evaporating fuel ethanol, for oxygen, and for carbon dioxide are analyzed in mixture fraction space. The results show that the contributions of the new terms dominate the spray flamelet equations for all species investigated, where the evaporation term is most important for the evaporating species ethanol, and the combined mixing/evaporation term for oxygen and carbon dioxide in regions where the spray resides. These results show that evaporation effects are important and they cannot be neglected as it is commonly done in the literature.

In summary, the present thesis emphasizes the importance of the evaporation in the

definition of the flame structure of spray flames and it presents and validates a set of multi-regime spray flamelet equations, which provides a framework for the development of a comprehensive multi-regime spray flamelet model for turbulent spray flames, as well as the fundamentals for the non-premixed spray flamelet model of Hollmann and Gutheil [42].

This work represents a major step in the development of a comprehensive multi-regime spray flamelet model for the simulation of turbulent spray flames. The development of such a model is of major importance, since it would allow for the proper prediction of pollutant formation of this widely used kind of combustion, having in this way a great impact in the development of new, more efficient and less contaminant combustion technologies.

Despite of the major progress made, the complete development of a comprehensive multi-regime spray flamelet model for the simulation of realistic turbulent spray flames requires the solution of several open issues, which have not been solved in the present work. Among these open questions are the definition of an appropriate reaction progress variable for spray flames, the formulation of a joint probability density function for the mixture fraction, its scalar dissipation rate and the mass evaporation rate and the definition of a flame index for the appropriate identification of the locally dominant combustion regime in turbulent spray flames, which would allow for the selective application of non-premixed, premixed or spray flamelet models to the simulation of complex practical flames. Solving these open issues would allow the development of a comprehensive multi-regime spray flamelet model, and it will therefore be the focus of future research.

Appendix

A. Nomenclature

Symbol	Description	Unit
A_k	Symbol of chemical species k	
a	Strain rate	s^{-1}
B_M	Spalding mass transfer number	
B_T	Spalding heat transfer number	
C_k	Concentration of species k	mol m^{-3}
C_p	Specific heat capacity of the mixture	J kg^{-1} K^{-1}
$C_{p,k}$	Specific heat capacity of species k	J kg^{-1} K^{-1}
Da	Damköhler number	
D_k	Diffusion coefficient of species k into the mixture	m^2 s^{-1}
D_{ki}	Diffusion coefficient of species k into species i	m^2 s^{-1}
f	Stream function	
h	Enthalpy of the mixture	J kg^{-1}
h_k	Enthalpy of species k	J kg^{-1}
K	Total number of droplet size groups	
Le	Lewis number	
M	Total number of chemical reactions	
M_k	Molecular weight of species k	kg mol^{-1}
$\overline{M}$	Mean molecular weight of the mixture	kg mol^{-1}
m	Droplet mass	kg
$\dot{m}_k$	Droplet mass vaporization rate in size group k	kg s^{-1}
N	Total number of chemical species	
P	Total number of variables for flamelet transformation	
p	Static pressure	Pa
p	Static pressure	Pa
R	Universal gas constant	J mol^{-1} K^{-1}
Re	Reynolds number	
Sh	Sherwood number	
S_e	Energy source term	J m^{-3} s^{-1}
S_m	Momentum source term	kg m^{-2} s^{-2}
S_v	Mass evaporation source term	kg m^{-3} s^{-1}
T	Temperature	K
t	time	s
u	velocity	m s^{-1}
$V_{k,i}$	Diffusion velocity of species k in i direction	m s^{-1}
x	Radial coordinate	m
X_k	Mol fraction of species k	
y	Axial coordinate	m
Y_k	Mass fraction of chemical species k	

Greek letter	**Description**	**Unit**
η	Similarity coordinate	
Λ	Reaction progress variable	
λ	Gas conductivity of the mixture	J m^{-1} K^{-1} s^{-1}
λ_k	Gas conductivity of species k	J m^{-1} K^{-1} s^{-1}
δ	Kronecker Symbol	
χ	Scalar dissipation rate	s^{-1}
μ	Gas viscosity	kg m^{-1} s^{-1}
ν'_{kj}	Stoichiometric coefficient of species k	
ρ	Gas density	kg m^{-3}
Θ	Gas flame index	
Θ_s	Spray flame index	
θ	Non-dimensional temperature	
τ	Transformed time	s
$\dot{\omega}_k$	Specific chemical reaction rate of species k	kg m^{-3} s^{-1}
Ξ	General characteristic variable	
ξ	Mixture fraction	

Subscript	**Description**
∞_-	Boundary condition at the left side of the counterflow
∞_+	Boundary condition at the right side of the counterflow
F	Fuel
f	Film around the droplets
g	Gas phase
l	Liquid phase
O	Oxygen
0	Initial condition

B. Acknowledgements

First, and foremost, I would like to express my most sincere and deepest gratitude to my advisor, Prof. Eva Gutheil for her continuous support, patience and encouragement. This dissertation would not have been possible without her excellent guidance and immense knowledge. She is my best role model for a scientist and mentor, and it is impossible to express in these few lines how thankful I am to her for the opportunity of pursuing my scientific passion at one of the best universities in the world and for the strong support provided during the application to my current position in Chile.

I would like to extend my cordial thanks to Prof. Hans-Robert Volpp, who always helped me to go through this period of PhD. I am very thankful for his immense amenity and great support to my work.

I express my sincere thanks to all my colleagues and friends who made my stay in Heidelberg more enjoyable and constantly helped me, the people whom I will always keep in my memories. I am thankful to L. Cao, X. Cui, H. Großhans, P. Hindenberg, Y. Hu, R. M. Humza, O. Noreña, S. Reddy, A. Sanches. Special thanks to Y. Hu and O. Noreña for proof reading this thesis and to H. Großhans and P. Hindenberg for the help translating the abstract. I also want to express my gratitude to Mrs. Vogel and M. Trunk, who made my life considerably easier.

I thank my parents José and Norma, and my brother, Alejandro, for the love, warm feelings and constant support during my entire life. I wish to thank my beloved wife, Ivelina, for the wonderful family she gave me and for being my daily support. And, of course, I want to thank my little David for showing me that there are many other important things in life.

Finally, I want to thank the German Academic Exchange Service (DAAD) and the Heidelberg Graduate School of Mathematical and Computational Methods for the Sciences (HGS-MathComp) of the Interdisciplinary Center for Scientific Computing (IWR) for the financial support provided during my PhD.

Bibliography

[1] International Energy Agency. "Key World Energy Statistic 2014". *International Energy Agency Publications,* http://www.iea.org/ (2014).

[2] International Energy Agency. "World Energy Outlook 2014". *International Energy Agency Publications,* http://www.iea.org/ (2014).

[3] R. Bilger. "The Role of Combustion Technology in the 21st Century". In: *Turbulent Combustion Modeling*. Ed. by T. Echekki and E. Mastorakos. Vol. 95. Fluid Mechanics and Its Applications Series. Springer Netherlands, 2011, pp. 3–18.

[4] R. E. Gullison, P. C. Frumhoff, J. G. Canadell, C. B. Field, D. C. Nepstad, K. Hayhoe, R. Avissar, L. M. Curran, P. Friedlingstein, C. D. Jones, and C. Nobre. "Tropical Forests and Climate Policy". *Science* **316**(5827) (2007), pp. 985–986.

[5] D. Veynante and L. Vervisch. "Turbulent combustion modeling". *Progress in Energy and Combustion Science* **28**(3) (2002), pp. 193–266.

[6] R. Cant and E. Mastorakos. *An Introduction to Turbulent Reacting Flows*. Imperial College Press, (2007).

[7] S. Pope. "Small scales, many species and the manifold challenges of turbulent combustion". *Proceedings of the Combustion Institute* **34**(1) (2013), pp. 1–31.

[8] M. Smooke. "The computation of laminar flames". *Proceedings of the Combustion Institute* **34**(1) (2013), pp. 65–98.

[9] N. Peters. "Multiscale combustion and turbulence". *Proceedings of the Combustion Institute* **32**(1) (2009), pp. 1–25.

[10] J. Buckmaster, P. Clavin, A. Linan, M. Matalon, N. Peters, G. Sivashinsky, and F. Williams. "Combustion theory and modeling". *Proceedings of the Combustion Institute* **30**(1) (2005), pp. 1–19.

[11] R. Bilger, S. Pope, K. Bray, and J. Driscoll. "Paradigms in turbulent combustion research". *Proceedings of the Combustion Institute* **30**(1) (2005), pp. 21–42.

[12] A. Demirbas. "Progress and recent trends in biofuels". *Progress in Energy and Combustion Science* **33**(1) (2007), pp. 1–18.

[13] A. K. Agarwal. "Biofuels (alcohols and biodiesel) applications as fuels for internal combustion engines". *Progress in Energy and Combustion Science* **33**(3) (2007), pp. 233–271.

[14] P. S. Nigam and A. Singh. "Production of liquid biofuels from renewable resources". *Progress in Energy and Combustion Science* **37**(1) (2011), pp. 52–68.

[15] URL: `http://www.metaefficient.com/`.

[16] J. M. Bergthorson and M. J. Thomson. "A review of the combustion and emissions properties of advanced transportation biofuels and their impact on existing and future engines". *Renewable and Sustainable Energy Reviews* 42 (2015), pp. 1393–1417.

[17] URL: `http://www.ecoworld.com/home/articles2.cfm?tid=389`.

[18] Food and agriculture organization of the united nations. "The state of food and agriculture. BIOFUELS: prospects, risks and opportunities" (2008).

[19] London Royal Society. "Sustainable biofuels: prospects and challenges" (2008).

[20] D. Turner, H. Xu, R. F. Cracknell, V. Natarajan, and X. Chen. "Combustion performance of bio-ethanol at various blend ratios in a gasoline direct injection engine". *Fuel* **90**(5) (2011), pp. 1999–2006.

[21] R. Lemaire, E. Therssen, and P. Desgroux. "Effect of ethanol addition in gasoline and gasoline-surrogate on soot formation in turbulent spray flames". *Fuel* **89**(12) (2010), pp. 3952–3959.

[22] "Biobutanol: a future fuel?" *Focus on Catalysts* **2010**(5) (2010), pp. 1–2.

[23] S. S. Merchant, E. F. Zanoelo, R. L. Speth, M. R. Harper, K. M. V. Geem, and W. H. Green. "Combustion and pyrolysis of iso-butanol: Experimental and chemical kinetic modeling study". *Combustion and Flame* **160**(10) (2013), pp. 1907–1929.

[24] A. Ranjan and V. S. Moholkar. "Biobutanol: science, engineering, and economics". *International Journal of Energy Research* **36**(3) (2012), pp. 277–323.

[25] J. Swana, Y. Yang, M. Behnam, and R. Thompson. "An analysis of net energy production and feedstock availability for biobutanol and bioethanol". *Bioresource Technology* **102**(2) (2011), pp. 2112–2117.

[26] S. Szwaja and J. Naber. "Combustion of n-butanol in a spark-ignition {IC} engine". *Fuel* **89**(7) (2010). 17th International Symposium on Alcohol Fuels, pp. 1573–1582.

[27] O. Doğan. "The influence of n-butanol/diesel fuel blends utilization on a small diesel engine performance and emissions". *Fuel* **90**(7) (2011), pp. 2467–2472.

[28] T. C. Ezeji, N. Qureshi, and H. P. Blaschek. "Bioproduction of butanol from biomass: from genes to bioreactors". *Current Opinion in Biotechnology* **18**(3) (2007). Energy biotechnology / Environmental biotechnology, pp. 220–227.

[29] S. Sarathy, M. Thomson, C. Togbé, P. Dagaut, F. Halter, and C. Mounaim-Rousselle. "An experimental and kinetic modeling study of n-butanol combustion". *Combustion and Flame* **156**(4) (2009), pp. 852–864.

[30] P. Dagaut and C. Togbé. "Oxidation kinetics of butanol-gasoline surrogate mixtures in a jet-stirred reactor: Experimental and modeling study". *Fuel* **87**(15-16) (2008), pp. 3313–3321.

[31] M. R. Harper, K. M. V. Geem, S. P. Pyl, G. B. Marin, and W. H. Green. "Comprehensive reaction mechanism for n-butanol pyrolysis and combustion". *Combustion and Flame* **158**(1) (2011), pp. 16–41.

[32] S. M. Sarathy, S. Vranckx, K. Yasunaga, M. Mehl, P. Oßwald, W. K. Metcalfe, C. K. Westbrook, W. J. Pitz, K. Kohse-Höinghaus, R. X. Fernandes, and H. J. Curran". "A comprehensive chemical kinetic combustion model for the four butanol isomers". *Combustion and Flame* **159**(6) (2012), pp. 2028–2055.

[33] A. Frassoldati, R. Grana, T. Faravelli, E. Ranzi, P. Oßwald, and K. Kohse-Höinghaus". "Detailed kinetic modeling of the combustion of the four butanol isomers in premixed low-pressure flames". *Combustion and Flame* **159**(7) (2012), pp. 2295–2311.

[34] E. Gutheil. "Issues in Computational Studies of Turbulent Spray Combustion". In: *Experiments and Numerical Simulations of Diluted Spray Turbulent Combustion*. Ed. by B. Merci, D. Roekaerts, and A. Sadiki. Vol. 17. ERCOFTAC Series. Springer International Publishing, 2011, pp. 1–39.

[35] P. Jenny, D. Roekaerts, and N. Beishuizen. "Modeling of turbulent spray combustion". *Progress in Energy and Combustion Science* **38** (2012), pp. 846–887.

[36] *Workshop on Measurement and Computation of Turbulent Spray Combustion (TCS),* http://www.tcs-workshop.org/.

[37] S. Pope. *Turbulent Flows*. Cambridge University Press, (2000).

[38] P. Davidson. *Turbulence: An Introduction for Scientists and Engineers*. Oxford University Press, (2004).

[39] T. Poinsot and D. Veynante. *Theoretical and Numerical Combustion, Second Edition*. R.T. Edwards, Inc., (2005).

[40] N. Peters. "Laminar diffusion flamelet models in non-premixed turbulent combustion". *Progress in Energy and Combustion Science* **10**3 (1984), pp. 319–339.

[41] C. Hollmann and E. Gutheil. "Modeling of turbulent spray diffusion flames including detailed chemistry". *Symposium (International) on Combustion* **26**(1) (1996), pp. 1731–1738.

[42] C. Hollmann and E. Gutheil. "Flamelet-modeling of turbulent spray diffusion Flames Based on a Laminar Spray Flame Library". *Combustion Science and Technology* **135**(1-6) (1998), pp. 175–192.

[43] B. Franzelli, B. Fiorina, and N. Darabiha. "A tabulated chemistry method for spray combustion". *Proceedings of the Combustion Institute* **34**(1) (2013), pp. 1659–1666.

[44] B. Fiorina, O. Gicquel, L. Vervisch, S. Carpentier, and N. Darabiha. "Approximating the chemical structure of partially premixed and diffusion counterflow flames using {FPI} flamelet tabulation". *Combustion and Flame* **140**(3) (2005), pp. 147–160.

[45] E. Knudsen and H. Pitsch. "A general flamelet transformation useful for distinguishing between premixed and non-premixed modes of combustion". *Combustion and Flame* **156**(3) (2009), pp. 678–696.

[46] E. Knudsen and H. Pitsch. "Capabilities and limitations of multi-regime flamelet combustion models". *Combustion and Flame* **159**(1) (2012), pp. 242–264.

[47] H. Pitsch and N. Peters. "A Consistent Flamelet Formulation for Non-Premixed Combustion Considering Differential Diffusion Effects". *Combustion and Flame* **114** (1998), pp. 26–40.

[48] O. Gicquel, N. Darabiha, and D. Thévenin. "Laminar premixed hydrogen/air counterflow flame simulations using flame prolongation of ILDM with differential diffusion". *Proceedings of the Combustion Institute* **28**(2) (2000), pp. 1901–1908.

[49] J. van Oijen, F. Lammers, and L. de Goey. "Modeling of complex premixed burner systems by using flamelet-generated manifolds". *Combustion and Flame* **127**(3) (2001), pp. 2124–2134.

[50] H. Barths, C. Hasse, and N. Peters. "Computational fluid dynamics modelling of non-premixed combustion in direct injection diesel engines". *International Journal of Engine Research* **1**(3) (2000), pp. 249–267.

[51] C. Hasse and N. Peters. "A two mixture fraction flamelet model applied to split injections in a DI Diesel engine". *Proceedings of the Combustion Institute* **30**(2) (2005), pp. 2755–2762.

[52] C. Felsch, M. Gauding, C. Hasse, S. Vogel, and N. Peters. "An extended flamelet model for multiple injections in DI Diesel engines". *Proceedings of the Combustion Institute* **32**(2) (2009), pp. 2775–2783.

[53] I. Dhuchakallaya, P. Rattanadecho, and P. Watkins. "Auto-ignition and combustion of diesel spray using unsteady laminar flamelet model". *Applied Thermal Engineering* **52**(2) (2013), pp. 420–427.

[54] N.-H. Chen, B. Rogg, and K. Bray. "Modelling laminar two-phase counterflow flames with detailed chemistry and transport". *Symposium (International) on Combustion* **24** (1992), pp. 1513–1521.

[55] S. Li, P. Libby, and F. Williams. "Experimental and theoretical studies of counterflow spray diffusion flames". *Symposium (International) on Combustion* **24**(1) (1992), pp. 1503–1512.

[56] J. Greenberg and N. Sarig. "An analysis of multiple flames in counterflow spray combustion". *Combustion and Flame* **104**(4) (1996), pp. 431–459.

[57] S. Li. "Spray stagnation flames". *Progress in Energy and Combustion Science* **23**(4) (1997), pp. 303–347.

[58] M. Massot, M. Kumar, M. D. Smooke, and A. Gomez. "Spray counterflow diffusion flames of heptane: Experiments and computations with detailed kinetics and transport". *Symposium (International) on Combustion* **27**(2) (1998), pp. 1975–1983.

[59] E. Gutheil. "Multiple solutions for structures of laminar counterflow spray flames". *Progress in Computational Fluid Dynamics* **5**(7) (2005), pp. 414–419.

[60] H. Olguin and E. Gutheil. "Influence of evaporation on spray flamelet structures". *Combustion and Flame* **161**(4) (2014), pp. 987–996.

[61] M. Mortensen and R. W. Bilger. "Derivation of the conditional moment closure equations for spray combustion". *Combustion and Flame* **156** (2009), pp. 62–72.

[62] G. Borghesi, E. Mastorakos, C. B. Devaud, and R. W. Bilger. "Modeling evaporation effects in conditional moment closure for spray autoignition". *Combustion Theory and Modelling* **15**(5) (2011), pp. 725–752.

[63] S. Ukai, A. Kronenburg, and O. Stein. "LES-CMC of a dilute acetone spray flame". *Proceedings of the Combustion Institute* **34**(1) (2013), pp. 1643–1650.

[64] A. Tyliszczak, D. Cavaliere, and E. Mastorakos. "LES/CMC of Blow-off in a Liquid Fueled Swirl Burner". English. *Flow, Turbulence and Combustion* **92** (2014), pp. 237–267.

[65] P.-D. Nguyen, L. Vervisch, V. Subramanian, and P. Domingo. "Multidimensional flamelet-generated manifolds for partially premixed combustion". *Combustion and Flame* **157**(1) (2010), pp. 43–61.

[66] H.-W. Ge and E. Gutheil. "Simulation of a turbulent spray flame using coupled PDF gas phase and spray flamelet modeling". *Combustion and Flame* **153**(1) (2008), pp. 173–185.

[67] H.-W. Ge, I. Düwel, H. Kronemayer, R. W. Dibble, E. Gutheil, C. Schulz, and J. Wolfrum. "Laser-Based Experimental and Monte Carlo PDF Numerical Investigation of an Ethanol/Air Spray Flame". *Combustion Science and Technology* **180**(8) (2008), pp. 1529–1547.

[68] N. Peters. *Turbulent Combustion*. Cambridge University Press, (2000).

[69] D. Spalding. "Mixing and chemical reaction in steady confined turbulent flames". *Symposium (International) on Combustion* **13**(1) (1971). Thirteenth symposium (International) on Combustion Thirteenth symposium (International) on Combustion, pp. 649–657.

[70] I. S. Erstevå g and B. F. Magnusse. "The Eddy Dissipation Turbulence Energy Cascade Model". *Combustion Science and Technology* **159** (2000), pp. 213–235.

[71] A. Klimenko and R. Bilger. "Conditional moment closure for turbulent combustion". *Progress in Energy and Combustion Science* **25** (1999), pp. 595–687.

[72] S. Pope. "PDF methods for turbulent reactive flows ". *Progress in Energy and Combustion Science* **11**2 (1985), pp. 119–192.

[73] D. Haworth. "Progress in probability density function methods for turbulent reacting flows". *Progress in Energy and Combustion Science* **36**(2) (2010), pp. 168–259.

[74] F. Williams. *Combustion Theory*. Oxford University Press, (1985).

[75] U. Maas and S. Pope. "Simplifying chemical kinetics: Intrinsic low-dimensional manifolds in composition space". *Combustion and Flame* **88** (1992), pp. 239–264.

[76] U. Maas and S. Pope. "Implementation of simplified chemical kinetics based on intrinsic low-dimensional manifolds". *Symposium (International) on Combustion* **24**(1) (1992), pp. 103–112.

[77] V. Bykov and U. Maas. "Extension of the ILDM method to the domain of slow chemistry". *Proceedings of the Combustion Institute* 311 (2007), pp. 465 –472.

[78] K. W. Mao and H. L. Toor. "A diffusion model for reactions with turbulent mixing". *AIChE Journal* 161 (1970), pp. 49–52.

[79] C. H. Gibson and P. A. Libby. "On Turbulent Flows with Fast Chemical Reactions. Part II. The Distribution of Reactants and Products Near a Reacting Surface". *Combustion Science and Technology* 61-2 (1972), pp. 29–35.

[80] K. Claramunt, R. Consul, D. Carbonell, and C. Perez-Segarra. "Analysis of the laminar flamelet concept for nonpremixed laminar flames". *Combustion and Flame* **145**(4) (2006), pp. 845–862.

[81] G. Continillo and W. Sirignano. "Counterflow spray combustion modeling". *Combustion and Flame* **81**(3) (1990), pp. 325–340.

[82] E. Gutheil and W. Sirignano. "Counterflow Spray Combustion Modeling with Detailed Transport and Detailed Chemistry". *Combustion and Flame* **113**(1) (1998), pp. 92–105.

[83] E. Gutheil. "Structure and extinction of laminar ethanol-air spray flames". *Combustion Theory and Modelling* **5**(2) (2001), pp. 131–145.

[84] D. Bradley, L. Kwa, A. Lau, M. Missaghi, and S. Chin. "Laminar flamelet modeling of recirculating premixed methane and propane-air combustion". *Combustion and Flame* **71**(2) (1988), pp. 109–122.

[85] W. A. Al-Masseeh, D. Bradley, P. Gaskell, and A. Lau. "Turbulent premixed, swirling combustion: Direct stress, strained flamelet modelling and experimental investigation". *Symposium (International) on Combustion* **23**(1) (1991), pp. 825–833.

[86] D. Bradley, P. Gaskell, and X. Gu. "The modeling of aerodynamic strain rate and flame curvature effects in premixed turbulent combustion". *Symposium (International) on Combustion* **27**(1) (1998), pp. 849–856.

[87] R. Borghi. In: *Recent Advances in Aeronautical Science*. Ed. by C. Bruno and C. Casci. Pergamon, 1984.

[88] "Length Scales in Laminar and Turbulent Flames in: Numerical Approaches to Combustion Modeling". *Progress in Astronautics and Aeronautics* 135 (1991), pp. 155–182.

[89] T. Mantel and R. Borghi. "A new model of premixed wrinkled flame propagation based on a scalar dissipation equation". *Combustion and Flame* **96**(4) (1994), pp. 443–457.

[90] A. Mura and R. Borghi. "Towards an extended scalar dissipation equation for turbulent premixed combustion". *Combustion and Flame* **133**(1) (2003), pp. 193–196.

[91] A. Mura, V. Robin, and M. Champion. "Modeling of scalar dissipation in partially premixed turbulent flames". *Combustion and Flame* **149**(1) (2007), pp. 217–224.

[92] T. Dunstan, Y. Minamoto, N. Chakraborty, and N. Swaminathan. "Scalar dissipation rate modelling for Large Eddy Simulation of turbulent premixed flames". *Proceedings of the Combustion Institute* **34**(1) (2013), pp. 1193–1201.

[93] C. M. Cha, G. Kosaly, and H. Pitsch. "Modeling extinction and reignition in turbulent nonpremixed combustion using a doubly-conditional moment closure approach". *Physics of Fluids (1994-present)* **13**(12) (2001), pp. 3824–3834.

[94] H. Pitsch, C. M. Cha, and S. Fedotov. "Flamelet modelling of non-premixed turbulent combustion with local extinction and re-ignition". *Combustion Theory and Modelling* **7**(2) (2003), pp. 317–332.

[95] L. Gomet, V. Robin, and A. Mura. "Lagrangian modelling of turbulent spray combustion under liquid rocket engine conditions". *Acta Astronautica* **94**(1) (2014), pp. 184–197.

[96] J. M. Richardson, H. C. H. Jr., and R. W. S. Jr. "The relation between sampling-tube measurements and concentration fluctuations in a turbulent gas jet". *Symposium (International) on Combustion* **4**(1) (1953), pp. 814–817.

[97] W. Jones and J. Whitelaw. "Calculation methods for reacting turbulent flows: A review". *Combustion and Flame* 480 (1982), pp. 1 –26.

[98] C. D. Pierce and P. Moin. "Progress-variable approach for large-eddy simulation of non-premixed turbulent combustion". *Journal of Fluid Mechanics* **504** (2004), pp. 73–97.

[99] M. Ihme, C. M. Cha, and H. Pitsch. "Prediction of extinction and re-ignition effects in non-premixed turbulent combustion using a flamelet/progress variable approach". *Proceedings of the Combustion Institute* **30** (2005), pp. 793–800.

[100] M. Hossain, J. Jones, and W. Malalasekera. "Modelling of a Bluff-Body Non-premixed Flame using a Coupled Radiation/Flamelet Combustion Model". English. *Flow, Turbulence and Combustion* **67**(3) (2001), pp. 217–234.

[101] H. Pitsch. "Unsteady flamelet modeling of differential diffusion in turbulent jet diffusion flames". *Combustion and Flame* **123**(3) (2000), pp. 358–374.

[102] H. Pitsch, M. Chen, and N. Peters. "Unsteady flamelet modeling of turbulent hydrogen-air diffusion flames". *Symposium (International) on Combustion* **27**(1) (1998), pp. 1057–1064.

[103] H. Pitsch and H. Steiner. "Scalar mixing and dissipation rate in large-eddy simulations of non-premixed turbulent combustion". *Proceedings of the Combustion Institute* **28**(1) (2000), pp. 41–49.

[104] O. Gicquel, N. Darabiha, and D. Thévenin. "Laminar premixed hydrogen/air counterflow flame simulations using flame prolongation of ILDM with differential diffusion". *Proceedings of the Combustion Institute* **28**(2) (2000), pp. 1901–1908.

[105] J. V. Oijen and L. Goey. "Modelling of Premixed Laminar Flames using Flamelet-Generated Manifolds". *Combustion Science and Technology* **161** (2000), pp. 113–137.

[106] D. Bradley, P. Gaskell, X. Gu, and A. Sedaghat. "Premixed flamelet modelling: Factors influencing the turbulent heat release rate source term and the turbulent burning velocity". *Combustion and Flame* **143**(3) (2005), pp. 227–245.

[107] H. Kolla and N. Swaminathan. "Strained flamelets for turbulent premixed flames, I: Formulation and planar flame results". *Combustion and Flame* **157**(5) (2010), pp. 943–954.

[108] H. Kolla and N. Swaminathan. "Strained flamelets for turbulent premixed flames II: Laboratory flame results". *Combustion and Flame* **157**(7) (2010), pp. 1274–1289.

[109] H. Olguin and E. Gutheil. "Derivation and Evaluation of a Multi-regime Spray Flamelet Model". *Zeitschrift für Physikalische Chemie* **229** (2015), pp. 461–482.

[110] H. Yamashita, M. Shimada, and T. Takeno. "A numerical study on flame stability at the transition point of jet diffusion flames". *Symposium (International) on Combustion* **26**(1) (1996), pp. 27–34.

[111] P. Domingo, L. Vervisch, and K. Bray. "Partially premixed flamelets in LES of nonpremixed turbulent combustion". *Combustion Theory and Modelling* **6**(4) (2002), pp. 529–551.

[112] P. Domingo, L. Vervisch, and J. Réveillon. "DNS analysis of partially premixed combustion in spray and gaseous turbulent flame-bases stabilized in hot air". *Combustion and Flame* **140**(3) (2005), pp. 172–195.

[113] P. Domingo, L. Vervisch, and D. Veynante. "Large-eddy simulation of a lifted methane jet flame in a vitiated coflow". *Combustion and Flame* **152**(3) (2008), pp. 415–432.

[114] H.-W. Ge and E. Gutheil. "PDF simulation of turbulent spray flows". *Atomization and sprays* **16**(5) (2006), pp. 531–542.

[115] K. Luo, H. Pitsch, M. Pai, and O. Desjardins. "Direct numerical simulations and analysis of three-dimensional n-heptane spray flames in a model swirl combustor". *Proceedings of the Combustion Institute* **33**(2) (2011), pp. 2143–2152.

[116] J. R. Kee, J. Warnatz, and J. A. Miller. "A FORTRAN Computer Code Package for the Evaluation of Gas-Phase Viscosities, Conductivities, and Diffusion Coefficients". *Sandia National Laboratories Report, No. SAND83-8209* (1988).

[117] S. Gordon and B. J. McBride. "Computer Program for Calculation of Complex Chemical Equilibrium Compositions, Rocket Performance, Incident and Reflected Shocks and Chapman-Jouguet Detonations". *NASA Report SP-273* (1971).

[118] C. Chevalier. "Entwicklung eines detallierten Reaktionmechanismus zur Modellierung der Verbrennungsprozesse von Kohlenwasserstoffen bei Hoch- und Niedertemperaturbedingungen". PhD thesis. Universität Stuttgart.

[119] E. Gutheil and F. Williams. "A numerical and asymptotic investigation of structures of hydrogen-air diffusion flames at pressures and temperatures of high-speed combustion". *Symposium (International) on Combustion* **23**(1) (1991), pp. 513–521.

[120] B. Abramzon and W. Sirignano. "Droplet vaporization model for spray combustion calculations". *International Journal of Heat and Mass Transfer* **32**(9) (1989), pp. 1605–1618.

[121] G. Hubbard, V. Denny, and A. Mills. "Droplet evaporation: Effects of transients and variable properties". *International Journal of Heat and Mass Transfer* **18**(9) (1975), pp. 1003–1008.

[122] B. Poling, J. Prausnitz, and J. O'Connel. *The properties of gases and liquids, Fifth Edition*. New York: McGraw-Hill, (2001).

[123] H. Olguin and E. Gutheil. "Theoretical and Numerical Study of Evaporation Effects in Spray Flamelet Modeling". In: *Experiments and Numerical Simulations of Turbulent Combustion of Diluted Sprays*. Ed. by B. Merci and E. Gutheil. Vol. 19. ERCOFTAC. Springer International Publishing, 2014, pp. 79–106.

[124] J. H. Ferzige. *Computational Methods for Fluid Dynamics*. Springer, (2002).

[125] H. Versteeg and W. Malalasekera. *An Introduction to Computational Fluid Dynamics: The Finite Volume Method*. Prentice Hall, (2007).

[126] E. Gutheil. "Numerical Analysis of the Autoignition of Methanol, Ethanol, n-Heptan and n-Octane Sprays with Detailed Chemistry". *Combustion Science and Technology* **105** (1995), pp. 265–278.